1. Report No. FHWA/TX-07/0-5239-1	2. Government Accession No.	3. Recipient's Catalog No.
4. Title and Subtitle NANOTECHNOLOGY SYNTHESIS STUDY: RESEARCH REPORT	5. Report Date November 2006 Published: April 2007	
	6. Performing Organization Code	
7. Author(s) Richard Liu, Zhibin Zhang, Rui Zhong, Xuemin Chen and Jing Li	8. Performing Organization Report No. Report 0-5239-1	
9. Performing Organization Name and Address Department of Electrical and Computer Engineering University of Houston 4800 Calhoun Rd. Houston, TX 77204-4005	10. Work Unit No.	
	11. Contract or Grant No. Project 0-5239	
12. Sponsoring Agency Name and Address Texas Department of Transportation Research and Technology Implementation Office P.O. Box 5080 Austin, TX 78763-5080	13. Type of Report and Period Covered Technical Report: Sep 1, 2005 – Aug 31, 2006	
	14. Sponsoring Agency Code	
15. Supplementary Notes Project performed in cooperation with the Texas Department of Transportation and the Federal Highway Administration. Project Title: Nanotechnology Synthesis Study URL: http://subsurface.ee.uh.edu/documents/0-5239.pdf		

16. Abstract:

In this project, we investigated the potential nanotechnology applications in highway pavements mainly in two different categories: smart materials for pavement construction and sensors for transportation and pavement infrastructure condition monitoring. The smart materials are applicable to pavement construction including concrete, asphalt, aggregates, and pavement marking materials; and the sensors, including temperature sensor, strain sensor, pressure sensor, accelerometer, and moisture sensor, now form a reliable, accurate, low-cost network and are suitable for transportation and pavement infrastructure condition monitoring. Radio frequency (RF) microelectronic monitoring system (MEMS) technology is an advanced and innovative MEMS sensor technology which transmits MEMS sensor data wirelessly at a high speed securely. Ultra-low-cost RF MEMS sensors can be placed in pavements, bridges, and even inside concrete and asphalt in large quantities to form a local RF MEMS sensor network for different pavement infrastructure monitoring purposes. Nanomaterials are very attractive to the Texas Department of Transportation (TxDOT). Though nanomaterials are still in the research and development stages and are not cost effective for implementation at this time, nano-based sensors are getting mature and can be used in TxDOT for monitoring and other applications. In order to demonstrate the applications of nanotechnology in transportations systems, a fully functional smart stop sign is developed and tested. This smart stop sign is able to detect any malfunction including direction change, fall down, or tilt and report wirelessly to the TxDOT office using nanosensors and MEMS radio technology.

17. Key Words MEMS Technology, Nanotechnology, Transportation Engineering, Sensor Application, Wireless Sensor Network, Smart Material	18. Distribution Statement No restrictions. This document is available to the public through National Technical Information Service, Springfield, Virginia, 22161, www.ntis.gov		
19. Security Classif. (of this report) Unclassified	20. Security Classif. (of this page) Unclassified	21. No. of Pages 122	22. Price

Form DOT F 1700.7 (8-72)   Reproduction of completed page authorized

This form was electrically by Elite Federal Forms Inc.

NANOTECHNOLOGY SYNTHESIS STUDY: RESEARCH REPORT

by

Richard Liu, Zhibin Zhang, Rui Zhong, Xuemin Chen and Jing Li

Technical Report 0-5239-1

by the

Subsurface Sensing Laboratory
Department of Electrical and Computer Engineering
University of Houston

DISCLAIMER

The contents of this report reflect the views of the authors who are responsible for the facts and accuracy of the data presented herein. The contents do not necessarily reflect the official views or policies of the Texas Department of Transportation (TxDOT) or the Federal Highway Administration (FHWA). This report does not constitute a standard, specification or regulation.

University of Houston
4800 Calhoun Rd.
Houston, TX 77204

ACKNOWLEDGEMENTS

TABLE OF CONTENTS

LIST OF FIGURES

LIST OF TABLES

CHAPTER 1 INTRODUCTION

Growing with the development of semiconductor fabrication industry, microelectrical mechanical systems (MEMS; also called nanotechnology) technology has begun to impact highway pavement construction materials and the pavement infrastructure condition monitoring sensor network. In this project, we investigated the potential nanotechnology applications in highway pavements mainly in two different categories: smart materials for pavement construction and sensors for transportation and pavement infrastructure condition monitoring. The smart materials are applicable to the pavement construction materials including concrete, asphalt, aggregates, and pavement marking materials, and the sensors, including temperature sensor, strain sensor, pressure sensor, accelerometer, and moisture sensor, now form a reliable, accurate, low-cost network and are suitable for transportation and pavement infrastructure condition monitoring.

Radio frequency (RF) MEMS technology is an advanced and innovative MEMS sensor technology which transmits MEMS sensor data wirelessly at a high speed securely, instead of using a traditional wired communication system. Ultra-low-cost RF MEMS sensors can be placed in the pavements, bridges, and even inside concrete and asphalt in large quantities to form a local RF MEMS sensor network for different pavement infrastructure monitoring purposes. Smart materials and applications of RF MEMS sensor networks are also investigated in this report. Nano materials are very attractive to the Texas Department of Transportation (TxDOT). Though nano materials are still in the research and development (R&D) stages and are not cost effective for implementation at this time, nano-based sensors are maturing and can be used in TxDOT for monitoring and other applications.

CHAPTER 2 NANO AND MEMS TECHNOLOGY

Nanotechnology is a result of semiconductor advancement. It is a miniaturization of materials, devices, and sensors using technologies developed in the semiconductor industry. Nano manufacturing can manufacture devices and materials from micro scales as small as molecules or particle levels. Therefore, the materials manufactured using nanotechnology are readily controllable to satisfy specific needs, such as long durability and stability. Nanotechnology is also called MEMS technology.

Since the concept of MEMS technology originated from R. Feynman's talk in 1960 [1], for decades scientists have been making great efforts to create innovative and tiny structures. MEMS technology is a process used to create tiny integrated devices or systems that combine mechanical and electrical components. MEMS products are fabricated using integrated circuit (IC) batch processing and can range in size from a few micrometers to millimeters. Most MEMS systems include a power system, signal processing unit, sensor, and actuator [2]. A typical MEMS sensor system is shown in Figure 1.
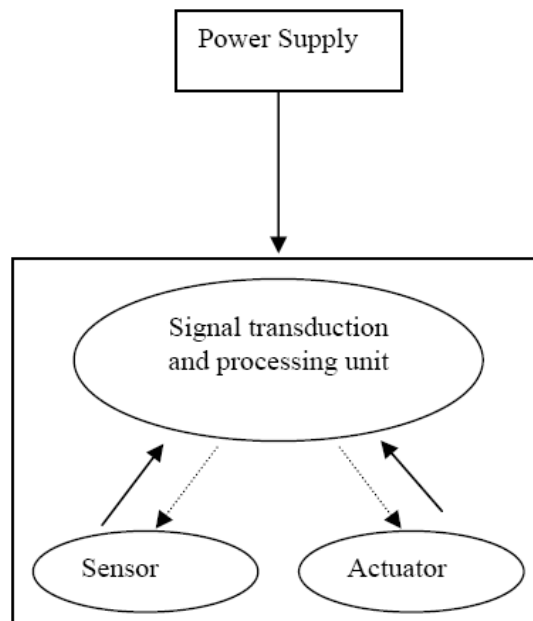
Figure 1 Basic MEMS

Because of the mature IC fabrication technology these days, MEMS products now are extremely low cost [3]. The following are a series of techniques that have been developed for building MEMS products.

2.1 Silicon-Based Microfabrication [4]-[11]

This kind of MEMS fabrication technology originated from IC fabrication [4], which has been employed to produce microcircuits for many years. As shown in Figure 2 [5], surface micromachining [6] [7] creates microstructures that reside near the surfaces of a substrate. As shown in Figure 3 [8], bulk micromachining [9] [10] creates free-standing mechanical structures (such as beams and membranes) or unique three-dimensional features (such as cavities, through-wafer holes, and mesas). In addition, this fabrication technology is based on the silicon wafer as shown in Figure 4 [11].
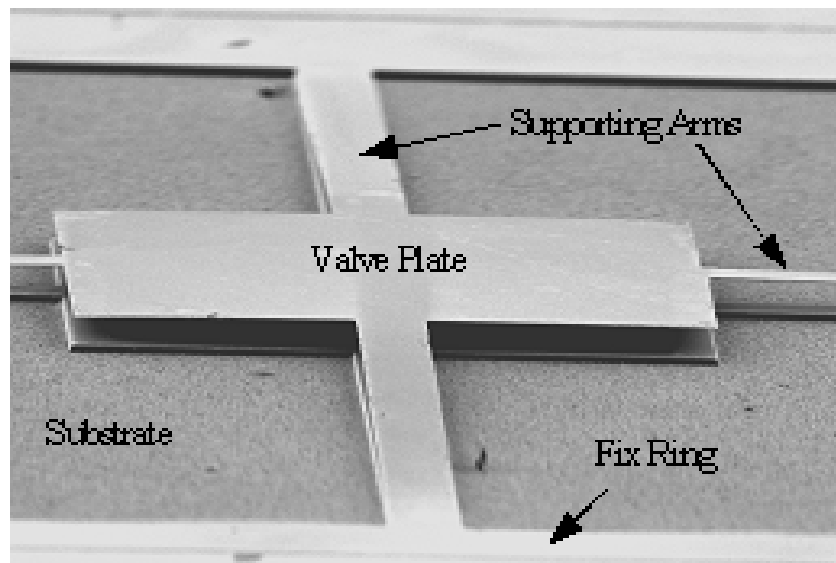
Figure 2 Example of surface micromachining (after C. S. Bien [5])
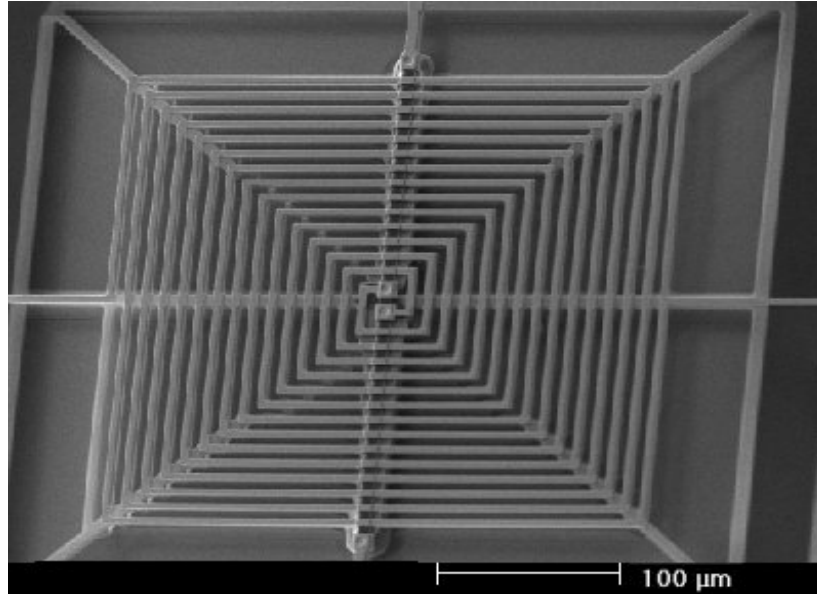
Figure 3 Examples of bulk micromachining (after the Micro and Nano System Research Group [8])
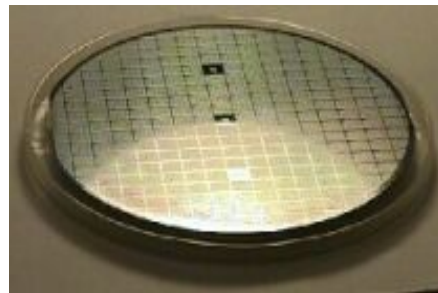
Figure 4 Silicon wafer as substrate (after MEMS Foundry Services [11])

2.2 Non-Silicon Fabrication Technology [12]-[15]

In recent years, many innovative materials have been used in MEMS fabrication process besides silicon-based materials [12]. For example, polymer materials are increasingly used in MEMS for realizing structures, sensors, and actuators. Polymers are large, usually chainlike molecules that are built from small molecules [13]. For instance, liquid crystal polymer (LCP) is a thermoplastic polymer material with unique structural and physical properties [14]. It contains rigid and flexible monomers that link to each other. Figure 5 shows a scanning electron micrograph (SEM) example of LCP-based MEMS products.
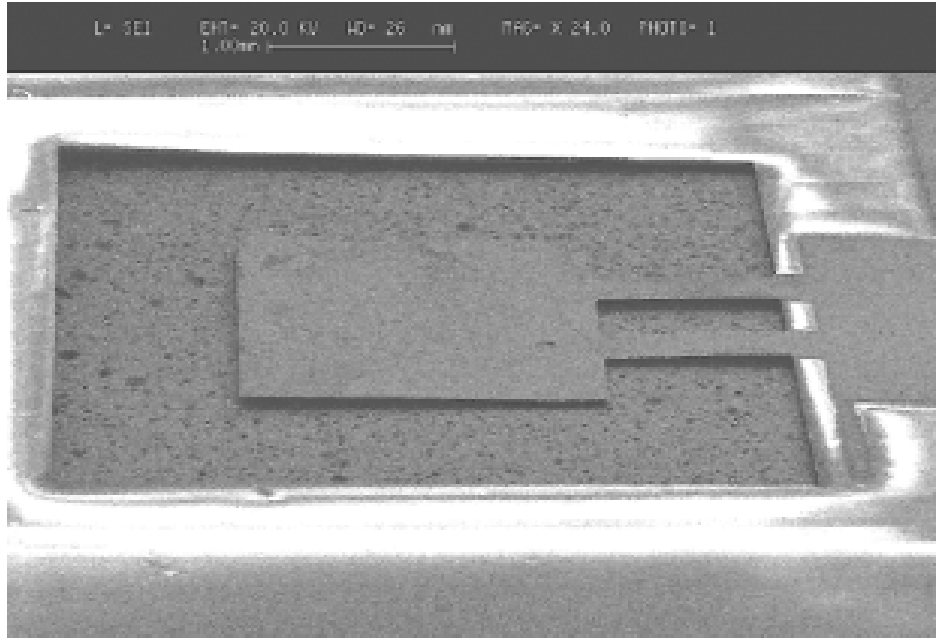
Figure 5 SEM micrograph example of LCP-based MEMS product (after J. Xie et al. [15])

However, MEMS technology is more than a manufacturing method. To create sensors and actuators, basic physics still plays a major role [16], for example, piezoelectric effect, piezoresistive effect, thermoelectric effect, etc.

With the above mature fabrication techniques, MEMS products are relatively low cost. Some new structures of smart materials with special features have already been created and applied to highway pavement engineering. A variety of smart material applications, such as smart aggregates, in which wireless sensors are embedded during construction, are constructed in the Federal Highway Administration's (FHWA's) Advanced Infrastructure Research Program [17]. These wireless MEMS sensors can be powered on and transmit data to the passing-by data reader. Several universities already have prototypes and are now at the testing stage.

The University of Houston (UH) [18] developed two sensor systems based on this method: a) a wireless moisture sensor system, which can be buried into pavement to measure moisture content of the concrete, base, and sub-base materials. Data collection vehicles

can collect both moisture and temperature data when they drive over the sensors. The mechanism and the architecture of the UH's wireless moisture sensor have a high potential to be applicable to building smart MEMS sensors of same functions, so as to provide a close-up look at the hydration process of individual cement grains to help gain insight into such concrete ills as alkali-silica reactivity (ASR); b) a passive ultra-high-frequency (UHF) RF identification (RFID) system, which can be used as a pavement monitoring system. The passive tag is buried into the pavement side and, when the vehicle passes by, the reader on the vehicle will transmit the RF signal, which is used to power up these passive tags, then read the tag information and write the corresponding information to the passive tag. This pavement monitoring system can be extremely low cost. Its maintenance is easy and it is very reliable.

Smart materials for structure crack self-healing have interested many researchers because they could lead to guardrails that heal themselves or concrete and asphalt that heal their own cracks. One way to accomplish self-healing is to incorporate a microencapsulated healing agent and catalysts within an epoxy matrix. A crack ruptures embedded microcapsules, releasing healing agents into the crack plane through capillary action. Polymerization is triggered by the embedded catalyst, bonding the crack faces. Nanomaterials can be used for many other applications, such as structure coating and reinforcement. It is time now to use the developed nanotechnology and implement it to the transportation applications.

New properties of MEMS products and smart materials have revealed wide applications for the development of new sensor systems and new smart construction materials for transportation engineering. MEMS products and smart materials can be manufactured as ultra-small size, lightweight, and at extremely low cost. Table 1 and Table 2 summarize the possible applications of nanotechnology to transportation engineering. Details of these technologies are explained in the following sections.

Table 1 Potential Innovative Materials for Transportation Application

Innovative Material or Research on Chemical Kinetics	Potential Application	Recommendations	Reference Page Number
Self-healing polymers	Automatically heal cracks	Research is still under way	11
Nanostructure for building steel	Low carbon, high performance steel	This technology has never been applied before in transportation	11
Nanotube crack-preventing material	Automatically heal structure cracks; increase structure strength	Research is still under way	12
Self-cleaning lotus leaf	Automatically clean pavement surface or traffic sign	Commercial product for transportation is not available	13
Superelasticity smart material	Self-rehabilitation concrete beams; blast protection of vehicular tunnels	Research is still under way	14
Shape memory alloy	Smart bridge	Successful application is transportation is available	15
Smart paints	Effective coating	Commercial product for transportation is in conceptual phase	17
Smart polymer coating	Radioactive contamination detection	Research is still under way	17
Steel and foam energy reduction barrier	Safer highway barrier	Successful product is available; cost and effectiveness needs more evaluation	17
Lead biosensor	Pavement lead contamination detection	Research is still under way	18
Smart fiber	Pavement environment monitoring	Commercial products are available	19
Helmholtz resonators	Noise-reduced pavement	Commercial products are available	19
Colloidal chemistry of ASR gels	Safer concrete	Research is still under way	20
Cement hydration kinetics	Safer cement	Research is still under way	20
Fly ash reactivity characterization	Reduce fly ash	Research is still under way	20
Aggregate ASR potential tests	Safer concrete	Research is still under way	21
Delayed ettringite formation damage	Safer concrete	Research is still under way	21

Table 2 Potential Sensor Networks for Transportation Application

Innovative Nano - and MEMS Sensor or Sensor Networks	Potential Application	Recommendations
Nanosensor		
MEMS strain sensor	Measure strain information of pavement and asphalt	Commercial products are available and advanced research is under way
MEMS moisture sensor	Moisture monitoring	Commercial products are available
MEMS accelerometer	Bridge and highway safety monitoring	Successful commercial products are available
MEMS load monitoring sensor network	Monitoring load condition on bridge and highway	Successful applications are available
MEMS crack corrosion and crack testing and monitoring sensor	Crack and concrete corrosion testing and monitoring	Research is still under way
National Science Foundation sponsored research projects for MEMS sensors	Ultra-small sensor monitoring pavement temperature, moisture, pH and so on	Sensors are reported to be successful
Microsensor		
UH wireless moisture and temperature sensors	Monitor moisture and temperature information of pavement	Sensors are available at UH; cost and effectiveness are evaluated
RFID system	Inventory tracking/pavement monitoring	Low cost and effective sensors are available in market
Bulky sensor		
Low-cost microwave weigh-in-motion (WIM) sensor	Monitor highway load condition	Sensors are available at UH; cost and effectiveness are evaluated
Sensor networks with communication and control of smart materials and sensors	Communication between MEMS sensors and smart materials to better monitor and control pavement	Successful applications are available

CHAPTER 3 INNOVATIVE MATERIALS

Advances in science and technology have led to the creation of new materials with new properties. These new materials will offer potential applications which will be beneficial for pavement engineering. Table 1 summarizes the potential application of these innovative materials to pavement engineering.

3.1 Self-Healing Materials [19]

Work on self-healing polymers is under way at the University of Illinois Urbana-Champaign by Professor Nancy Sottos and her Sottos Research Group, which has developed a structural polymeric material with the ability to autonomically heal cracks. Autonomic (spontaneous) healing is accomplished in this program by incorporating a microencapsulated healing agent and a catalytic chemical trigger within an epoxy matrix. An approaching crack ruptures embedded microcapsules, releasing the healing agent into the crack plane through capillary action. Polymerization of the healing agent is triggered by contact with the embedded catalyst, bonding the crack faces. A similar process has been described in which micro-sized hollow fibers filled with crack sealant would be introduced into concrete. If the concrete cracked, the fibers would also break and release sealant. This would be especially applicable for bridge piers and columns suffering from microcracking and requiring costly epoxy injection, and the ability to self-heal may not be limited to encapsulated microcapsules or fibers.

3.2 Building Steel through Nanotechnology [19]

In 1992, the FHWA began partnering with the American Iron and Steel Institute and the U.S. Navy to develop new, low-carbon, high-performance steel (HPS) for bridges. HPS was deemed to require improved strength and weld ability, and a boost in the overall quality of steels used in bridges in the United States. In 1996, the first of these steels was produced. Steel is a nanostructured material. In low-carbon HPS steel, copper nano particles form at the steel grain boundaries. The resulting microstructure changes make

the HPS steel tougher, easier to weld, and more corrosion-resistant. Separately, Sandvik Materials Technology is producing an ultra-high-strength stainless steel using nanotechnology. The new product, Sandvik Nanoflex, allows ultra-high-strength to be combined with good formability, corrosion resistance, and a good surface finish. Because of its attributes, Nanoflex is suited to mechanical applications where lightweight, rigid designs are required. A high modulus of elasticity combined with extreme strength can result in thinner and even lighter components than those made from aluminum and titanium. While currently being used for medical equipment, such as surgical needles and dental tools, other areas of use are anticipated. It is not unimaginable that this technology could be applied to bridge structural elements.

3.3 Crack-Preventing Materials [20]

Self-healing materials are able to automatically heal structure cracks. A concept of crack-preventing materials presumably can prevent pavement cracking. It has been found that carbon nanotubes can have distinct properties depending on their atomic structures, i.e., they can be stiffer than steel, and can also be resistant to damage from physical forces. When an external force is applied to the tip of a nanotube, the nanotube bends; when the force is removed, it recovers its original shape. Specially designed nanotubes used to build new core/shell microparticles in which the core is made of nanotubes and the thin outer shell is made of bonding material.

When construction material, like cement, is incorporated with a large quantity of strong, firm, rigid microparticle, it forms a new composite material with great strength, equivalent to rebar-frame reinforced concrete in microscale, a crack-free material.

3.4 Self-Cleaning Materials [21]

The lotus leaf, or water lily leaf, exhibits an extraordinary ability to keep itself clean and dry. The particular cleanness of the lotus plant is well known since early in history. Lotus plants are a symbol for purity in Asian religions. W. Barthlott and C. Neinhuis [22] from the University of Bonn, Germany, brought this biological approach into the minds of

non-biologists and opened up a huge field of possible industrial applications. Nevertheless, even after numerous scientific awards, the lotus effect is still not yet fully understood. Now nanotechnology is being used to mimic the lotus leaf surface and to create new products that outperform existing non-stick products, and it is clear that this technology will have immediate benefits for traffic and work zone signage. Typically, on a hydrophobic (water-repellent) easy clean surface, particles of dirt are just moved around by moving water, but on a lotus-effect surface, dirt and grime are collected by water drops and rinse off. Figure 6 is a picture showing the lotus-effect surface.
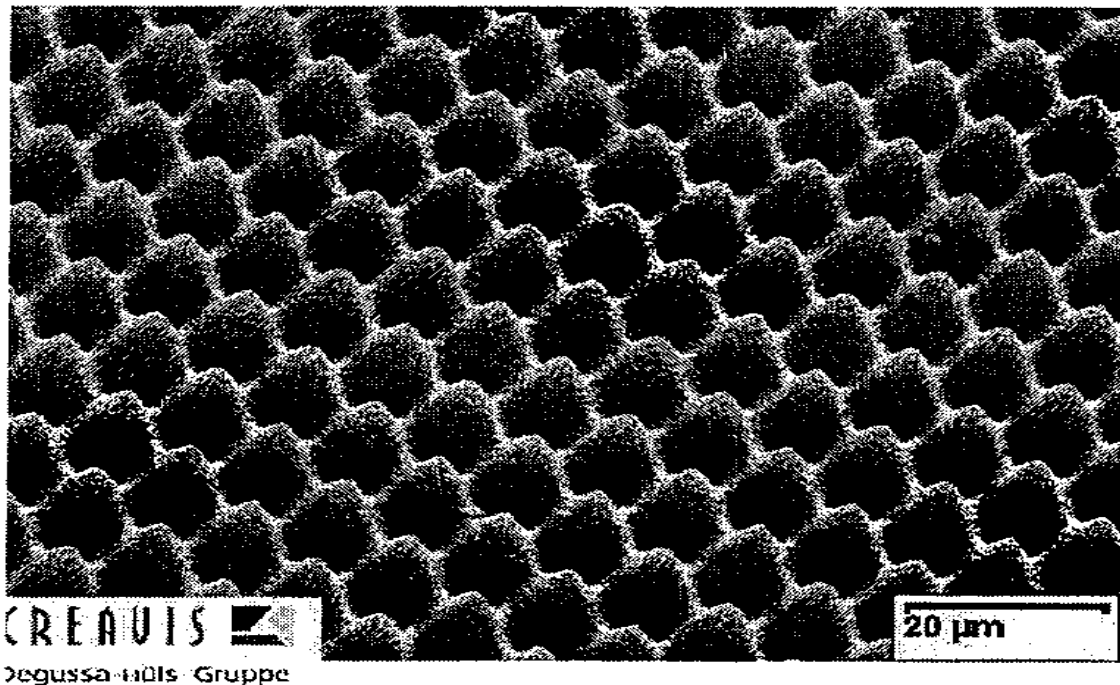
Figure 6 SEM picture of a polymer lotus-effect surface (after M. Oles et al. [21])

Before, only one commercial product was available which utilizes this effect: exterior house paint. Now this technology can be brought to the market for use with traffic signs and, in particular, traffic control devices, which require labor-intensive periodic washing to remove road grime and enhance visibility.

Researchers at the Washington Department of Transportation (WSDOT) have developed a technique utilizing the lotus effect [23]. Their technology has the potential to solve even mundane problems like dirty signs. Coatings that mimic the properties of the lotus leaf — to which nothing sticks — may well lead to signs that shed dirt and never need washing,

freeing up time for more important activities. These coating are plastic coatings which have been developed to mimic the lotus effect.

Another self-clean material involves polycyclic aromatic hydrocarbons, and it is especially effective in decontaminating soil. Using polymeric nanoparticles, it could be an efficient tool to deal with soil particles with tightly adherent contaminants [24]. In addition, it is possible that the nanoparticles could be tailored for a particular set of soil-decontamination conditions [25].

3.5 Superelasticity Smart Material [26]

Superelasticity smart material has the ability to go back to its original length after stress-induced phase changes. Therefore, it may be used as self-rehabilitation material in concrete beams. Developed by the U.S. Air Force Research Laboratory, this elastomeric coating is formulated for spray application on walls of structures to improve their blast resistance. For extra strength, high-strength fibers can be added to the formulation. An obvious application of this material is in blast protection of major vehicular tunnels in Virginia, many of which are under navigable waters, as these can be considered potential targets of attacks by terrorists. Virginia Department of Transportation's (VDOT's) Structure & Bridge Division indicates that the Association of American State Highway and Transportation Officials (AASHTO) are developing blast design and protection guidelines for tunnels. Although this material may not prevent damage caused by bomb blasts in such tunnels, it likely could minimize the effects of such blasts and, thereby, facilitate speedy resumption of traffic operation.

3.6 Shape Memory Alloy (SMA) Material [27]

Differential settlement between bridges and pavements causes bumps or uneven joints at the bridge ends. When vehicles, especially heavy trucks, approach and leave bridges, the bumps cause large impact loads to the bridges and pavements. It is well known that these uneven joints can cause pavement and bridge deterioration, damage automobiles, or cause accidents. The damage includes separation of pavement topping from its base, spalling of joints, fatigue cracking of pavements, and fatigue damage to bridges. A

similar problem is associated with uneven settlement between the piers of the bridge or the approach spans. When differential settlement occurs, not only is the drivability of the bridge affected, but additional internal forces are also created for the structure. Maintenance of joints is a big problem and expense for engineers and highway officials. Traditionally, in dealing with these problems, engineers focus on improvement in foundation design. However, they have not been very successful in resolving these problems associated with the unevenness of the joints and differential settlement.

Temperature change and time-dependent effects, such as creep and shrinkage, also cause internal restraint forces for indeterminate structures. These forces alone or together with other external load effects cause cracking of existing structures and pavements, or increase the cost for new construction meant to cope with these effects (such as increase in section dimensions). Another problem is that associated with the performance of bridge bearings. Malfunctioning bearings due to material deterioration, clogging of dirt, and other factors result in tremendous stresses near the bearing region. This causes changes in the force redistribution and thus makes the bridges behave differently from the intended design. These problems are common factors in bridge failures and in maintenance requirements. Finding a way to automatically adjust forces among the bearings in order to alleviate all of the above problems is desirable. The two-way memory effects of SMA can be used to make SMA actuators that can rise and fall to adjust their heights. SMA can also be used to manufacture smart strands. After mechanically deforming the strands and embedding them in concrete, the prestressing and self-repair effects can be activated as needed during the life of the structure. The smart strands are actually actuators that can be activated by external heating or internal stress changes.

The applications of the smart bearings and smart strands can be used to develop a smart bridge as shown in Figure 7. The smart bearings will adjust their heights through the shape memory effect of the SMA. This height adjustment will correct the unevenness problem as well as the internal forces induced from differential settlements, time-dependent deformations (creep and shrinkage of concrete, relaxation of prestressing

steel), and temperature changes as discussed earlier. When needed, the prestress forces can also be adjusted to deal with cracking issues in both positive and negative moment zones. With the combined application of the smart bearings and smart strands, the bridge can adjust its internal force distribution and mobilize each element to adapt itself to different environmental loads like those induced by differential settlement, time-dependent effects, temperature effects, and overweight trucks.
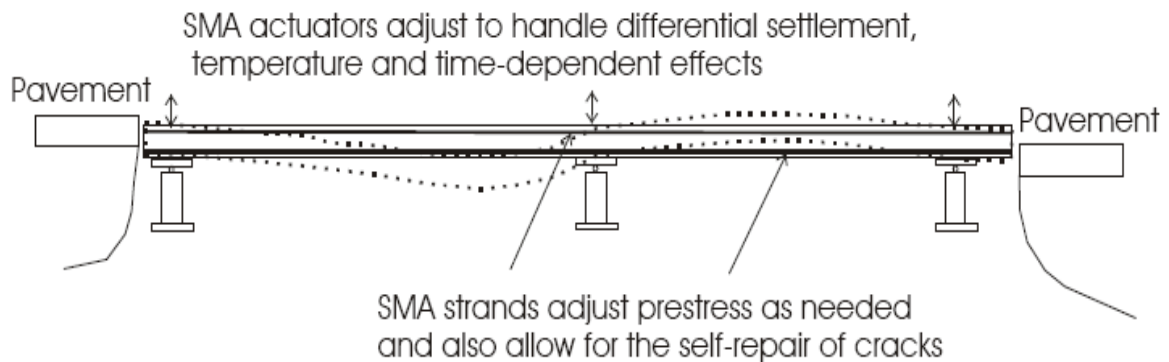
Figure 7 SMA smart material applied to bridge (after C. S. Cai et al. [27])

3.7 Smart Paints [28]

Smart paints can monitor their own condition and their effectiveness in protecting the underlying steel substrate from corrosion and, therefore, provide a prediction of their remaining life. Smart paints are new and have tremendous potential in improving the effectiveness of managing coating programs for bridges and structures.

3.8 Smart Polymeric Coatings [28]

These peelable coatings are being developed at the University of Texas at Tyler expressly for the cleanup of working surfaces that are accidentally contaminated with radioactive materials. They are in the conceptual stage, and they may have potential application as a less-expensive alternative to the current expensive methods for removing lead in deteriorating leaded paints on bridges. A lead-removal method based on this concept would offer two inherent advantages: (1) the envelope or tent around a structure to

contain the resulting lead-loaded debris generated by the current blasting methods would not be required, and (2) the breathing apparatus for workers required with the current methods would not be required. Toward the development of such a method, it is necessary to identify a polymeric solution that can effectively "draw" the lead to its resulting coating before it is peeled off the structural steel. It may be desirable also to identify and incorporate a suitable color indicator for lead, which can vary the intensity of its characteristic color with the concentration of lead drawn from the structural steel.

3.9 Steel and Foam Energy Reduction Barrier [28]

An ideal safety barrier must be able to absorb or attenuate the very high energy resulting from vehicular impact, safely redirect the direction of an errant vehicle along the line of the barrier, and prevent crossover of the vehicle into the path of oncoming vehicles. The desirable result is to provide protection to the driver and passengers inside the errant vehicle with minimum damage to the roadway and interruption to traffic. The safety barriers being used on highways today are commonly made of steel, concrete and steel, or molded plastic barrels filled with an energy-absorbing material such as sand or water. Aside from their shortcomings, the use of these barriers has not been entirely successful in accidents involving tall vehicles carrying heavy loads. Recently, new designs that use sandwich panels made with a facing material (such as aluminum, fiber-reinforced plastic, or wood) and a core made of either honeycombed materials (such as aluminum, Nomex, Aramid, etc.) or foam materials (such as polyurethane, polyvinylchloride, etc.) have been introduced. The steel and foam energy reduction barriers, also called soft walls, are somewhat similar to these panels but are made of a steel skin or tubing and a backing of polystyrene blocks. Since these barriers have been used successfully in motor speedways, they may have applications in highways, even for bridge parapets. Their effectiveness in various highway applications must be established and their costs must be compared with those for other barriers.

3.10 Biosensor for Lead [29]

The biosensor is being developed by a team at the University of Illinois at Urbana-Champaign to meet the need for a comparatively sensitive and yet simple and

inexpensive method for detecting lead. The prefix "bio" denotes the biological nature of the sensor, which is a combination of nanoparticles (13 billionths of a meter in diameter) of gold and a solution of a lead-specific synthetic deoxyribonucleic acid (DNA). The synthetic DNA causes the nanoparticles of gold to aggregate in clusters that give off a blue color. When this comes in contact with lead, the DNA breaks apart, which in turn causes the aggregation of gold nanoparticles to fail and generate a color shift to red. In addition, the intensity of the red color is directly proportional to the amount of lead present, thereby providing the basis for a quantitative measure of lead. A prototype test method based on a solution of this biosensor was able to detect lead in paint as low as 20 parts per billion, far below the safety limits used by the U.S. Environmental Protection Agency. Although already relative simpler than the methods used currently (such as anodic stripping voltammetry, electrothermal vaporization atomic adsorption, and X-ray fluorescence spectrometry), the research team hopes to develop this into a method using paper strips with the biosensor deposited on their surface so that the strips can be used to detect lead in a manner similar to the use of litmus or pH papers. As it is, the prototype test method is already useful for testing old paints or coatings on structural steel for the presence of lead. Therefore, it is one new material that can be assessed by field trials for its cost-effectiveness.

3.11 Smart Fibers [29]

These fibers are simply optical-quality glass fibers with a modified surface—some at only one end, and some at selected locations and intervals along each fiber—to change their light transmission or reflection properties in response to a change in their surroundings, such as the force to which they are subjected, moisture content, pH, etc. As such, each fiber is useful for monitoring changes in any one of these parameters (to which it is designed to respond) in the surrounding in which it is embedded, as long as the expected range of changes is within the dynamic range of the fiber's response. These fibers have been modified to respond to the strain in its surrounding medium. As indicated by the fact that the contacts for this material are commercial companies, the technology is in various stages of maturity: it is ready for some applications but requires modifications for others. With some additional developments, mostly to facilitate the

embedment and survivability of the fibers, these fibers would be applicable in health monitoring of critical components of modern bridges, such as the post-tensioned tendons, to alleviate the lack of a proven nondestructive inspection technique that is effective, convenient, and inexpensive. Similar sensors for moisture would be very useful, since this substance is a precursor to corrosion. A unique advantage of optical fibers is that numerous sensing spots can be engineered onto each single fiber at pre-determined locations or intervals so that, once embedded, the fiber can sense changes in either strain, moisture, or any of the other applicable parameters at different areas in its surrounding medium.

3.12 Helmholtz Resonators [30]

Since about 1990, European researchers have been evaluating techniques to reduce noise caused by tire-pavement interaction using carefully engineered voids cast into the pavement, termed Helmholtz resonators. These voids serve to dampen sound induced by excessive air pressure created as a tire rolls over the pavement. The scanning team observed these resonators firsthand on the Roads to the Future project. In this case, they were precast into a concrete layer used on some test sections.

3.13 Colloidal Chemistry of Alkali-Silicate Reaction (ASR) Gels [31]

ASR occurs between alkalis from cement and a reactive form of silica from the wrong aggregates, which can result in an alkali/silica gel. If there is enough moisture, the gel will expand, damaging the concrete. The FHWA's work involves fundamental research into the chemical and physical processes that cause ASR gel damage. The research includes the application of neutron scattering and positron annihilation spectroscopy to measure nanoscale and sub-nanoscale changes in gel microstructure as a function of gel chemistry, temperature, and relative humidity. An efficient way to combat control ASR is also being evaluated [31].

3.14 Cement Hydration Kinetics [32]

It is essential to have an accurate model of the rate of reaction of cement with water as a function of temperature, water/cement ratio, and grain size, but this fundamental

information has been very difficult to obtain using conventional analytical methods because the reactions take place in the nanoscale pores of the cement gel. In collaboration with the National Institute for Science & Technology's Center for Cold Neutron Research, Turner-Fairbank researchers have been applying an array of neutron scattering methods to determine the effects of the various factors on the rate of development of cement's fractal nanoscale structure.

3.15 Fly Ash Reactivity Characterization [32]

This FHWA-funded research is a fundamental look into the interactions between fly ash and the Portland cement gel nanostructure that affect the strength and durability of concrete, including ASR reactivity. It includes the use of small-angle neutron scattering to quantify the changes on a nanoscale as a function of time and fly ash composition. A unique vibrational spectroscopy is also being employed to nondestructively measure the reactivity of fly ashes.

3.16 Aggregate ASR Potential Tests [33]

ASR in concrete can be precluded by using nonreactive aggregates. This FHWA research involves fundamental research into the formation of ASR gels by reaction with different types of aggregates, using solid state nuclear magnetic resonance to measure the formation of silicate chains on the nanoscale.

3.17 Delayed Ettringite Formation Damage [34]

Delayed ettringite is an internal sulfate attack on concrete. The FHWA research is exploring how delayed ettringite forms and causes damage in concrete when transforming from an amorphous ettringite gel to nanoscale crystals. The research involves the application of synchrotron radiation to study the relationship between ettringite crystal formation and concrete expansion.

CHAPTER 4 NANO AND MEMS SENSORS

The majority of the potential MEMS applications in transportation infrastructure condition monitoring will act as sensors. The advantage of these nano and MEMS sensors is their dimensions. With a scale of a micrometer, the sensors can be embedded into the structure during the construction process. These sensors can be used in monitoring temperature, measuring cracks, corrosion testing, monitoring ASR, and other related reactions in concrete, and for the reliability of welding units in structural steel. Since the MEMS sensors are fabricated with the microfabrication techniques commonly used in integrated circuit processing, they can be integrated with electronics to develop a high-performance system. Generalized MEMS could consist of a sensor and electronics, all integrated in the same environment. The sensor would provide information about the environment, the electronics would process the information from the sensors, and the electronic circuitry samples the signal and processes the signal. Many applications in transportation condition monitoring are buried in the structure with no physical connection to the outside world. Therefore, they need to integrate the sensors and the communication system into one chip. This kind of application is often made up of two parts: the nano and MEMS sensors and communication system. Table 2 summarizes the MEMS sensors potential for transportation applications, and they are explained in the following sections. These sensors can be categorized into three groups: nanosensor, microsensor, and bulky sensor. Nanosensor refers to a scale of from 10^{-9} m to 10^{-5} m; microsensor refers to a scale of 10^{-4} m to 10^{-2} m; sensors larger then 10^{-1} m are called bulky sensors.

4.1 Nanosensors in Transportation

Nanosensor refers to a scale of from 10^{-9} m to 10^{-5} m and usually these sensors use MEMS technology.

4.1.1 MEMS Strain Sensor [35]-[41]

The MEMS strain gauge can be used to optimize the use of accelerated load testing facilities and to improve the application of results from these facilities. Its design method originates from the mechanical strain sensors, and it can be applied to monitoring systems of asphalt pavement and concrete pavement. Even nowadays, the mechanical strain sensor is still being widely used. The Laboratory of Traffic Facilities of the Federal Institute of Technology EPFL in Switzerland has recently launched a program investigating the strain gauge in highway pavement and bridge aging monitoring systems in a laboratory situation [35]. Figure 8 and Figure 9 show their four-point-bending-test setup. To transfer the load from the press load plate to the beam, two rollers are situated in the third-points on the top, ideally as two line loads. This brings a constant bending moment in the area where the strain gauge is embedded. Four displacement gauges are placed. Two of them are placed on the upper side above the roller supports; the others are at the bottom center line of the beam, one in the middle and one at a distance of 10 mm from the edge of the beam.
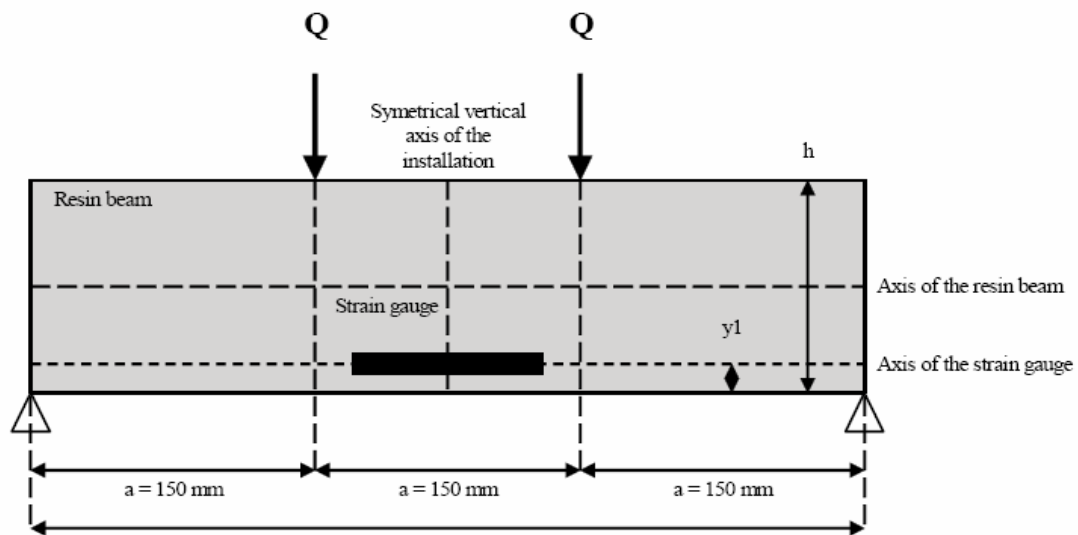
Figure 8 Scheme of the four-point-bending test (after M. Heinrich and M. Janauschek [35])

Figure 9 Test zone of the four-point-bending setup (after M. Heinrich and M. Janauschek [35])

Their analytical results of the strain gauge fit the laboratory test data well, and they show the availability of the product of strain gauge in application. Since the pavement strain gauge has come into reality, many state and local institutions have invested a lot of money into the strain gauge application in pavement. For instance, scientists at National Center for Asphalt Technology (NCAT) have developed a real-time data analysis system using strain gauges [36] and Figure 10 and Figure 11 show asphalt strain gauge real-time data processing results.
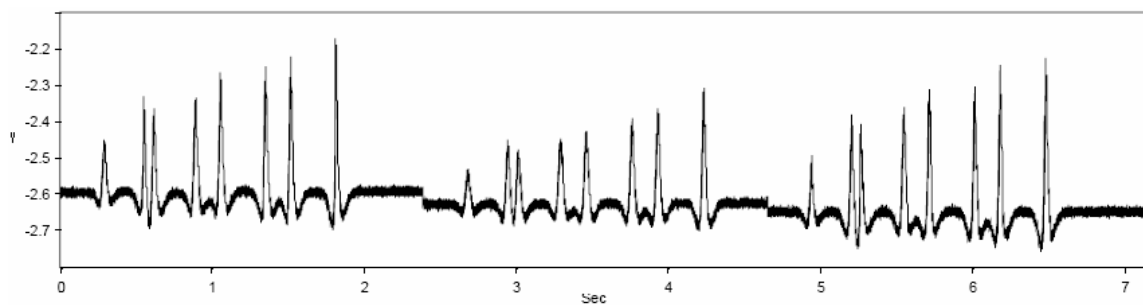
Figure 10 Longitude asphalt strain gauge before signal processing (after D. H. Timm and A. L. Priest [36])
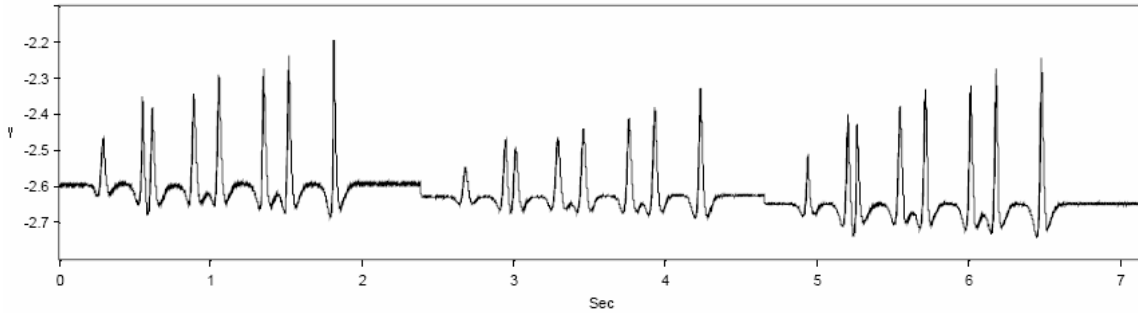
Figure 11 Longitude asphalt strain gauge after signal processing (after D. H. Timm and A. L. Priest [36])

Their research efforts provide a more accurate and real-time data description of pavement status. Furthermore, researchers at VDOT and the University of Virginia have successfully applied strain gauges to the evaluation of continuously reinforced hydraulic cement concrete pavement in Virginia [37]. Their research focused on sections of Virginia's Smart Road. Virginia's Smart Road is 7.7 miles long. This road consists of two concrete lanes. One lane is 12 ft wide, and the other is 14 ft wide. The additional 2 ft of concrete was part of the shoulder; the remainder of the shoulder is asphalt concrete. Below the concrete pavement is a 3-inch thick open graded drainage layer (OGDL). The OGDL was stabilized with 4 percent cement for 1,263 ft and with 2.5 percent asphalt for 984 ft. Under the OGDL is a 6-inch layer of cement-stabilized aggregate containing 4 percent cement by weight, which was placed on 3-inch aggregate base. Longitudinal and transverse reinforcing steel was placed on steel chairs and tied. The percentage of steel was 0.7 percent. Both the temperature and strain information are collected in this project. Figure 12 and Figure 13 show the strain gauge data.
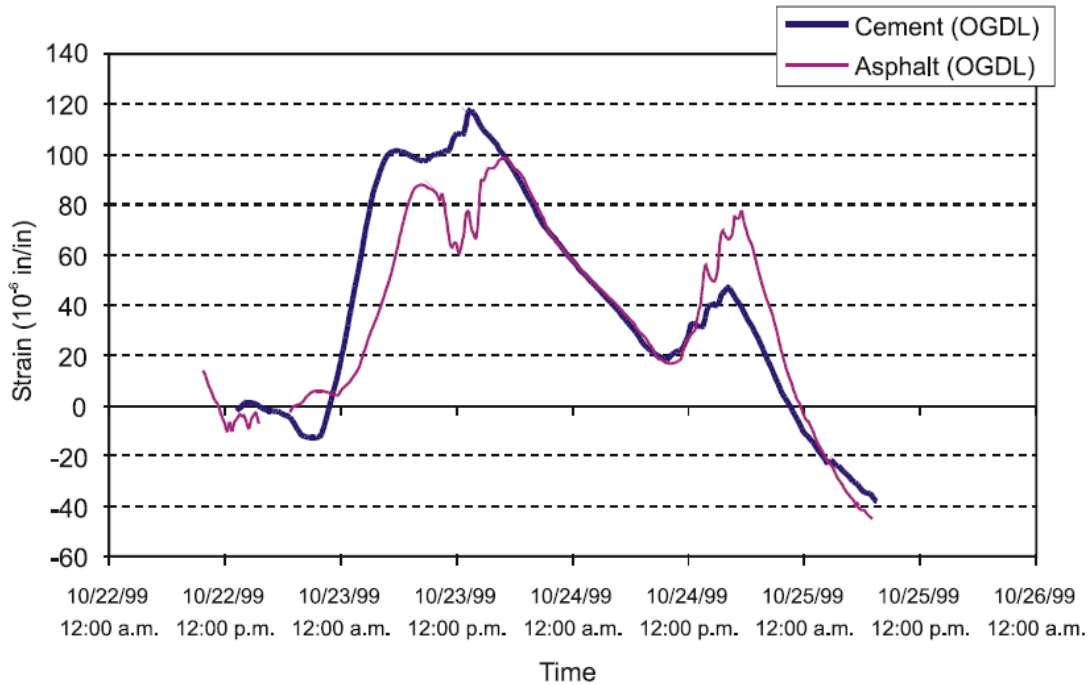
Figure 12 Strain data for top section of slab for 12-ft lane (after C. Ozyildirim [37])
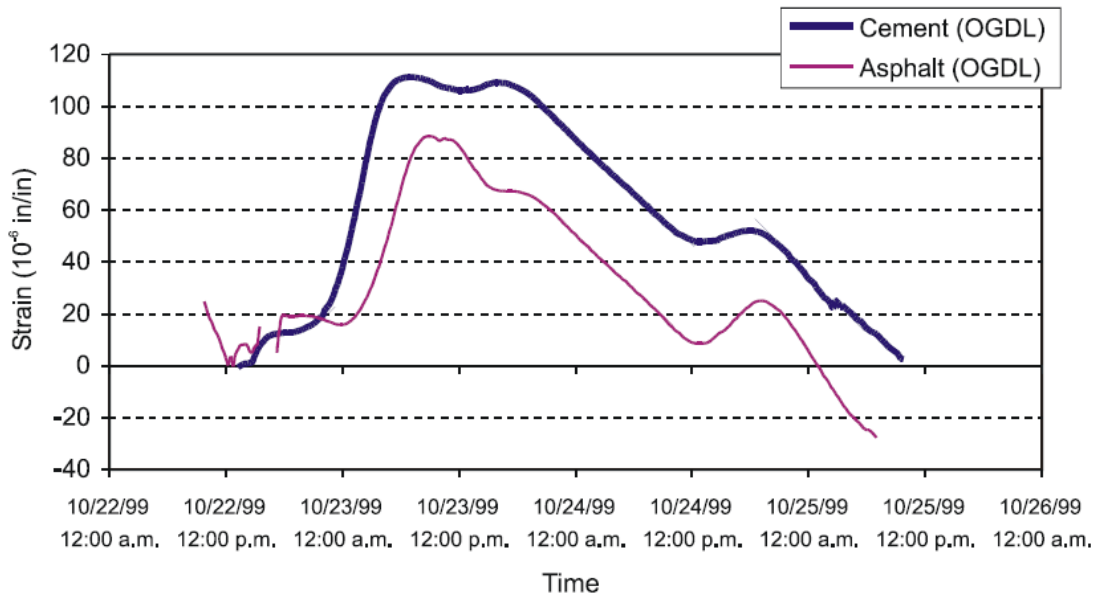
Figure 13 Strain data for bottom section of slab for 12-ft lane (afterC. Ozyildirim [37])

In this project, in order to get a though monitoring of the crack status in the pavement, it is suggested that multiple data sources are needed (including temperature, strain, etc.). Strain gauges in this project play a key role in evaluating the crack status in pavement.

Scientists at Delft University of Technology have recently conducted research on asphalt concrete [38]. Their results show that, in order to have a good asphalt concrete response evaluation, the model should include multiple data sources, for instance, the strain rate and temperature sensitivity of the material. The research group at National Airport Pavement Test Facility (NAPTF) also developed a mechanical strain gauge in order to sense the asphalt pavement status in the airport. The Asphalt Strain Gages (ASGs) are used at the NAPTF to measure asphalt concrete (AC) strains. Results from speed tests (vehicle speeds ranging from 0.08 m/sec [0.25 ft/sec] to 2.2 m/sec [7.33 ft/sec]) performed on flexible pavements on a high-strength subgrade are presented. Tests were conducted at pavement temperatures of 11.1°C (52°F) (4/20/00) and 22.2°C (72°F). The objective was to measure AC strains at low speeds and heavy wheel loads. Vehicle speed and pavement temperature both have a significant effect on the strains induced in the asphalt layers. Increasing the vehicle speed from 0.08 m/sec (0.25 ft/sec) to 2.2 m/sec (7.33 ft/sec) reduced the longitudinal strains by 50-55 percent and reduced the transverse strains by 45-50 percent (for a given load level). The rate of change in strain with speed was higher at slow speeds (speeds less than 0.61 m/s [2 ft/sec]). Slower speeds result in higher load durations, which reduce the AC dynamic modulus (increasing the amount of viscous deformation relative to the elastic deformation). This results in very high strains at the bottom of the AC layers. An increase in the temperature of the pavement from 11.1°C (52°F) to 22.2°C (72°F) resulted in an increase in AC strains ranging from 100 to 120 percent (for the three load levels at all speeds). The effect of increasing temperature is also due to increasing the proportion of viscous deformation relative to the elastic deformation. Figure 14 and Figure 15 are testing example results at the NAPTF.
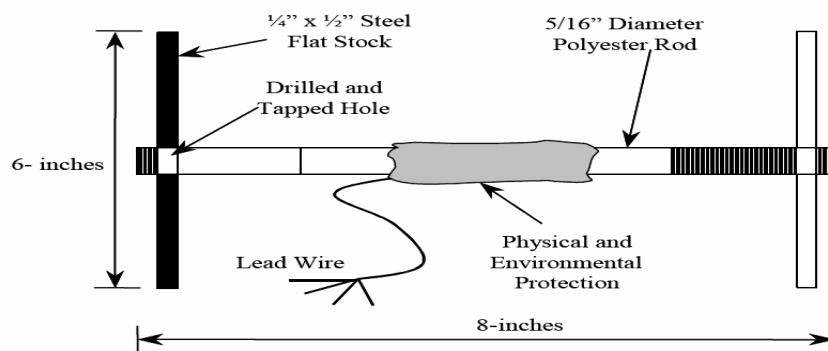
Figure 14 Asphalt Concrete Strain Gauge used at the NAPTF (after N. Garg and G. F. Hayhoe [39])
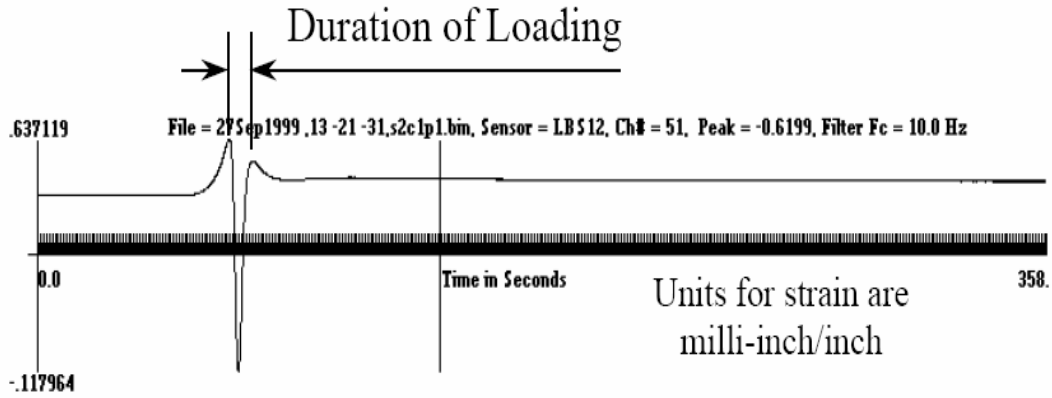
Figure 15 Longitudinal ASG response signal (after N. Garg and G. F. Hayhoe [39])

A research program sponsored by Virginia Transportation Research Council was conducted at Virginia Polytechnic and State University to reinforce the functionality of the strain sensor by adding wireless ability to them [40]. The wireless system is shown in Figure 16.
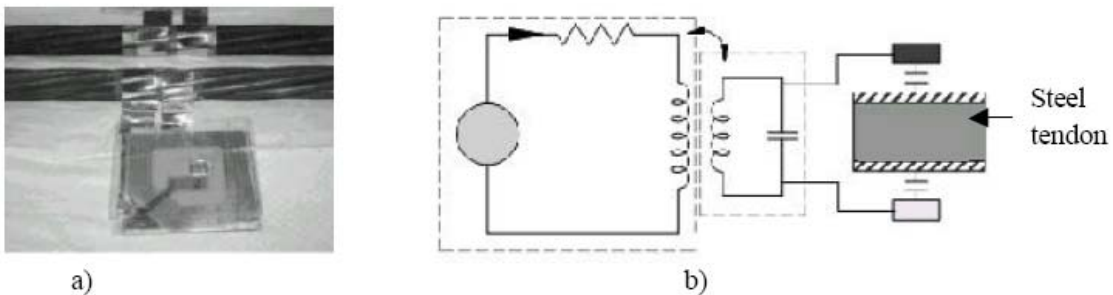
Figure 16 Wireless sensor system a) a wireless sensor for corrosion monitoring attached to a steel tendon; b) the schematic diagram (after J. C. Duke [40])

Using such wireless technology, multiple measurement sites can report to one central processing site, avoiding the need to string wires access long distances, which might require considerable effort as well as traffic control. Furthermore, scientists at University of California-Berkeley have taken great efforts in manufacturing a MEMS strain gauge. For example, they have developed a micro strain gauge with a mechanical amplifier [41]. A detailed design process is published. Figure 17 and Figure 18 show the layout and principle of the mechanical amplifier in this sensor.
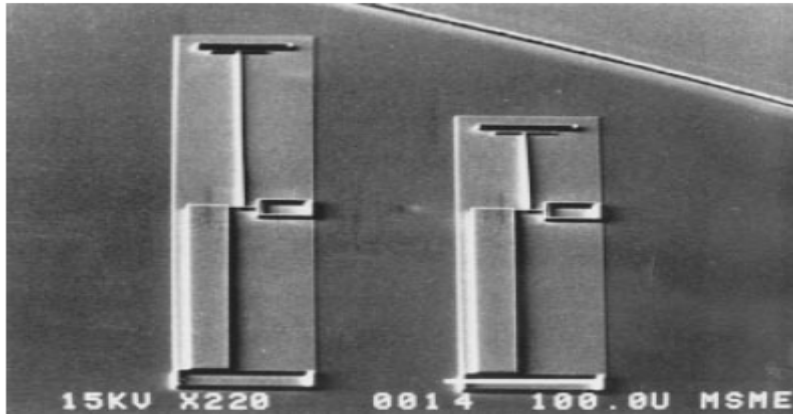
Figure 17 SEM microphoto of two strain gauges (after L. Lin et al. [41])
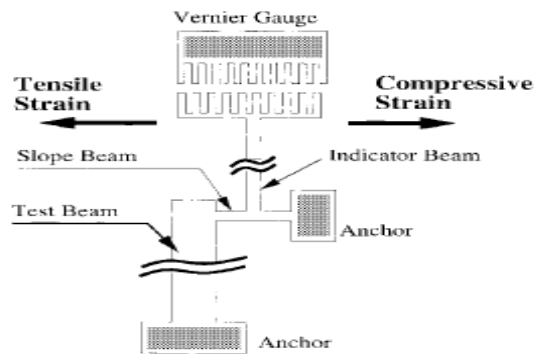
Figure 18 Schematic of a MEMS strain gauge based on the mechanical amplifier (L. Lin et al. [41])

4.1.2 MEMS Moisture Sensor [42]-[53]

Networks of nanosensors embedded in roadways could provide real-time information to better manage congestion and incidents, or to detect and warn drivers about fast-changing environmental conditions, such as fog and ice.

In several countries outside the United States, standards for floor moisture were developed based on measuring relative humidity (RH) within the concrete floor slab. Problems resulting from concrete floor moisture can cause serious consequences, for instance, delamination, peeling, blistering, staining, etc. Understanding how concrete floors and floor coverings can be protected from moisture exposure can help prevent troubles from arising. Protection begins with choosing the appropriate concrete mix. Proper placement and curing procedures will help ensure the slab has the strength and

durability performance potential. For interior floors, a vapor retardant should be used below the slab. For floors to receive moisture-sensitive floor coverings, attention should be paid to the floor's moisture level during and after curing. Proper curing of concrete is crucial for obtaining design strength and maximum durability, especially for concrete exposed to extreme environmental conditions at an early age.

To "cure" concrete is to provide concrete with both adequate moisture and temperature to foster cement hydration for a sufficient period of time [42]. Research has shown that a high curing temperature (up to 212^oF or 100^oC) generally accelerates cement hydration and concrete strength gain at an early age. The relative humidity in concrete also significantly influences the rate of cement hydration. Normally, the moisture in the freshly placed concrete is in excess of that required for complete cement hydration. If this moisture can be kept within the concrete, it will promote cement hydration. However, if the moisture evaporates and the relative humidity of the concrete falls below 80 percent, cement hydration may cease [43]. Furthermore, loss of moisture also causes concrete to shrink. Finally, curing time is another key for proper cement hydration and concrete strength development. So, in order to monitor the cement curing process during or after concrete construction, a MEMS moisture sensor with small volume and wireless ability is strongly recommended for its easy implementation during concrete construction process, friendly data access interface, and low-cost maintenance.

Researchers at Iowa State University working with the Iowa Department of Transportation (IDOT) measured the moisture content in the lab stage [42]. They measured moisture content from a set of three mortar prisms at age 1 and 3 days. In the tests, a 2-inch by 2-inch by 4-inch mortar prism was fractured along the designed notches into three pieces: top, middle, and bottom. Each piece was weighed to the nearest 0.01 g (Wi) and then put in an oven at a constant temperature of 105ºC to remove free water. After heating for 48 hours, the pieces of samples were weighed again (W). The moisture content (MC) is given by

$$MC = (Wi - W) / W$$

Its procedure is shown in Figure 19.
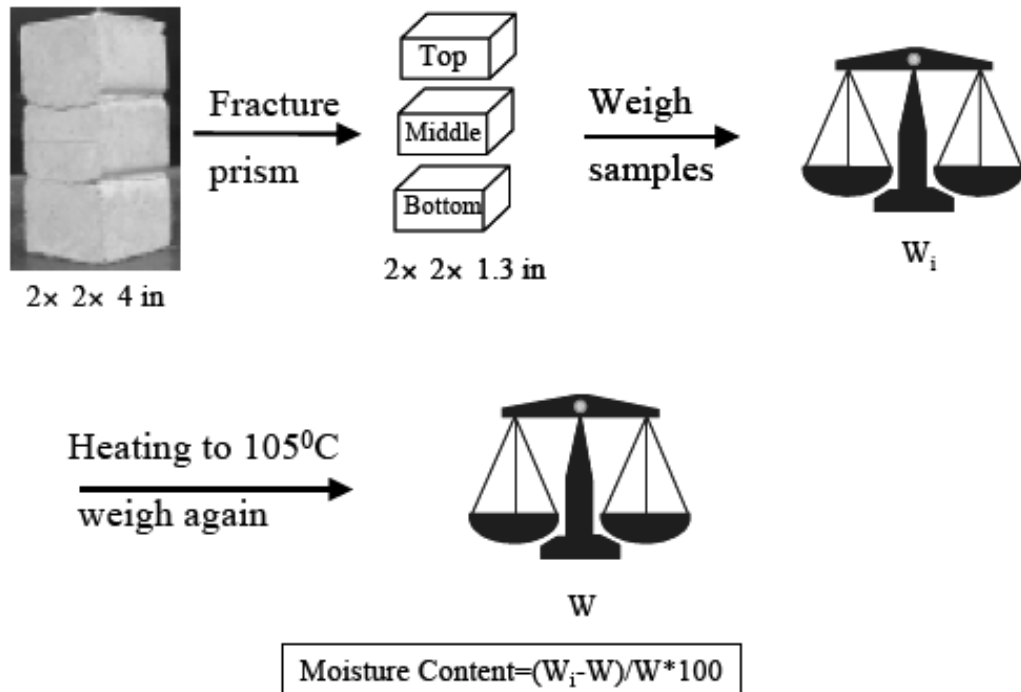
Figure 19 Moisture test at Iowa State University for IDOT (after K. Wang et al. [42])

By comparing their application and the application at the University of Houston, it is obvious that the wireless MEMS sensor is a better choice for its small volume, wireless ability, easily implementation during the concrete construction process, friendly data access interface, and low-cost maintenance.

More specifically, researchers in Germany summarized the microwave techniques for detecting the moisture level in concrete and pavement as shown in Table 3 [44].

Table 3 Summary of Microwave Moisture Sensor (after K. Kupfer [44])

Subject *Comments*	Method Frequency range	Experiments - Results
Microstrip sensors used in microwave aquametry	1 – 10 GHz	Microstrip radiating sensors & antennas; near field experiments & monitoring of particleboards; New: active integrated antennas, photonic band gap patch antennas
Moisture distribution using TDR	TDR-Imaging	New technique for 2D MC- distribution in a composite material using CG-based inversion
Microstrip resonator technique for moisture / permittivity measurement	Spectral Domain Analysis 8.4 – 10.2 GHz	Determination of complex permittivity using spectral domain analysis of multi-layer microstrip embedded in a dielectric cover
One sided moisture sensors		Open ended types: induct.coupled $\lambda/4$ resonator; T-junction $\lambda/4$ coax line, $\lambda/2$ microstrip resonator
Integrated network analyser module for microwave moisture sensors	Ultra wideband principle 5 GHz	Can replace NWA or TDR in microwave sensors; using of MLBS-signals simplification of measurment system & application of digital circuit concept (ASIC)
Construction & assessment of a coax-capacitor for dielectric grain measurements	< 5 MHz	Analysis of capacitive meas. Methods; coax capacitor for determination of dielectric properties of grains
Sample area of TDR-Probes in proximity to sharp dielectric permittivity boundaries	TDR	Permittivity is a function of probe geometry & interface location; the spatial TDR-probe sensitivity is a function of distribution of dielectric permittivities in transverse planes
Conversion models of open coax-probes	FDTD	Analysis of the conversion stability due to imperfect contact of open ended coaxprobe models; (antenna model, capacitive model, Misra model, virtually conical cable m.)
Microstrip sensor for measuring sand water content & ion conductivity	100 - 600 MHz 3 GHz	Detection of MC & ion conductivity ~ insertion loss in MW & RF range; MW- & RF microstrip sensors
Modular MOIST-System Portable setup contains 5 sensing heads, 2 portable & 1 online control units	2.45 GHz	Selection of sensing heads with different measuring principles for different penetration depths; applications for many moisture problems
Portable NMR-system in one-sided access technique	NMR	Content & mobility of H in the material; linear distribution of MC & moisture mobility; depth profiling of MC

Acronyms in this table are defined below. **CG:** Conjugate Gradient; **FDTD:** Finite-difference time-domain Method; **MC:** moisture content; **MLBS:** multilayer boards; **NWA:** network analyzer; **NMR:** Nuclear magnetic resonance; **TDR:** Time-domain Deflectometer.

There are also other feasible moisture sensors still in the lab stage. Scientists in the UK developed a fiber-optic based humidity sensor which can be used for the measurement of moisture absorption in concrete [45] (see Figure 20). The sensor was fabricated using a fibre Bragg grating (FBG) coated with a moisture-sensitive polymer. To test the sensor and to investigate the use of this sensing technique for the detection of moisture ingress in concrete, the sensor was embedded in various concrete samples of different water-to-cement ratios which were then immersed in a water bath. A direct indication of the humidity level within a sample is given by the shift of the Bragg wavelength caused by the expansion of the humidity-sensitive material coated on the fiber. The sensor itself exploits the inherent characteristics of the FBG, with its operation being based on the strain effect induced in the Bragg grating through the swelling of the polymer coating. This sensor is created by coating an optical fiber containing an FBG with a moisture-sensitive polymer that absorbs the moisture present, causing it to swell. This swelling effectively stretches the fiber, thereby causing a strain in the FBG contained within it. This consequently changes the wavelength of the reflected signal of the FBG, which can be monitored using an optical spectrum analyzer or any other similar wavelength-based interrogation technique. Different chemical coatings will have different responses to humidity change [46]. Polyimide was used as the coating material, as a linear response is preferred.
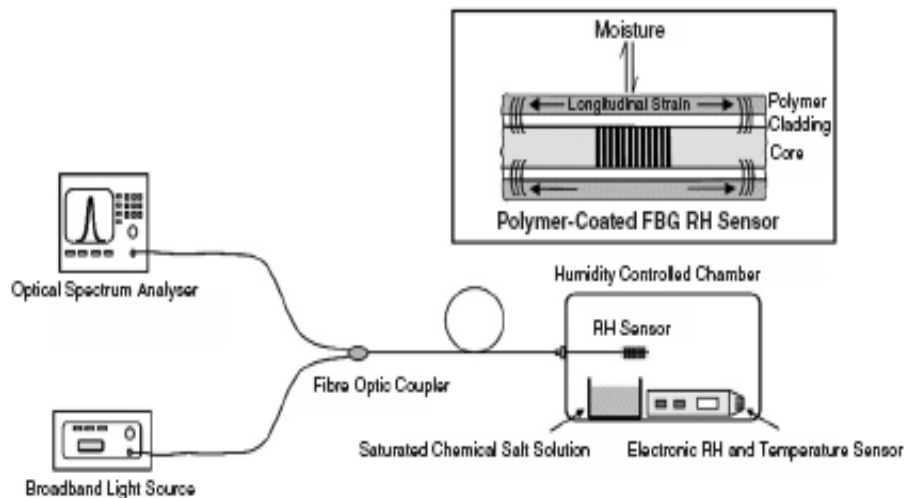
Figure 20 Schematic for FBG sensor calibration and test (after T. L. Yeo et al., UK [45])

In recent years, more and more attention has been paid to MEMS-based moisture sensors. Chia-Yen Lee and Gwo-Bin Lee of China developed the idea of MEMS moisture sensor that is shown in Figure 21 [47].
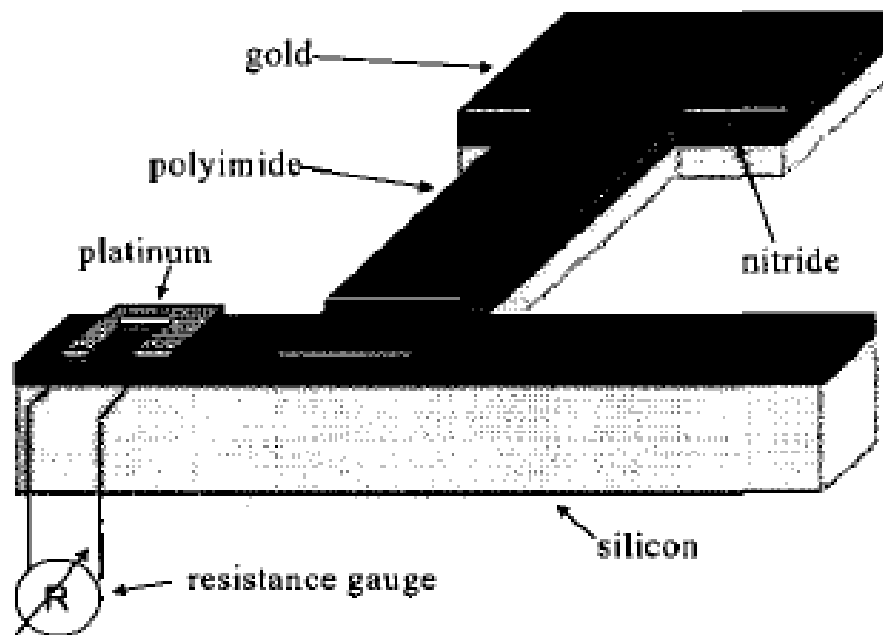
Figure 21 Schematic of suspended structure of the humidity sensor (after C. Y. Lee and G. B. Lee in China [47])

In this design, the movable electrode of a capacitance-type humidity sensor is made of microfabricated cantilevers coated with a material that absorbs water when exposed to humid conditions. The absorption of water molecules causes the upper layer of the cantilever to expand, and this induces a surface tensile stress. As a result, a change in the capacitance between the suspended structure and the glass substrate is caused by the bending of the cantilever. An Au layer is deposited directly on both the moveable cantilever part of the sensor and on the stationary glass substrate. Some researchers in India simulated this design in Coventor [48] (see Figure 22).
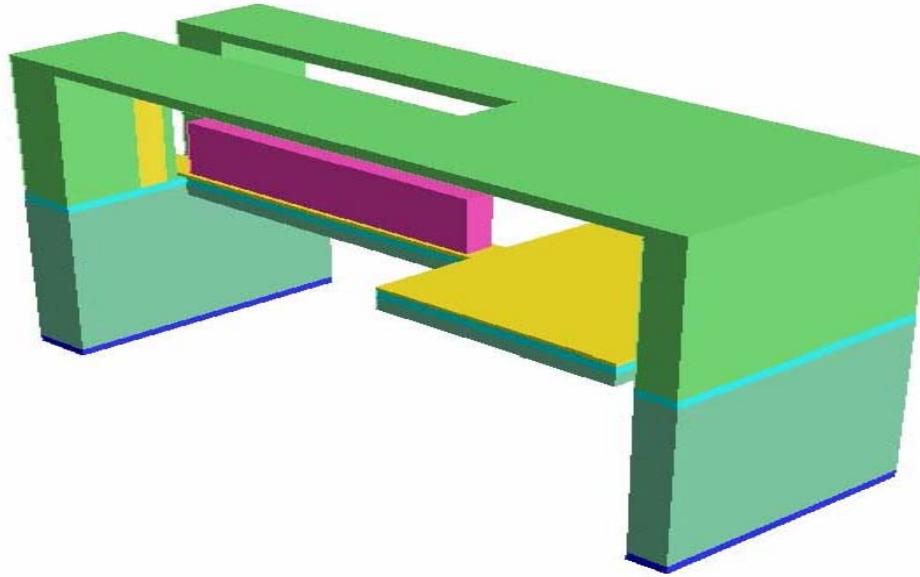
Figure 22 View of the MEMS moisture sensor (after K. Govardhan and Z. C. Alex, India [48])

Figure 23 shows the electro-mechanical displacement analysis in Coventor of the design shown in Figure 22. Figure 24 shows the relationship between the environmental humidity and sensor capacitance.
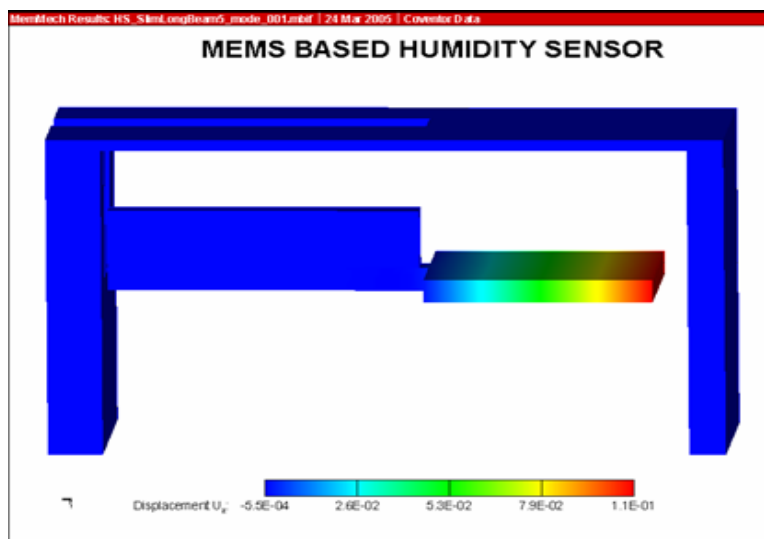
Figure 23 Electro-mechanical displacement analysis in Coventor (after K. Govardhan and Z. C. Alex, India [48])
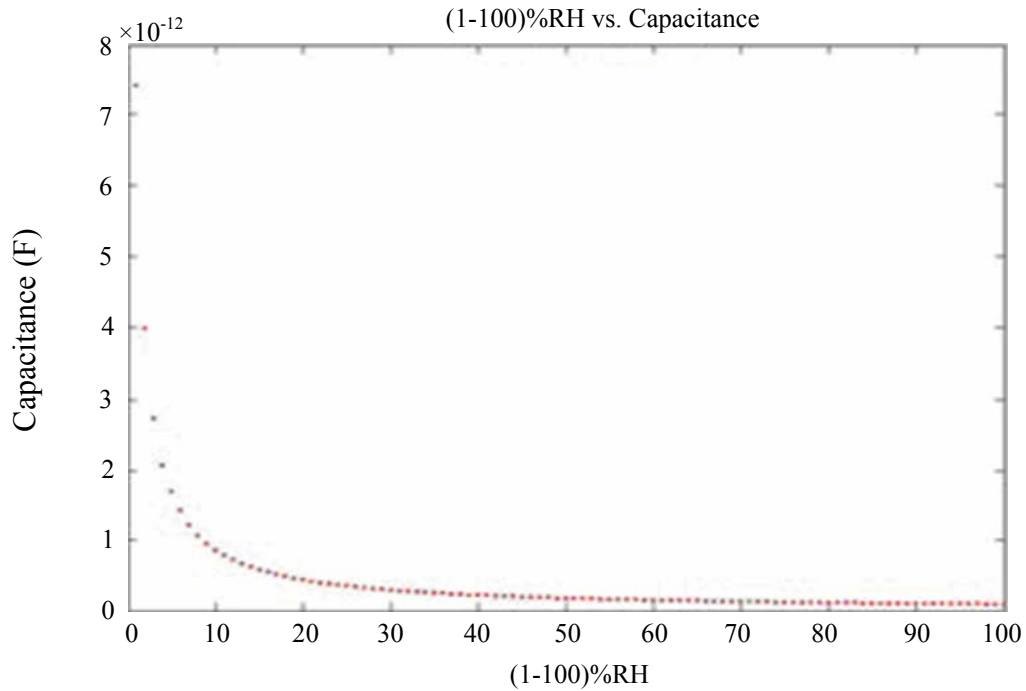
Figure 24 Humidity vs. capacitance (after K. Govardhan and Z. C. Alex, India [48])

The group led by Dr. Harpster at the University of Michigan developed a MEMS-based passive moisture sensor system [49] [50] [51] as shown in Figure 25.
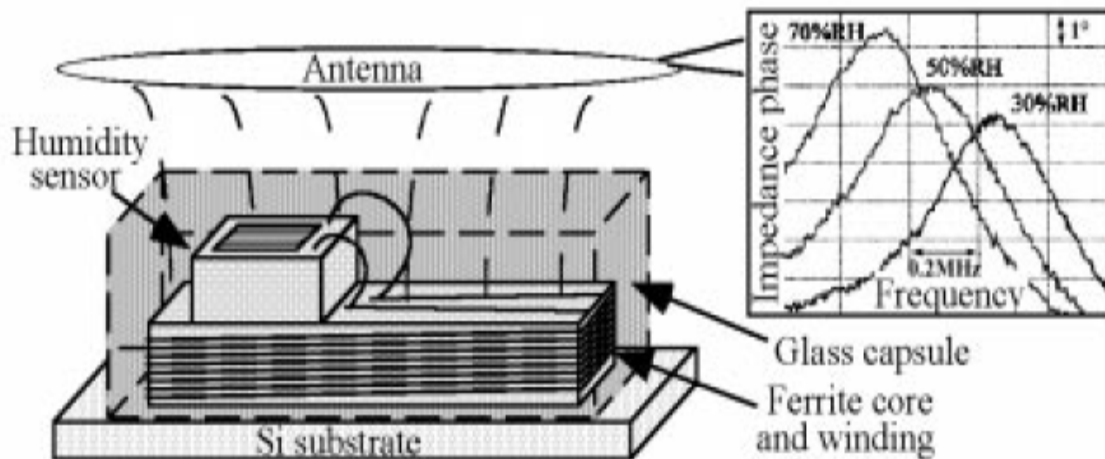
Figure 25 Schematic of passive MEMS humidity (moisture) sensor (after T. J. Harpster et al., University of Michigan [49] [50] [51])

The MEMS passive wireless humidity monitoring system (shown in Figure 26) is for continuous remote monitoring of humidity changes inside miniature hermetic packages. It consists of a high-sensitivity capacitive humidity sensor that forms an LC tank circuit together with a hybrid coil wound around a ferrite substrate. The resonant frequency of the circuit changes when the humidity sensor capacitance changes in response to changes in humidity. This humidity monitoring system can resolve humidity changes of 2.5 percent RH over a 2 cm range.

Figure 26 Demo of passive MEMS humidity (moisture) sensor (after T. J. Harpster et al., University of Michigan [49] [50] [51])

The A. D. DeHennis and Khalil Najafi [52] group built a remote MEMS passive sensing system for relative humidity, temperature, and pressure, as shown in Figure 27 to Figure 29.
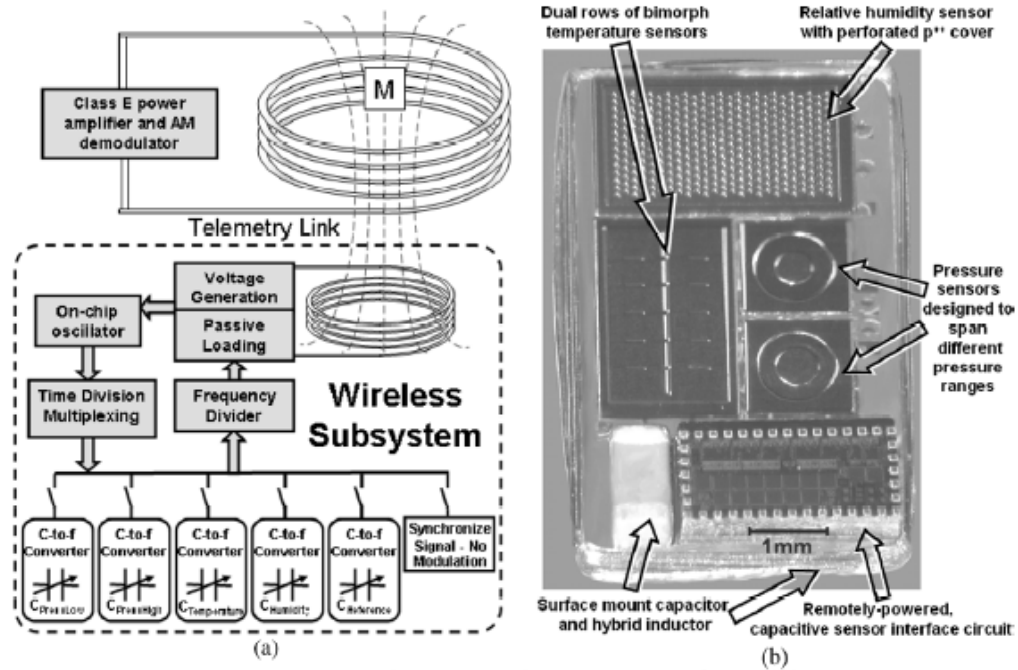
Figure 27 Schematic of remote sensing system for relative humidity, pressure, and temperature (after A. D. DeHennis and Khalil Najafi, Fellow, IEEE [52])

Figure 28 Demo of remote sensing system for relative humidity, pressure, and temperature (after A. D. DeHennis and Khalil Najafi, Fellow, IEEE [52])
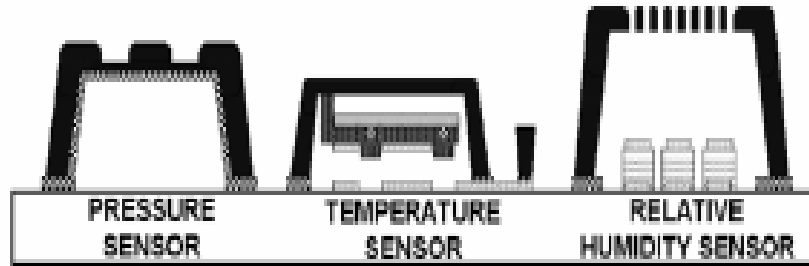
Figure 29 MEMS sensing device of the remote sensing system (after A. D. DeHennis and Khalil Najafi, Fellow, IEEE [52])

The working principle of the humidity (moisture) sensor [53] in this system is based on the idea of the humidity-to-capacitance transducer, and it has a faster humidity response than the normal humidity sensor method. This high-speed capacitive humidity sensor integrated on a polysilicon heater. High speed is achieved using multiple polyimide columns having diameters of a few microns and allowing moisture to diffuse into them circumferentially (Figure 30). Using structures that eliminate the air-gap capacitance between the columns, the simulated sensor output drifts by only 1 percent when the relative dielectric constant in the air region changes from 1 to 10.
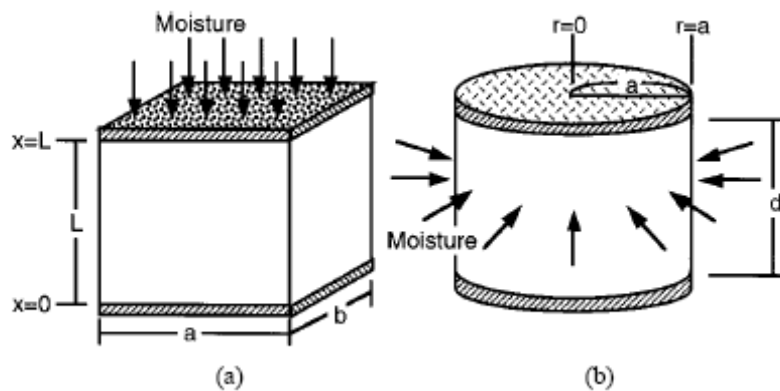
Figure 30 High-speed humidity sensor, a) Conventional structure; b) high-speed structure (after Uksong Kang and Kensall D. Wise, Fellow, IEEE [53])

Figure 31 shows some of the results from the remote sensing system shown in Figure 30.
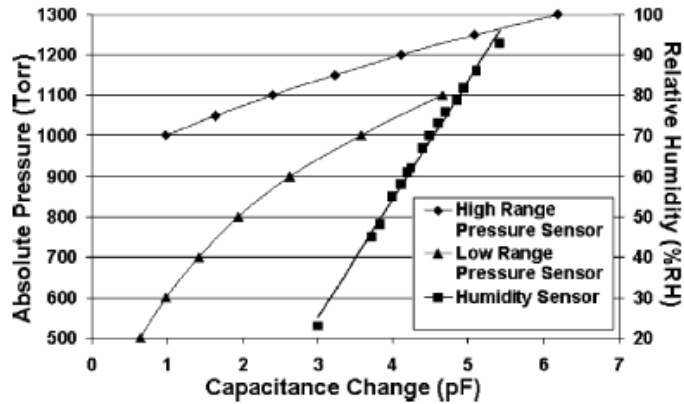
Figure 31 Plot showing the capacitance vs. pressure and humidity characteristics in their respective domains (after A. D. DeHennis and Khalil Najafi, Fellow, IEEE [52])

4.1.3 MEMS Accelerometer [54]-[75]

For the accelerometer sensor network application, the Ohio Department of Transportation and the Federal Highway Administration have conducted a comprehensive market survey and laboratory evaluation to identify the most promising sensors and data-acquisition systems for infrastructure application, especially for highway bridge monitoring [54]. This system was implemented on a typical steel-stringer bridge in Cincinnati for high-speed traffic and long-term environmental monitoring. This multi-disciplinary research program gives accurate results on the actual loading environment and the corresponding bridge responses and helps to provide an objective measure of the state-of-health and alerts officials to bridge deterioration or failure. The system is shown in Figure 32.
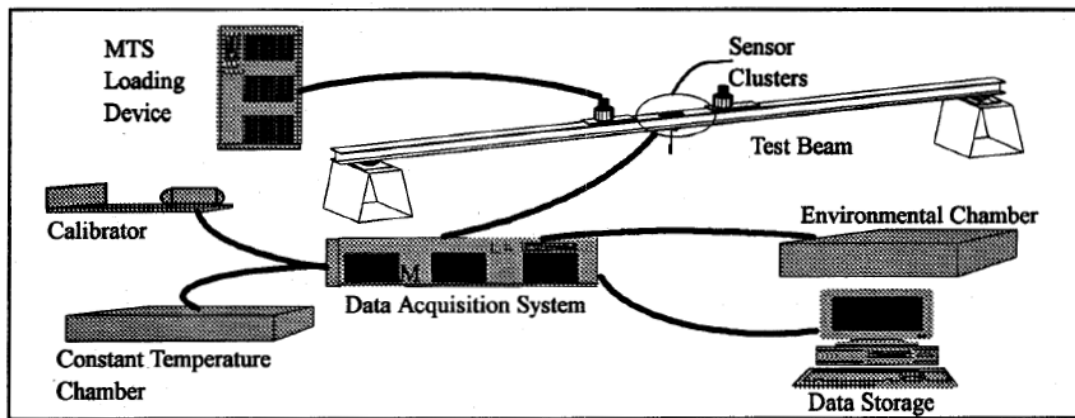
Figure 32 Bridge monitoring system by Ohio Department of Transportation and FHWA (after A. J. Helmicki et al. [54])

Researchers in Morocco [55] added wireless ability to the above monitoring system.
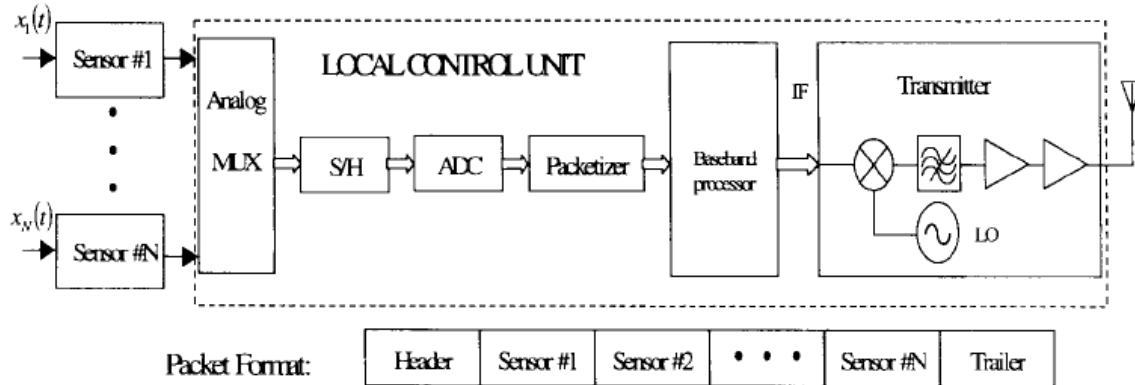
Figure 33 An exemplary local control unit block and telemetry packet format (after Ali Iraq et al. [55])

The sensors shown in Figure 33 are not only a constraint to the MEMS accelerometer but can also be a magnetic flux sensor which can be applied to bridge inspection [56]. This continual monitoring system, which can be applied to civil engineering constructions as water dams, bridges, highways, or landing surfaces in airports, is of vital technical and economic importance. For example, today there are 187,000 deficient bridges in the National Bridge Inventory [57], and this number steadily increases with age. And about 1 percent (5000 bridges) become deficient each year. Techniques of nondestructive evaluation should be used effectively and efficiently to collect quantitative data about the condition of bridges and other elements of civil infrastructure, and many measurement techniques may be used for this purpose. This telemetric system for monitoring civil engineering constructions consists of a set of sensors deployed on the construction to be monitored, linked—via telecommunication means—with a computer-based central control unit. The measurement information on sensors (for example, accelerometer) is acquired and then sent to the central control unit where it is integrated and transformed into a useful form, e.g., into an approximate mapping of the acceleration distribution. An intermediate level of data processing may be recommendable in a larger telemetric system if the distance between sensors and control unit requires the use of powerful

telecommunications means. The sensors may be then grouped into clusters, each connected with and served by a local control unit equipped with some computation power and an emitter for wireless communication with the central control unit. The number of sensors to be used and the scheme of their deployment depend on the construction to be monitored and the nature of the information needed. For example, for continuously monitoring the state of an old lift bridge, accelerometer sensors could be mounted transverse to the plates' long axis. A typical mounting of accelerometers contains one transverse and one longitudinal sensor to monitor both components of acceleration. Before networking the sensors, each one must be calibrated separately. The parameters of calibration of all sensors can be stored in the central control unit, which receives the data, identifies the sensor, and effectuates the data processing to reconstruct the measured value of acceleration.

A practical example of accelerometer highway applications is the case of Geumdang Bridge [58], which is a special 7.7 km segment of the north-south Jungbu Inland Highway near Icheon, South Korea. This case study has focused upon the deployment of a large-scale wireless structural monitoring system within the long-span Geumdang Bridge. In total, 14 wireless sensing units were installed throughout the span's concrete box girder. A tethered structural monitoring system has been installed in parallel with the wireless monitoring system so that the measurement quality and time synchronization error of the wireless monitoring system could be assessed in a realistic field setting. The results obtained from the wireless sensing units were impressive. Acceleration time-history response records were accurately measured using MEMS accelerometers. Furthermore, accurate clock synchronization across the network of wireless sensing units was possible, often within one sample increment. Researchers at the University of Michigan, Stanford University, and Korea Advanced Institute of Science and Technology (KAIST) work together on this program focused upon improvement of the wireless sensing unit hardware in preparation for future installation in the Geumdang Bridge.

The novel wireless sensing unit shown in Figure 34 that integrates the latest embedded system technologies is proposed by Wang et al. [59]. The hardware design of the prototype

unit emphasizes measurement accuracy, long-range communication, and minimal total power consumption.

Figure 34 Wireless MEMS sensor in the Geumdang Bridge (after J. P. Lynch et al. [58])

The wireless sensing unit can be regarded as a node of a wireless data acquisition system to which traditional sensors (e.g., accelerometers and strain gauges) can be interfaced. To collect measurement data from a variety of different structural sensors, the wireless sensing unit contains a multichannel analog-to-digital converter (ADC). With a resolution of 16 bits, the Texas Instruments ADS8341 ADC can sample data from four simultaneous sensing channels at rates as high as 100 kHz. To provide sufficient space to store up to 64,000 data points at one time, the Cypress CY62128B 128-kB static random access memory (SRAM) chip is included in the unit design. To control the flow of data through the wireless sensing unit, the unit employs a low-power microcontroller. The 8-bit Atmel ATMega128 microcontroller is selected for integration with the unit because of its low power demand and on-chip computing resources. Software for unit operation and embedded data processing is stored in the ATMega128's 128 kB of read only memory (ROM). To freely transfer data between wireless sensing units and to transmit data to centralized repositories, a wireless radio with far-reaching communication ranges is needed. In the design of the wireless sensing unit, the 900-MHz Maxstream 9XCite wireless modem is selected for integration. This wireless modem provides an excellent balance between low power consumption and far communication ranges. For example, the line-of-sight communication range of the XCite radio is over 300 m. Meanwhile, the

XCite modem only consumes 50 mA of current when transmitting and 30 mA when receiving data.

Figure 35 is the layout of wireless sensors on the Geumdang Bridge, which was completed in 2002 and carries two lanes of southbound Jungbu Inland Highway traffic. The bridge is designed using two different structural system types. The northern 151 m span of the bridge is constructed from four precast concrete I-girders that support a 27 cm concrete deck. The southern 122 m length of the Geumdang Bridge is constructed from a precast concrete box girder. The precast concrete box girder is approximately 2.6 m deep and supports a 12.6 m wide roadway. The box girder is a continuous span that is supported along its length by three piers (the piers are denoted as Piers 4, 5, and 6 in Figure 35) and the southernmost concrete bridge abutment. At each support (pier and abutment), the span sits on elastomeric pads that serve as simple supports.
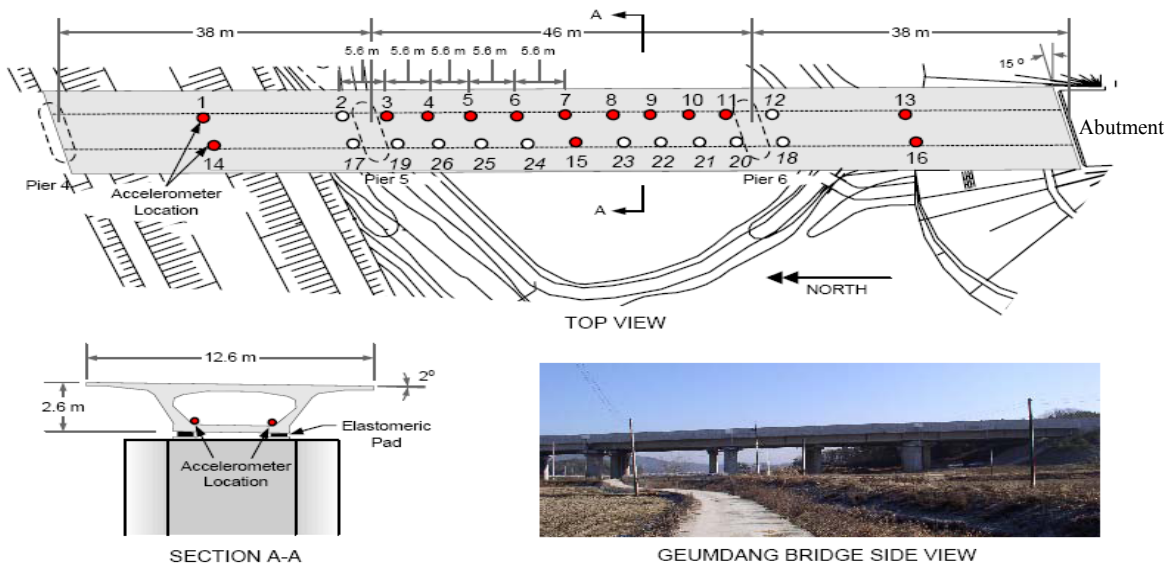
Figure 35 Engineering schematic of the Geumdang Bridge including the location of the instrumented accelerometers (after J. P. Lynch et al. [58])

To validate the performance of the wireless monitoring system, the Geumdang Bridge is intentionally loaded in a well-controlled manner using truck traffic. During testing, the bridge is closed to highway traffic, allowing the research team to have full control over

the loadings applied. To excite the bridge in the vertical direction, three large trucks of varying weight are employed: 15, 30, and 40 tons. The three trucks utilized during testing are also shown in Figure 36.

Figure 36 Three trucks (15, 30, and 40 tons) as vibration sources in the Geumdang Bridge (after J. P. Lynch et al. [58])

As shown in Figure 37, the wireless monitoring system proves to be capable of collecting data with high measurement fidelity when compared to the tethered monitoring system. For example, if the bridge acceleration response data collected by both monitoring systems are compared, there exists a strong one-to-one correspondence. To facilitate a fair comparison with the tethered monitoring system, the wireless sensing unit at sensor location 8 is configured to sample the accelerometer output at 200 Hz for this one test. The wireless sensing unit is sufficiently accurate to fully capture the bridge response during the period when the trucks transverse the bridge span. As is witnessed for the 40-ton truck, the wireless monitoring system is also able to capture the free vibration response of the span even after the trucks have exited the bridge.
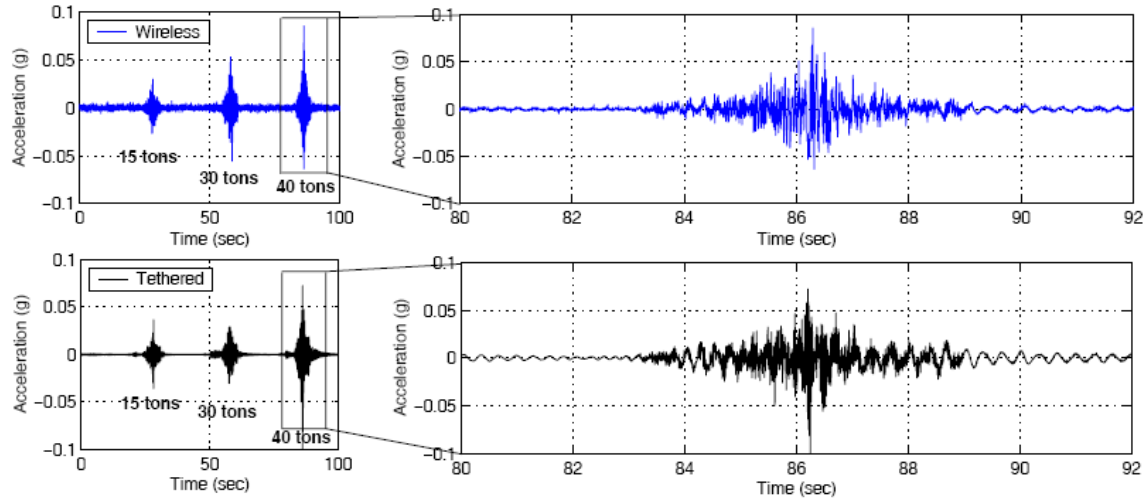
Figure 37 Acceleration response of the Geumdang Bridge at sensor location 8 while three trucks (15, 30, and 40 tons) transverse sequentially at 80 km/hr. The wireless (top) and tethered (bottom) monitoring systems both collect data at 200 Hz (after J. P. Lynch et al. [58])

Another similar example is the Alamosa Canyon Bridge [60] [61] [62] [63] in New Mexico, which is instrumented with wireless sensing units and a traditional cable-based monitoring system in parallel. Forced vibrations are applied to the bridge and monitored using both (wireless and tethered) data acquisition systems. The performance of the wireless sensing units is compared to that of the commercial wire-based monitoring system.

The architectural design of the wireless sensing unit shown in Figure 38 can be divided into three major subsystems: multichannel sensor interface, computational core, and wireless communications. The first subsystem, the sensor interface, represents the unit's ability to collect measurements from a variety of sensing transducers that could provide measurement of structural responses and environmental loads. To accommodate multiple sensors simultaneously, a multichannel interface is designed. At the core of the sensing interface subsystem is a single-channel, ADC that can resolve the output of an analog sensor to a 16-bit digital representation. Most sensors used for structural monitoring (including accelerometers, strain gauges, and anemometers) employ analog voltages and can, therefore, be interfaced. Sampling rates as high as 100 kHz can be attained using the Texas Instruments ADS7821 16-bit ADC. Two additional sensing channels are provided

that accept duty-cycle modulated outputs from a wide class of digital sensors. Many commercial MEMS-based accelerometers provide duty-cycle modulated outputs with resolutions of 14 bits.
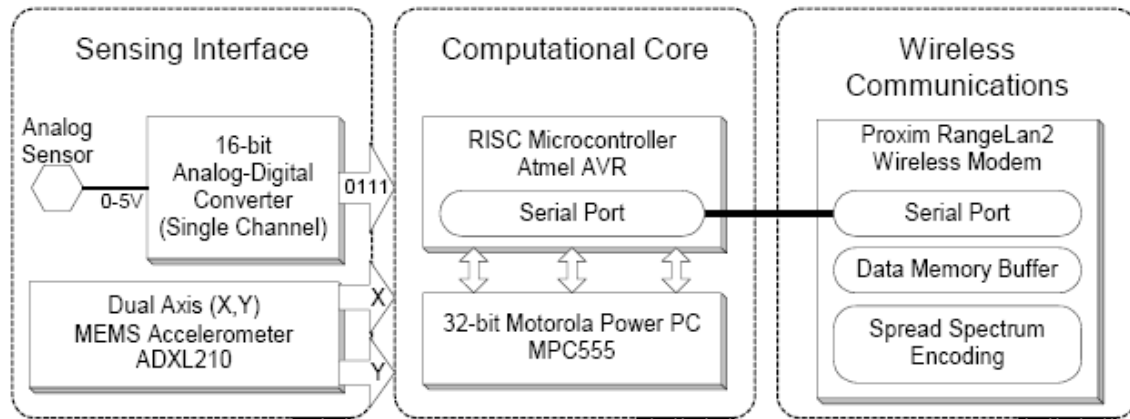
Figure 38 Wireless sensing unit in Alamosa Canyon Bridge case (after J. P. Lynch et al. [60])

The computational core is responsible for the overall operation of the wireless sensing unit. To collect data, the core will initialize the sensing interface and receive a stream of measurement data from the interface for storage in memory. Upon completion of acquiring raw time history data, the computational core can perform data interrogation tasks or transfer measurement data to the wireless sensor network using the wireless communication channel. In designing the sensing unit core, a balance between computational capabilities and low power consumption is sought. To achieve a suitable balance, a two-processor core design is created; a low-power 8-bit microcontroller is chosen for simple unit operation and a powerful 32-bit microcontroller is added to carry out intensive data interrogation tasks. The 8-bit Atmel AT90S8515 AVR microcontroller is selected for its capability-rich hardware design, low cost, and efficient power characteristics. For the execution of computationally demanding data interrogation algorithms, the 32-bit Motorola MPC555 PowerPC microcontroller is selected. With 448 kB of flash ROM and 26 kB of RAM, sufficient onboard memory is provided to serve as storage for measurement data. Special data registers are provided by the MPC555 to perform rapid floating-point calculations in hardware. The MPC555 microcontroller is kept turned off to conserve power and is turned on by the 8-bit microcontroller only when

intensive computational tasks are required. After completion of those tasks, the MPC555 is turned off and no longer consumes power.

The Proxim RangeLAN2 radio modem is chosen to serve as a reliable wireless communication technology of the wireless sensing unit. Operating on the 2.4-GHz unregulated Federal Communications Commission (FCC) industrial, scientific, and medical (ISM) band, data rates of 1.6 Mbps can be attained, with communication ranges of up to 1000 ft in unobstructed open space. Within structures constructed from heavy construction materials (e.g., concrete), the communication range reduces to about 450 ft. To ensure reliable wireless communication, data packets are modulated using frequency-hopping spread spectrum (FHSS) techniques.

The locations of accelerometers are distributed throughout the structure to provide good spatial separation for identification of the lower modes of response of the structure. To make identification of the sensor locations easy, the girders of the span are numbered through 1 to 6. In total, seven locations are selected, with each location denoted by a unique location number such as S1, S2, etc. Except for location S4, all accelerometers are mounted at the midpoint of the girder's web. The accelerometers installed at location S4 are situated 4 in. above the bottom flange surface of the girder. Figure 39 shows the locations of the seven accelerometers installed including a picture of the accelerometers mounted at sensor location 5. The PCB336 accelerometer is installed at the girder midpoint on the left and the CXL01LF1 accelerometer on the right, with wireless sensing units placed upon the girder flange. A 30-ft cable is used to connect the accelerometer to the Dactron SpectraBook that is situated beneath the bridge span. In order to test the whole system, forced excitation is applied to the Alamosa Canyon Bridge (see Figure 40).
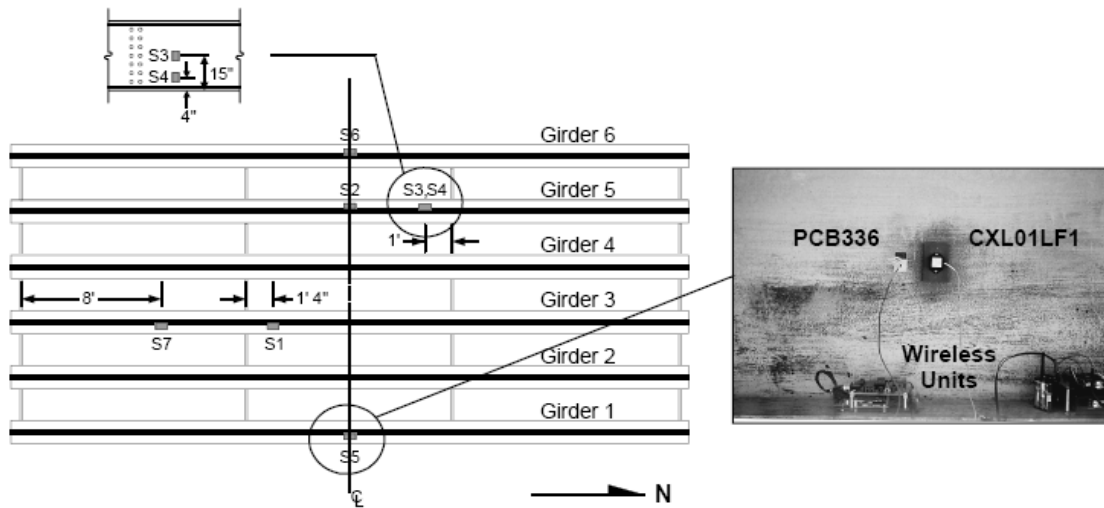
Figure 39 Accelerometer installation locations on the Alamosa Canyon Bridge (after J. P. Lynch et al. [60])

Figure 40 Methods of forced excitation of the Alamosa Canyon Bridge; (left) modal hammer and (right) flatbed truck driving over a wood stud place in the center of the span (after J. P. Lynch et al. [60])

Figure 41 shows the frequency response function of the recorded time history at S7 as calculated by the wireless sensing unit. The Alamosa Canyon Bridge serves as a realistic deployment of the wireless sensing unit with a controllable environment well suited for testing.
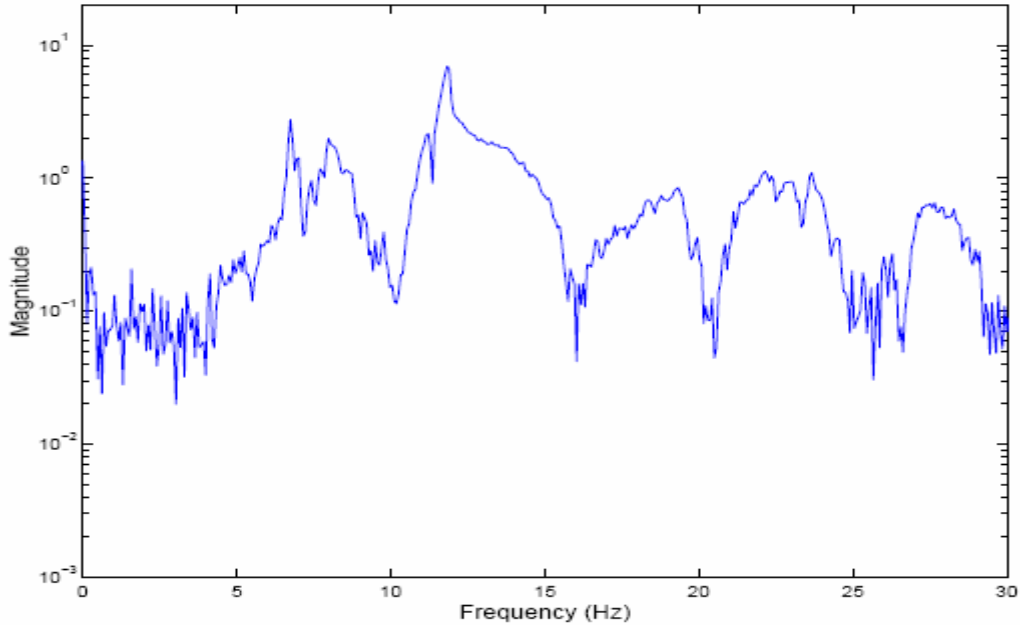
Figure 41 Frequency response functions derived from the acceleration response to the vehicle at S7 (after J. P. Lynch et al. [60])

In recent years, a more complex concept, which is to implement an active control scheme using trucks passing over a bridge to reduce the bridge vibration, has been considered by many researchers and scientists. For example, Victor DeBrunner et al. have an idea of a control system based on the nonlinear black-box model to minimize the vibration of bridges and highways. Their idea is shown in Figure 42. For details about the symbols please see Reference [64] section.
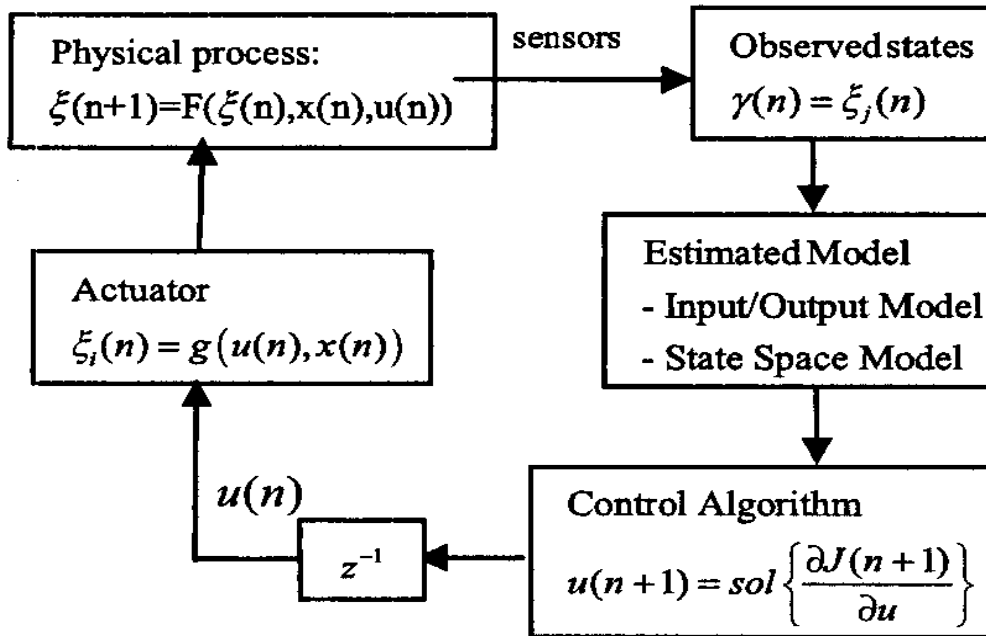
Figure 42 Control architecture based on the nonlinear black-box model (details, please see V. DeBrunner et al. [64])

For the sensor part, MEMS accelerometers are a mature product of MEMS technology, and there are a lot of successful MEMS accelerometer products on the market. Its design methodology can be roughly classified into two major categories: silicon-based design [65] and non-silicon-based design [66]. An example of silicon-based MEMS accelerometer is shown in Figure 43 [67].
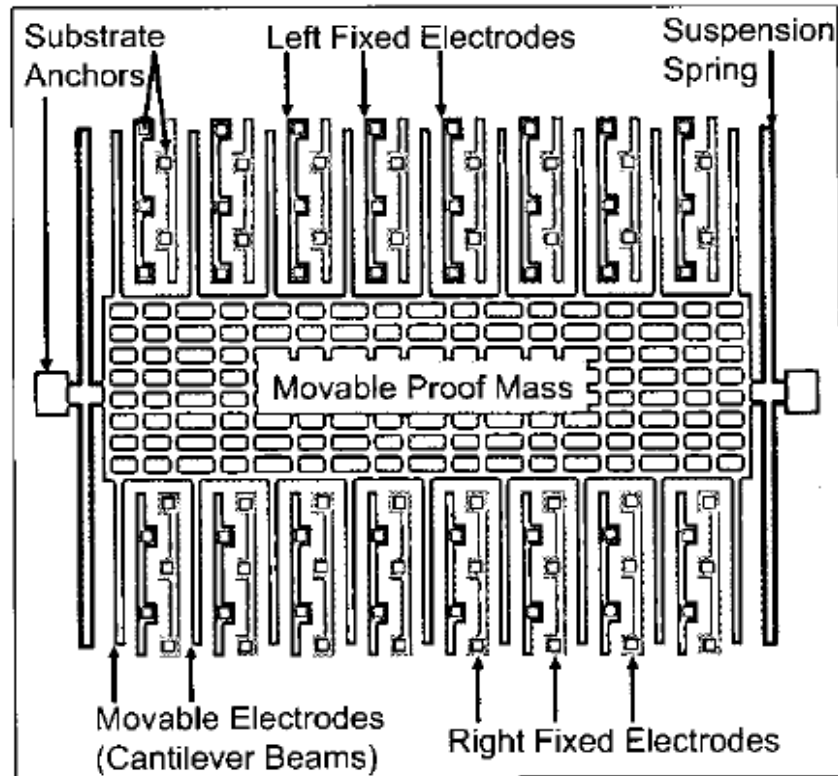
Figure 43 Standard lateral accelerometer layout schematic (after G. J. O'Brien and J. Hammond [68])

These MEMS accelerometers have a basic structure, shown in Figure 44. It represents a differential capacitor comprised of three polysilicon layers, each representing one of three plates used to create the differential capacitor. The middle plate (polysilicon layer 2) is a movable seismic mass suspended by two cantilever beams, while the other polysilicon layers (layers 1 and 3) are fixed. The seismic mass is centered between the two fixed layers, creating two equal capacitances. The bottom capacitance is formed between polysilicon layers 1 and 2, while the top capacitance is formed between layers 2 and 3.
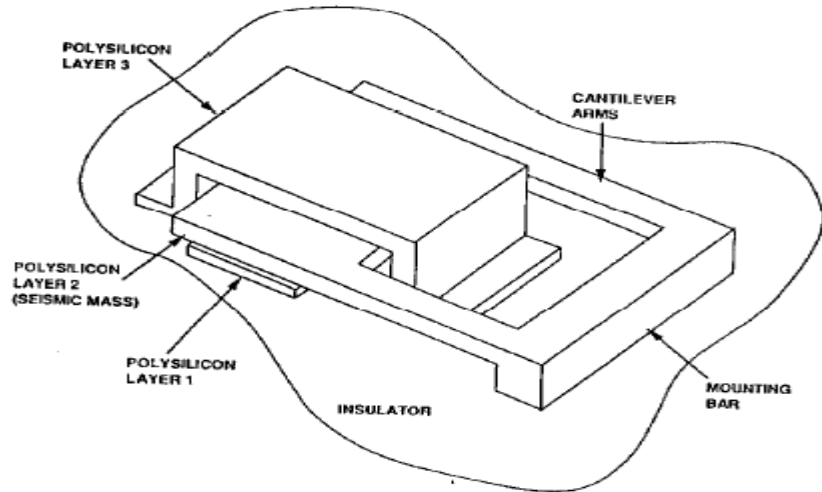
Figure 44 Basic structure of silicon-based accelerometer (after L. Ristic [66])

This structure is sensitive to acceleration in the direction perpendicular to the chip surface. The displacement of the seismic mass due to acceleration will change the capacitances between plates. This capacitance difference is proportional to the acceleration. The top and bottom capacitance form an active capacitance divider, where the resultant capacitance, due to an applied acceleration, can be converted into an output signal via the custom designed signal processing circuit. Figure 45 shows a more sophisticated commercial product.
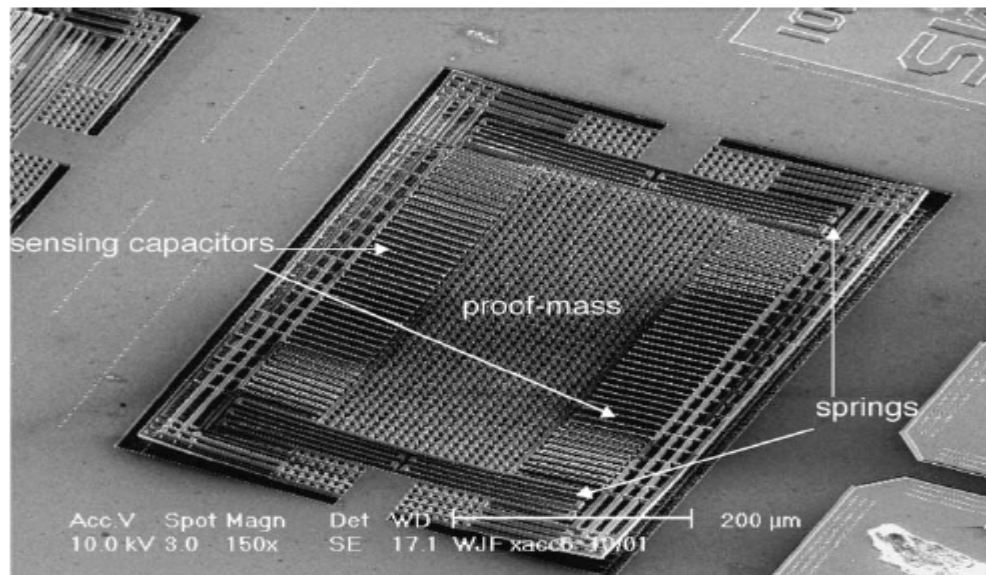
Figure 45 Demo of the silicon-based accelerometer (after J. Wu et al. [69])

An example of a non-silicon-based MEMS accelerometer design is shown in Figure 46 [67].
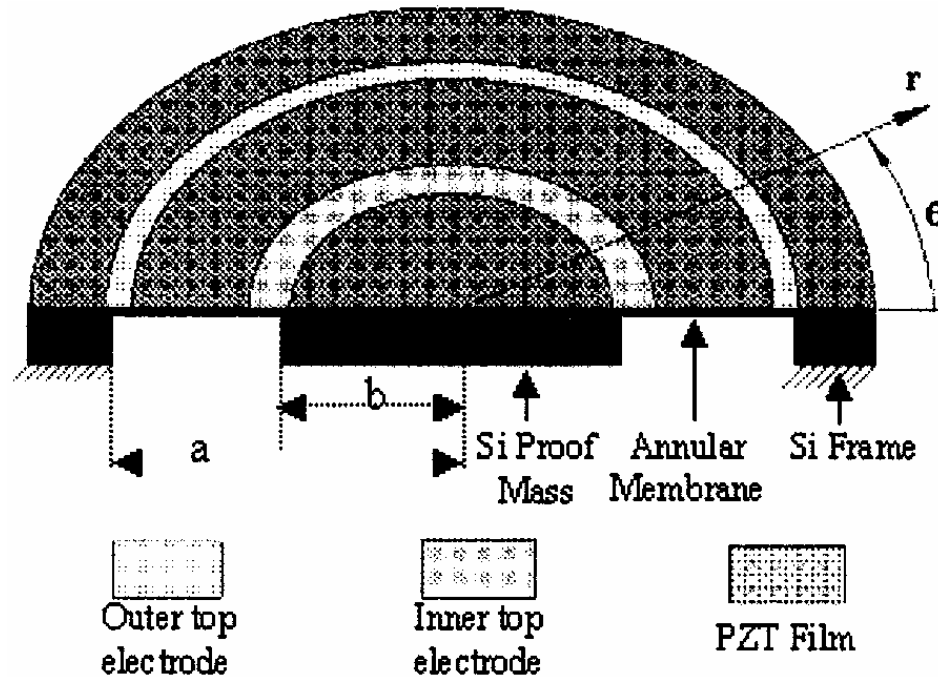
Figure 46 Schematic of cross section of non-silicon-based MEMS accelerometer
(after L. P. Wang et al. [67])

This non-silicon-based MEMS accelerometer is based on piezoelectric lead zirconate titanate (PZT) thick films with annular diaphragm sensing structures. The design provides good sensitivity along one axis, with low transverse sensitivity and good temperature stability. Test results show high sensitivities and broad usable frequency ranges. Measured sensitivities range from 0.77 to 7.6 pC/g for resonant frequencies from 35.3 kHz to 3.7 kHz. This MEMS sensor has a circular diaphragm sensing structure, specifically, an annular membrane supported by a silicon frame with a proof mass suspended at the center of the diaphragm. The thickness of the Si layer supporting the PZT film/electrode stack is between 6 and 45 μm. The piezoelectric film is deposited on a Pt/Ti/SiO stack so that it can be poled through its thickness, and the annular top electrodes are adjusted so that the areas are identical. The pyroelectric effect is cancelled when these two areas are poled in the opposite directions. Compared with beam-type sensing structures, this design uses an area efficiently, yielding a high-sensitivity accelerometer. Because the structure is stiff, the sensor has a high resonant frequency and

wide bandwidth. Furthermore, the symmetry yields natural insensitivity to transverse acceleration. From a fabrication standpoint the design does not require through-etching the silicon to release the membrane; therefore, the fabrication process is simplified and yield can be enhanced.

The basic idea of the MEMS sensor is still to transform acceleration information into an electrical charge. The structure was modeled using Timoshenko plate theory [70], and the boundary conditions under quasistatic inertial load were treated as in the Reference [71] section. In this structure, both radial stresses and tangential stresses contribute to the piezoelectric charge. However, the stresses are of opposite signs for the outer (i.e., close to the frame) and inner sides of the diaphragm; therefore, the top electrodes are separated in order to pole the two sections in opposite directions. When the outputs of the electrodes are connected in parallel, the pyroelectric output of the sensor is cancelled. To lower the overall sensor capacitance (to 6 nF), the top electrodes are placed only over highly stressed areas.

An issue related to the MEMS accelerometer is its noise characteristics. Scientists at George Washington University have conducted a research program for analyzing the noise sources of the MEMS accelerometers on the market, including ADXL202, ADXL105, and ADXL190 accelerometers from Analog Devices [72] [73]. Figure 47 shows an example of noise characteristics of the ADXL105.
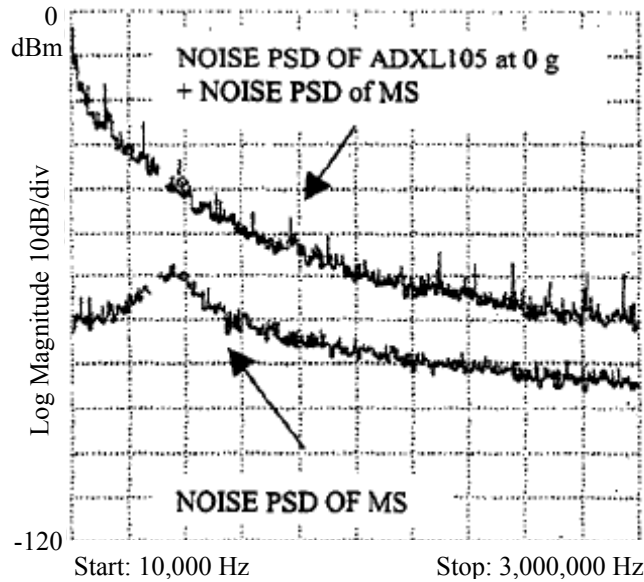
Figure 47 ADXL105 noise position sensing device (PSD) (after F. Mohad-Yasin et al. [72])

By comparing these MEMS accelerometer noise characteristics, F. Mohad-Yasin et al. conclude that MEMS accelerometer noise sources have 1/f-type noise characteristics and are acceleration dependent. In addition, there are impulse-type noise harmonics originating from the oscillators inside the accelerometers.

Furthermore, a passive MEMS accelerometer system can be accomplished using a wireless RF power supply. P. Singh et al. [74] have developed a circuit for receiving RF power. Its idea and demo system are shown in Figure 48 and Figure 49.
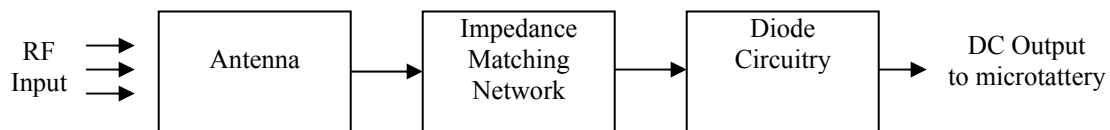
Figure 48 RF power (P. Singh et al. [receiving circuit after 74])

The direct current (DC) output coming from this circuit will charge up a mini-battery [75], which stores the power.
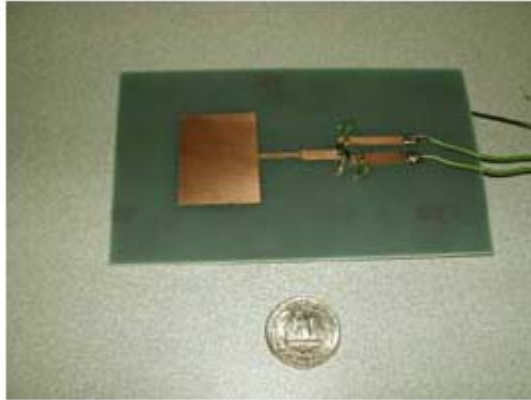
Figure 49 Demo of RF power receiving circuit (after P. Singh et al. [74])

This wireless RF power system can generate a 3.5-V DC power supply with a power delivery of 63 mW, sufficient to power up a MEMS accelerometer monitoring system.

4.1.4 MEMS Load Monitoring System [75]-[85]

Nanosensors, such as accelerometers and pressure sensors, can be integrated into pavement materials, such as concrete and asphalt, to monitor pavement performances. These accelerometers and pressure sensors might monitor the vibration and loads on bridges. These data might enable researchers to assess structural weaknesses and conditions, and fix them long before they are even apparent to human inspector.

For load-monitoring purposes on bridge and pavements, multiple kinds of MEMS sensors are needed. Scientists in Europe developed a wireless sensor network for large structural monitoring and it is suggested that in this sensor network, the MEMS sensor, which monitors the load condition of bridges and pavement, can be installed [75] (see Figure 50).
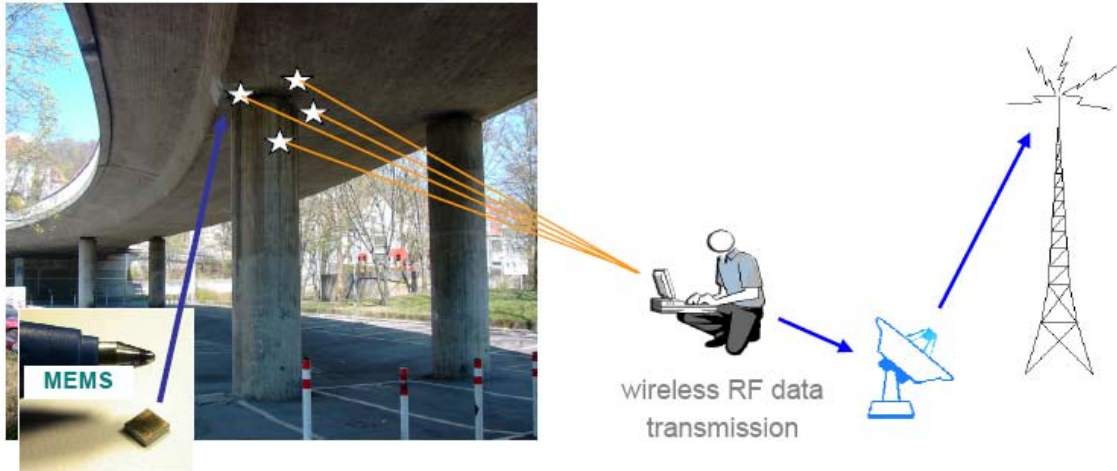
Figure 50 Diagram of wireless sensing of large structures using radio frequency transmission technique (after C. U. Grosse et al. [77])

This wireless monitoring system with MEMS sensors could reduce installation and maintenance costs dramatically. A wireless sensor mote with a MEMS pressure sensor could then be fabricated at a price varying from 100 to about 400 Euro each. As a result, the use of monitoring systems equipped with MEMS sensors and wireless communication could enormously decrease the costs to only a small percentage of a conventional monitoring system, and therefore will increase its application beyond monitoring bridges.

Figure 51 shows the layout of the wireless monitoring system. The sensor motes have to be power- and cost-optimized so they can provide data only at small distances. For that reason, there is the demand to install a central processing unit (CPU) on site in addition to the installation of the sensor motes. This central unit has to collect and store the data in a database, and further analyze the data from the sensor motes until these data are requested by the user or until a sudden event is detected that results in an alarm message. The central unit also should allow a calibration and wireless reprogramming of the sensor nodes to keep the whole system flexible.
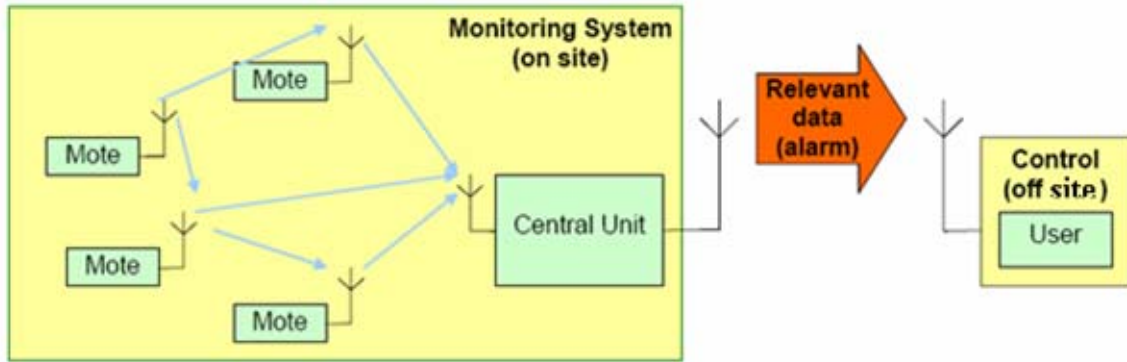
Figure 51 Layout of the wireless monitoring system with sensor motes (after M. Krüger and C. U. Grosse [76])

The sensor motes shown in Figure 52 are the main components of a wireless monitoring system. There are different tasks a sensor mote has to perform, which are to collect and digitize data from different sensors, to store sensor data, to analyze data with simple algorithms, to send and receive selective and relevant data to and from other nodes as well as the central unit, and to work for an adequate time period without a wired power supply. Therefore, a sensor mote consists of a CPU or Digital signal processing (DSP) chip with sufficient memory, a low-power radio, an aligned ADC module, a power supply, and one or more MEMS sensors.
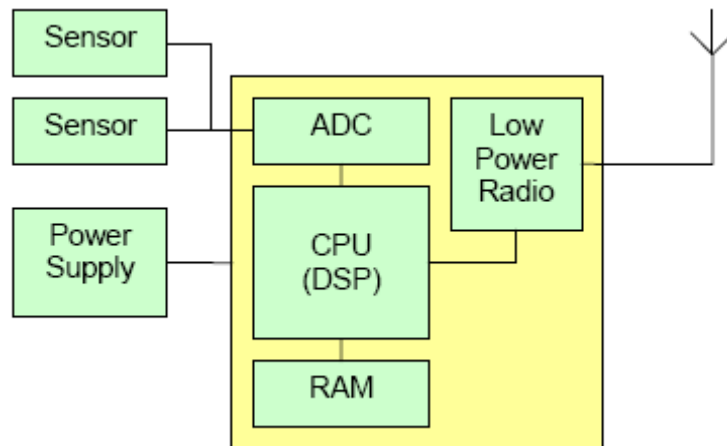
Figure 52 Schematic of sensor mote (after M. Krüger and C. U. Grosse [76])

Researchers at Cincinnati [78] use 300 hundred strain sensors on the bridge to monitor the load condition. Figure 53 shows their setup. These researchers conducted a comprehensive survey of commercially available sensors and data acquisition systems, and they selected a kind of sensor which has been investigated through a rigorous system calibration conducted in the laboratory [79].
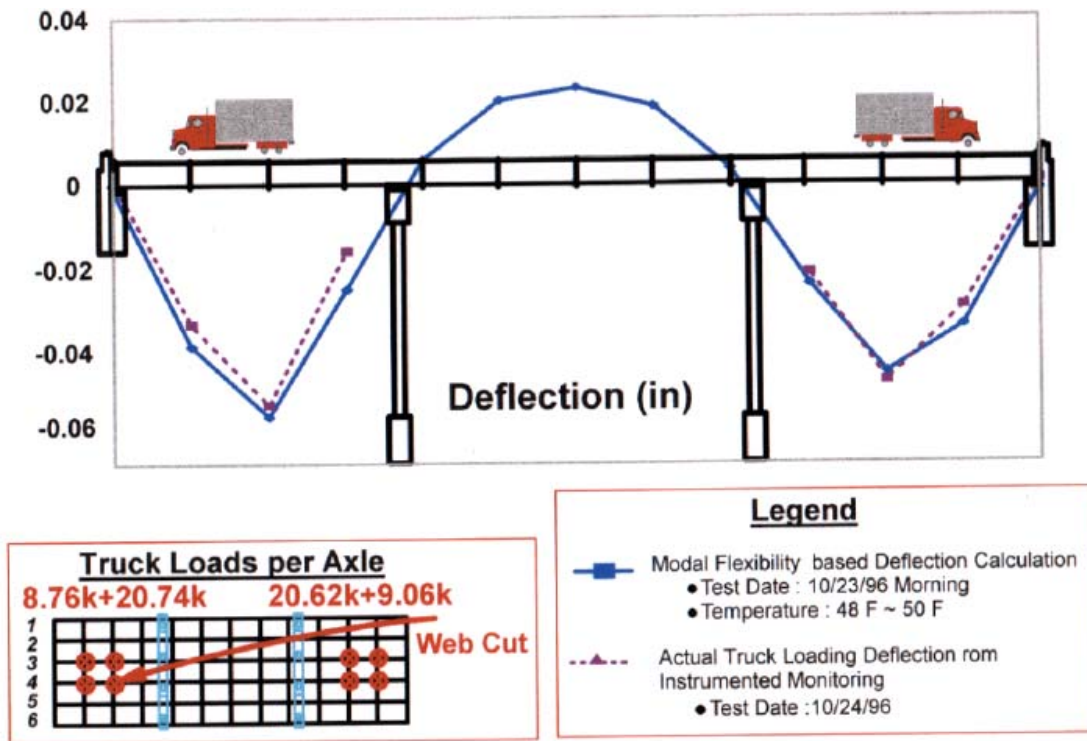
Figure 53 Overview of load monitoring system in Cincinnati (after A. E. Aktan et al. [78])

Figure 54 provides the time history recording of the strain resulting at midspan in the steel superstructure due to the pouring of the deck in September 1996. As expected, the net effect is to place the upper flange of the girder into compression and the lower flange into tension. The net strain offset due to the dead-load of the deck was measured and compared favorably with analytical results obtained from computer simulations as shown. This observation serves to verify the design calculations of researchers in Cincinnati.
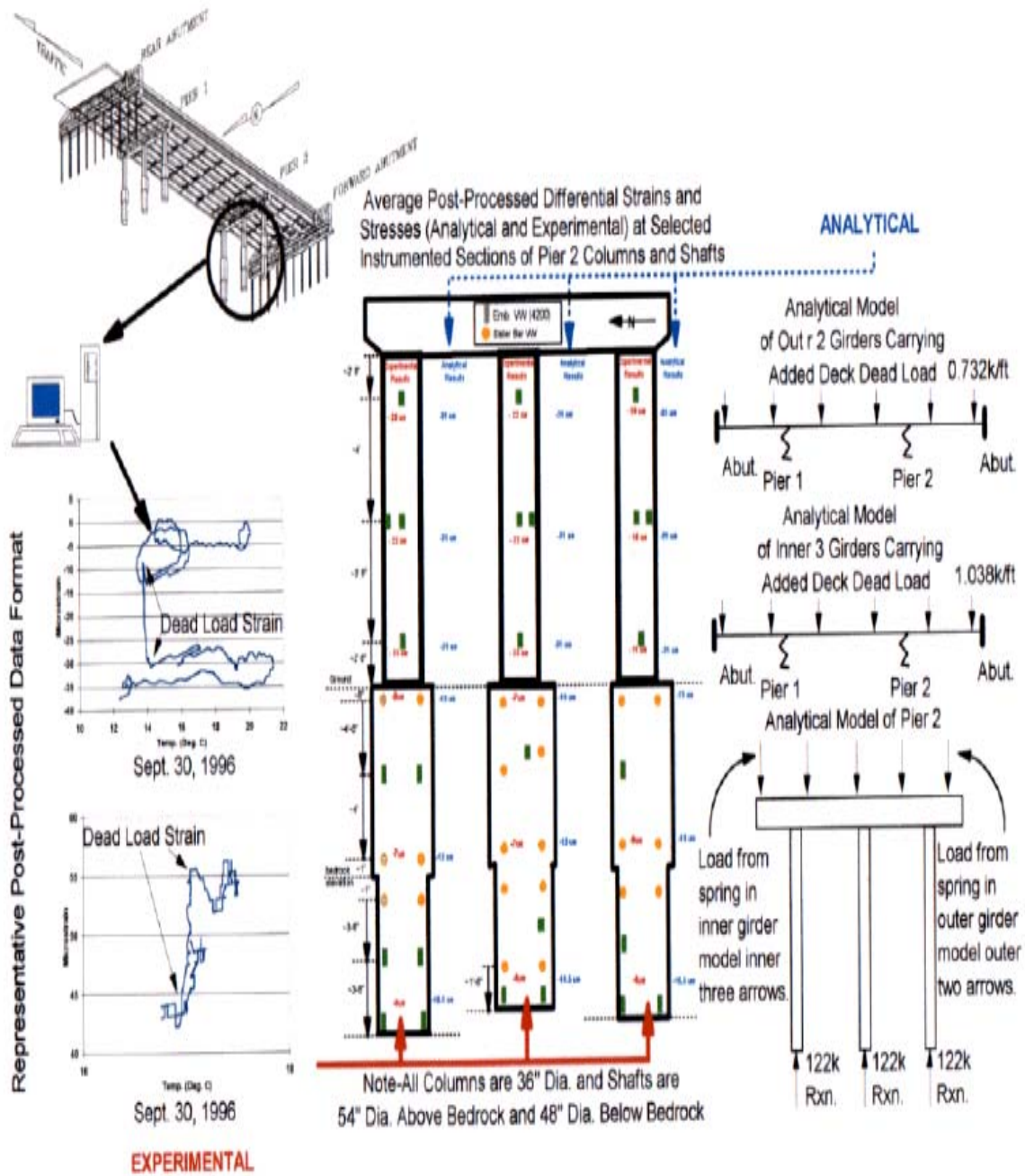
Figure 54 Details on load effects test setup (after A. E. Aktan et al. [79])
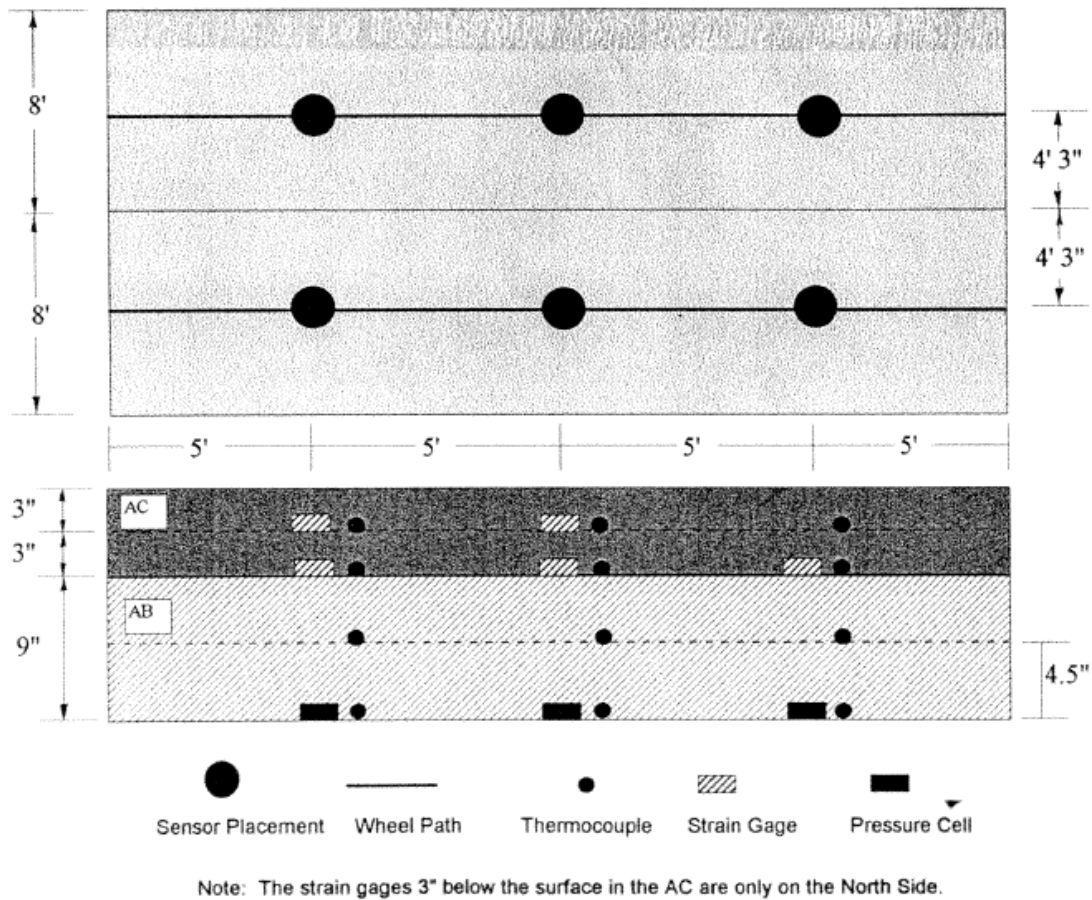
Figure 55 Location of sensors on plan and through section depth (after National Transportation Library [80])

Figure 55 shows six soil pressure cells, Model 3500 Dynamic Series with Ashkroft K1 transducers (from Geokon). On the plan, this is along the centerline of each wheel (pair of tires) at the quarter-span points. The centerline of the wheel paths for the north and south lanes are symmetrically located at 1280 mm (51 in.) from the middle of the pit. Three pressure cells were therefore placed on each wheel path, at about 1.5 m (5 ft) from the east and west ends. Eight strain gauges (Dynatest Model PAST-2AC) were placed in the above figure, along the centerline of the wheel paths. This line is the same line along which the pressure cells were placed. Three gauges were installed at the bottom of the asphalt concrete layer below each of the two test sections, right on top of the AB-3 base. A small amount of cold asphalt mix patching material was placed on top of these gauges

to protect them during hot asphalt paving. Detailed load monitoring results are shown in National Transportation Library [80].

Figure 56 shows a research program conducted in Korea [81] [82].

Symbol	Sensor	Quantity	Behavior	Symbol	Sensor	Quantity	Behavior
●	Thermometer	21Ea	Cable & Member	■	1-D Accelerometer	12Ea	Cable
		12Ea	Tower	□	2-D Accelerometer	4Ea	Tower Top & Deck
==	Static Strain Gage	8Ea@4	Anchor Bolt			10Ea	Deck
		42Ea	Deck. Cross Section	□	3-D Accelerometer	3Ea	Tower Foundation
		10Ea@4	Anchor Plate	○	Anemometer	4Ea	Wind
		8Ea	Link Shoe	×	Laser Disp. Sensor	3Ea	
―	Dynamic Strain Gage	76Ea	Deck. Cross Section	♠	Potentiometer	4Ea	Expansion Joint
		99Ea	Etc.	SL	Static Data Logger	2Ea	
♦	2-D Tiltmeter	10Ea	Tower Inclination	DL	Dynamic Data Logger	2Ea	

Figure 56 Sensor locations of Youngjong Bridge (after C. B. Yun [81])

Data collected at each bridge can be processed exclusively at each field station for real-time monitoring and alarming the sudden abnormal behavior. However, data that are useful for long-term evaluation of bridge condition as well as the periodical inspection data of the bridge are transmitted through high-speed Internet lines to the management center, which is located far from the site. Once the data are collected at the center, the integrated bridge management software (BMS) handles them for classifying, storing, and retrieving. This integrated BMS itemizes bridge maintenance details, not only physical information, but knowledge such as detailed rating category for all members. Based on the inspection results, it manages status assessment, rating, repairing, and retrofitting activities. Although the health monitoring system itself plays an important role for

studying the behavior of structures in the real environment and to reduce uncertainties in further design process, it can be combined with other technologies such as system identification and damage detection theory, bridge management system, and artificial intelligence to give an overall estimation of the bridge condition, to make a proper maintenance decision, and finally to lengthen the service life of the structure.

Fiber sensors can also be used to monitor the load condition of bridge and pavement. Because intra-core Bragg reflection gratings fabricated in germania-doped optical fiber [83] are increasingly considered as strain-sensing elements in mechanical structures [84], and considerable experience of single-element grating design and fabrication now exists worldwide. Modern military bridges are generally lightweight, welded aluminum structures of modular design for rapid transportation and deployment. In the battlefield, it is important to know the structural health of the bridge and to determine its load capacity, if damaged. Optical fibers for strain sensing offer a means of structural health monitoring for bridges, since they have the potential for wide area coverage with single-fiber arrays. Figure 57 shows such an application.
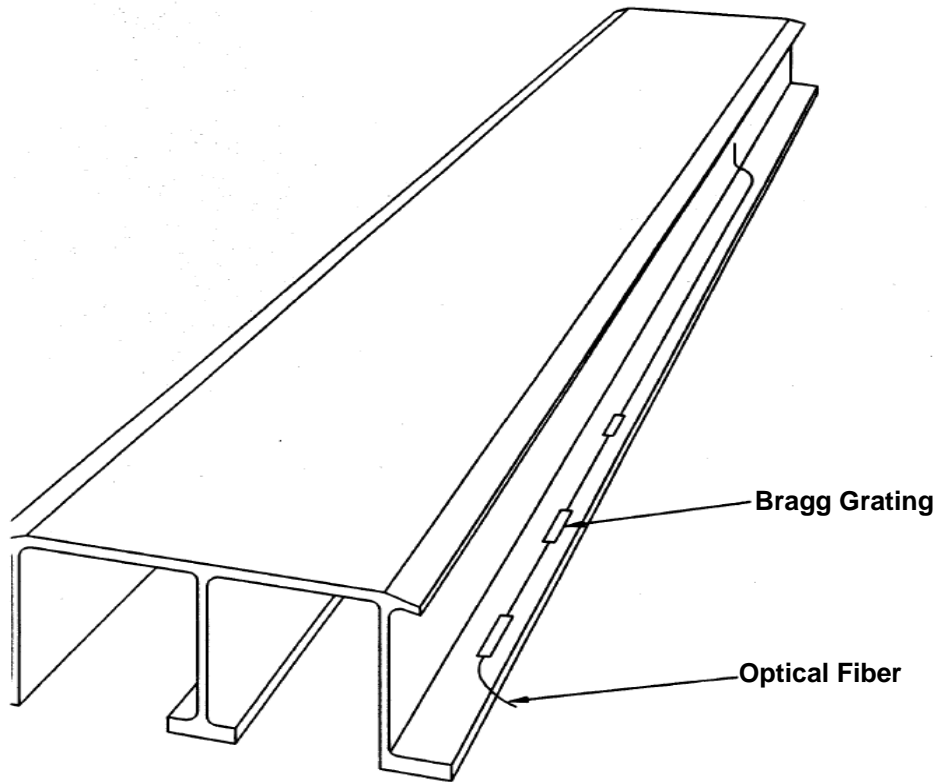
Figure 57 Alloy bridge section (after J. A. J. Fells et al. [85])

The University of Houston team, which is supported by the National Science Foundation (NSF), developed a remote bridge vibration monitoring sensor to measure highway bridge vibration. This system has a series of wireless accelerometers embedded into the pavement on the bridge. Accelerometers are manufactured by Analog Devices using MEMS technology. These low-cost accelerometers continuously measure the acceleration of the bridge in three axes and wirelessly send the data to a data collection center. The acceleration data are then analyzed to obtain bridge and load conditions. A conceptual network layout is shown in Figure 58, and measured vibration data from a sensor fixed at the end of a spring is shown in Figure 59. The wireless concept and network protocols can be used in many areas of transportation sensor networks.
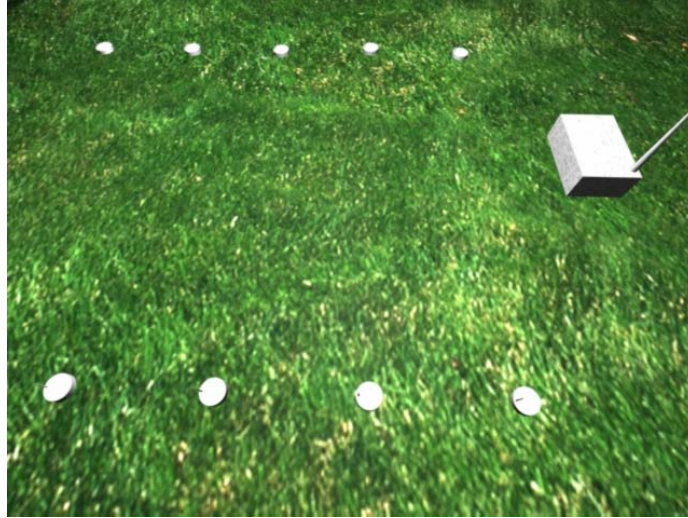
Figure 58 Schematics of distributed wireless sensor network. The distance between sensors (the circular objects in the figure) and data collection center (the rectangular box in the figure) is about 100 ft.
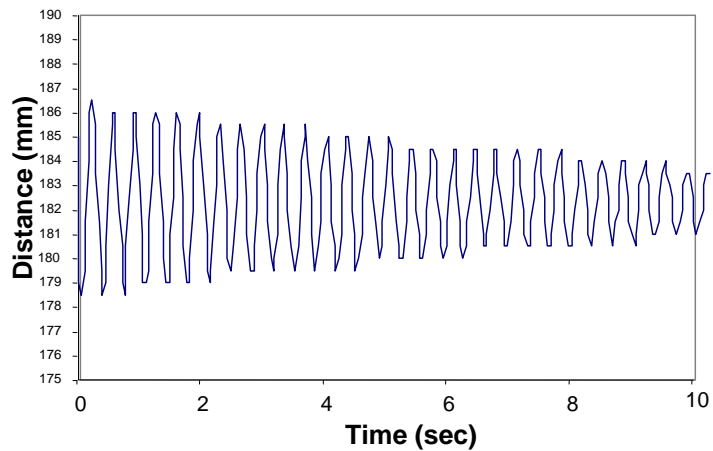
| (a) | (b) |

Figure 59 Lab test setup. (a) vibration measurement system; (b) results of the steel spring tests. The MEMS sensor is installed on the tip of the wire.

4.1.5 MEMS Concrete Corrosion, Crack Testing, and Monitoring Sensor [86] [88]

Concrete is a porous material, ranging from air voids to nanometer-scale pores produced by cement-water chemical reaction [86]. These nanoscale pores control the properties of

the calcium-silicate-hydrate hydration product, which is the main "glue" that holds concrete together. The assault of deicing chemicals, which penetrate concrete's porous structure and oxidize the reinforcing steel within, causes crack and deterioration to the structure.

By sensing the electrochemical reactions through a potentiometric or amperometric method, corrosion in steel structures, especially welding joint and load transfer devices in rigid pavement, can be detected and monitored. The potentiometric device can be used to measure and monitor equilibrium potential established between the sensor surface and the material in contact, while the amperometric device measures the current.

Normally, the steel in reinforced concrete platforms is protected against corrosion by high pH levels in Portland cement. When contaminants like deicing salts penetrate the concrete, the naturally stable pH environment is chemically upset, and corrosion begins. The platform can also deteriorate when carbon dioxide permeates the cement's pores and converts the calcium hydroxide into calcium carbonate. By sensing the change of the pH value, detecting special chemical elements and sensing the change of their concentration around the steel structure by the electrochemical sensor, the corrosion procedure can be tested and monitored.

For crack monitoring purposes, I. J. Oppenheim et al. developed a MEMS transducer for an ultrasonic flaw detection system. The sensor can be used to detect the initiation of a crack [87] (see Figure 60).
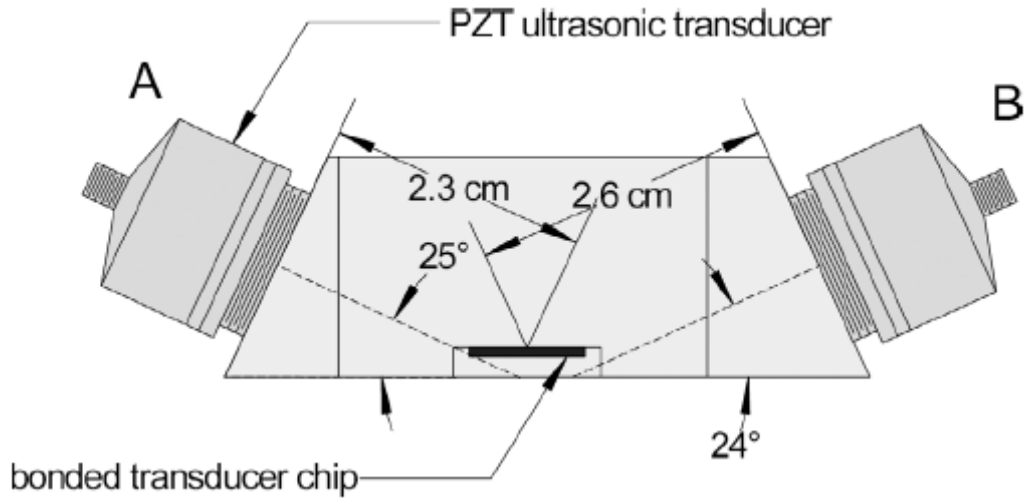
Figure 60 Drawing showing plexiglass test specimen with two off-axis locations for the emitting transducer (after I. J. Oppenheim et al. [87])

A Krautkramer MSW-QC ultrasonic transducer was coupled to the plexiglass specimen and driven by a Krautkramer USPC-2100. Transducers with various resonant frequencies were used (1, 3.5, and 5 MHz). The transducer could be attached in different locations to provide for uniform illumination (not shown) or off-axis incident illumination with various source distances and incidence angles. Individual detectors were contacted using a standard probe station. The output signal was recorded using an HP 54601A oscilloscope triggered by the pulse exciting the PZT transducer. The test results are shown in Figure 61.
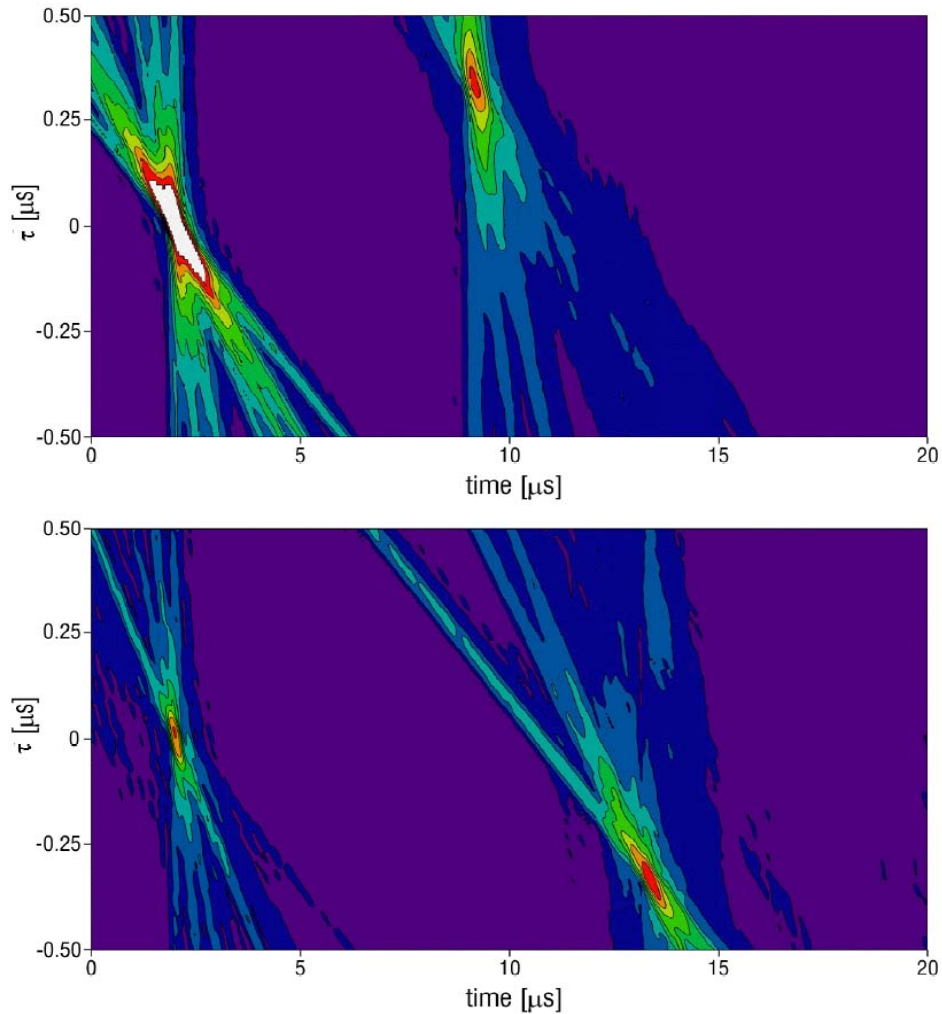
Figure 61 Summed MEMS transducer signal: (top) emitting transducer in position A; (bottom) emitting transducer in position B (after I. J. Oppenheim et al. [87])

From this contour plot, the angular position of a source is related to the peak position on the τ axis (τ is delay time), and the distance is proportional to the peak location on the t axis [110]. Further investigation on this MEMS sensor will result in an efficient pavement crack detector.

Other sensors and data telemetry system developed for military uses can also be used in TxDOT projects. Oak Ridge National Laboratory (ORNL) is developing a medical telesensor for military troops in combat zones. This chip shown in Figure 62 on the fingertip will report measurements of vital functions of a soldier to remote recorders [88].

The goal is to develop an array of chips to collectively monitor bodily functions and send the data by wireless transmission to an intelligent monitor. The monitor could alert medics if the data show that the soldier's condition fits one of five levels of trauma. The monitor also would receive and transmit global satellite positioning data to help medics locate the wounded soldier. TxDOT can use this technology in monitoring pavement conditions with minor changes in sensors.
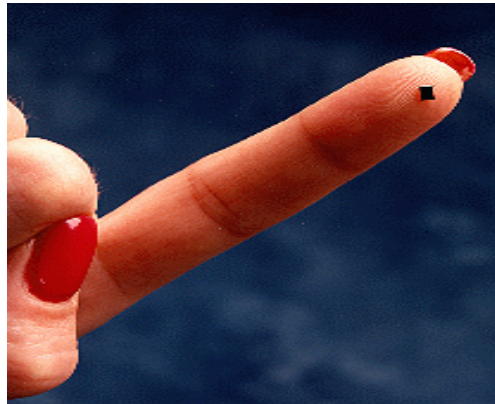
Figure 62 Wireless telesensor developed by ORNL for military applications (after K. B. Jacobson [88])

4.1.6 National Science Foundation Sponsored Research Projects for MEMS Sensors [89] [98]

NSF sponsored research projects for the development of a silicon-based MEMS sensor that can be mixed with concrete to make multiple analyses of steel-reinforced concrete more reliable and safe from deterioration and collapse. These detectors can be poured along with the concrete into a bridge deck or roadbed, providing data for up to 100 years. Many of these new devices, perhaps hundreds, could be embedded in a new bridge, building, or roadway. The ultra-small sensor would monitor moisture, temperature, and pH as well as the concentration of chloride, sodium, and potassium ions within the concrete. These devices will provide critical data for evaluating concrete performance from its freshly mixed stage to its casting, through the concrete's service life to its period of deterioration and repair.

ORNL [89] is claiming a new world's record by detecting just 5.5 femtograms with its silicon MEMS sensor. The silicon cantilever, 2 µm long by 50 nm thick, can be made to detect virtually any material by coating cantilevers with various materials sensitive to proteins, cells, or trace amounts of almost any chemical contaminants.

O. T. -C. Chen et al. [90] propose a multifunction amperometric microsensor, originally designed for medical applications. This microsensor consists of an electrochemical cell, a current-to-voltage amplifier, and a voltage-controlled resistor. The sensor can be used in various applications, including highway research. The microsensor is implemented by using 0.5 µm CMOS technology with a die size of 1.0 mm by 1.0 mm. This electrochemical cell is a two-electrode scheme and its enzyme area is 600 µm by 800 µm to generate the induced current that is proportional to the concentration of the test material. The microsensor can effectively perform the operation of amplification and signal transformation from the chemical reaction. The proposed microsensor chip is shown in Figure 63.
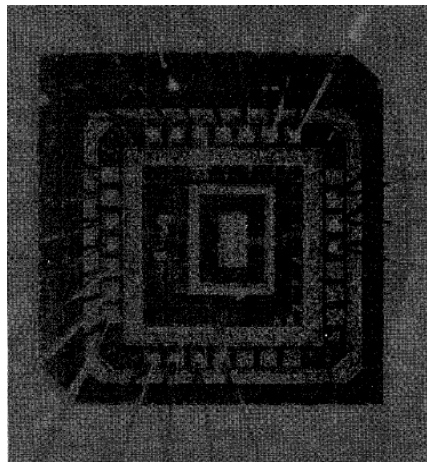
Figure 63 The chip structure (after O. T. -C. Chen et al. [90])

This sensor is especially useful when buried into concrete to monitor the concrete maturity process and analyze concrete cracks. Due to the small size and low cost of the sensor, large quantities of such sensors can be mixed with concrete. Combined with wireless MEMS chips, data can be obtained through wireless link over a specially designed data link protocol.

M. Mayer et al. [91] reported the integrated temperature microsensors for characterization and optimization of the thermosonic ball bonding process. Ball bonding technology is used to connect internal integrated circuits to the external circuit. The in situ temperature during ball bonding is measured and analyzed. Figure 64 (a) shows the in situ microsensor, designed for thermosonic ball bond process monitoring. The measurements were performed on an ESEC (ESEC is a company whose core business is making the die bonders, wire bonders, and flip chip bonders needed to lay down the itty bitty pathways on microchips) gold ball bonder with a ceramic 100 µm pitch bottleneck capillary. A 25 µm diameter AW14 wire was used. The circular shaped aluminum line meanders are used as temperature microsensors. Figure 64 (b) shows the dimension of the temperature microsensors. This temperature sensor can be integrated into any of other sensors to measure pavement temperatures including temperature in concrete to monitor concrete maturity. Since this sensor is very low in cost and very small in size, embedding this sensor into concrete will not affect the strength of the concrete. However, it has to be wired for data transmission.

(a)   (b)
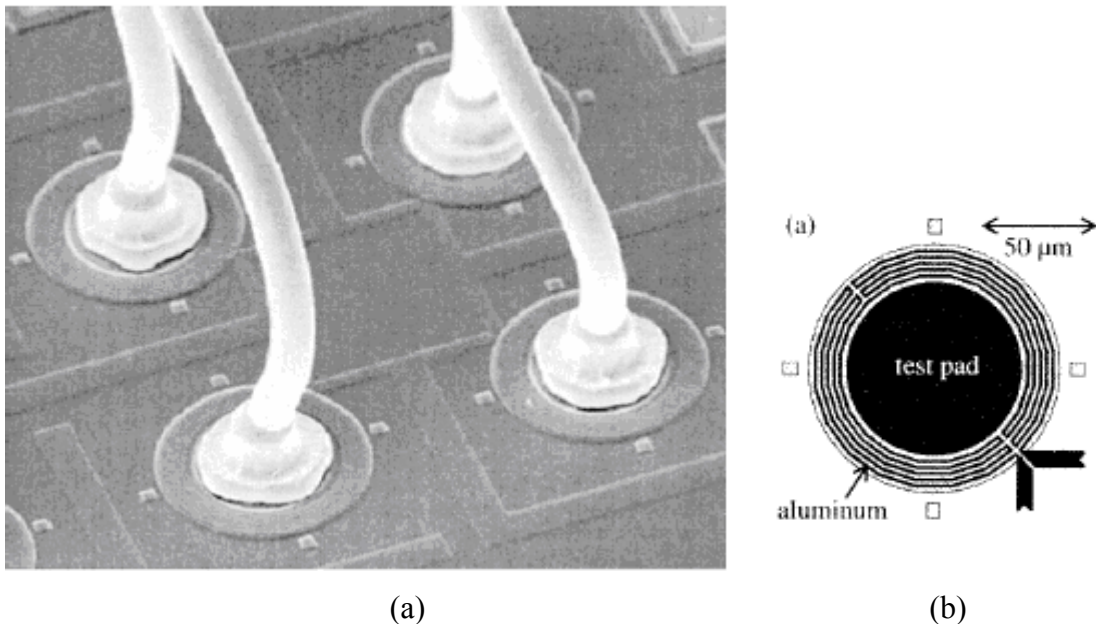
Figure 64 Integrated temperature microsensor, (a) SEM picture of gold balls bonded to test pads surrounded by circular shaped aluminum line meanders used as temperature microsensors; (b) group of eight microsensors with connection pads. Test pad pitch is 200 µm (after M. Mayer et al. [91])

H. Nam et al. [92] reviewed the recent development of electrochemical sensors, which are commonly used to determine the presence and concentrations of chemical species in samples by measuring the changes in electrical currents and/or potentials. These sensors can be miniaturized into mass producible microelectrodes or even nano-sized electrodes suitable for in vivo sensors. Figure 65 (a) shows a cross section of the completed sensor made by his lab, (b) shows the SEM image of the ion-selective membrane, and (c) shows the packaged sensor. TxDOT can use this kind of sensor for studying the effects of chemical agents in concrete and other pavement materials. By continuously monitoring the chemicals, it is possible to improve pavement lifespan and build better pavements for Texas.
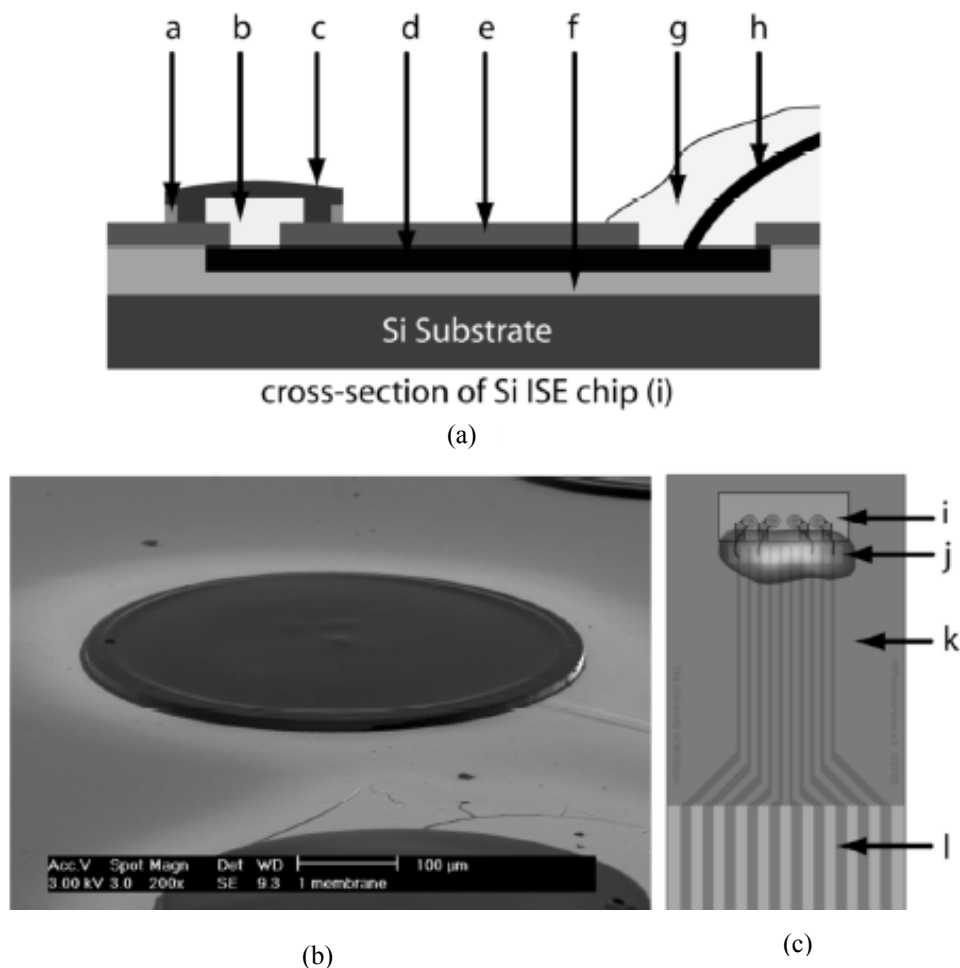
Figure 65 Schematic and SEM of a silicon based ion-selective device. (a) Cross section of silicon chip; (b) containment ring; (c) AgCl electrode (after H. Nam et al. [92])

Currently TxDOT uses humidity sensors for concrete maturity monitoring. I. Stiharu et al. [93] report the implementation of a relative humidity microsensor. The low-cost and high-reliability micromachined sensor is built on the same chip with the conditioning circuitry. The layer view of a unit cell of the humidity resistive transducer is shown in Figure 66. This sensor is a candidate for applications in pavement maturity monitoring at a low cost.
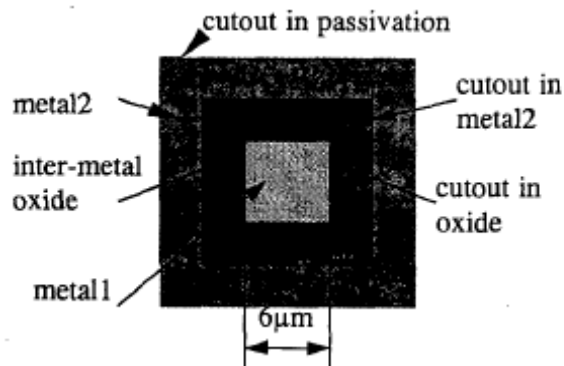
Figure 66 Layer of a unit cell of humidity resistive transducer (I. Stiharu et al. [93])

Accelerometers have been used by TxDOT in profilers. The current accelerometers are based on magnetic coils. Scientists (J. Tieman et al. [94]) describe the design of a low-cost, compact, MEMS-based smart sensor system for three-axis acceleration measurement using only commercial off-the-shelf (COTS) components. Analog devices, ADXL150 and ADXL250, were used. Figure 67 shows a view of the ADXL150 inside the open package.

Pressure sensors can be used for pavement loading measurements, material compaction detection, and joint distance measurement. O. Tohyama et al. [95] developed a fiber-optic pressure microsensor with a sensing element only 270 pm by 270 pm by 150 pm in size and applied it to actual balloon catheters. The sensors have been fabricated using silicon micromachining such as anisotropic etching and direct wafer bonding. Figure 68 shows the view of the sensor.
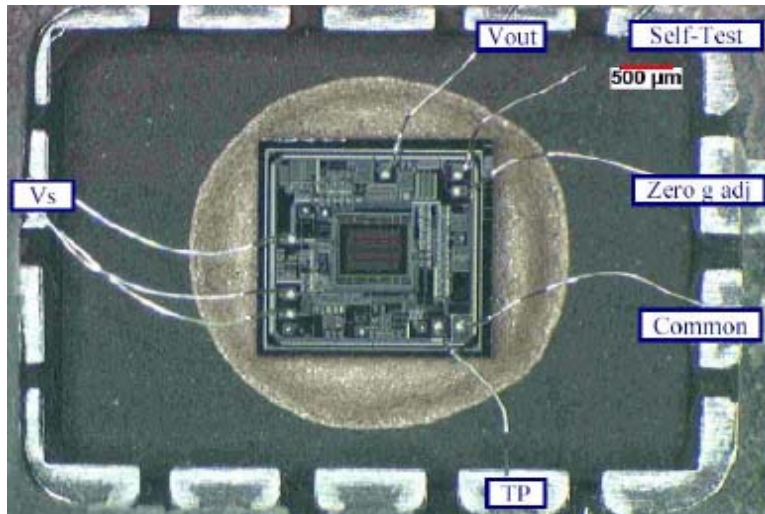
Figure 67 View of ADXL150 inside the open package (after J. Tieman et al. [94])

Figure 68 Fiber-optic pressure sensor (after O. Tohyama et al. [95])

Deep understanding of the electrochemistry, physics, and microelectronics at the molecular scale offers tremendous promise for an enhanced generation of sensing devices. TxDOT can take advantage of these sensors and use them in pavement design, monitoring, and maintenance. Nanosensors have the promise of being extremely sensitive, selective, and responsive. Therefore, the sensors can be smaller, have higher performance, consume less power, and be less expensive. Some recent development on the nanosensor includes the following.

Massachusetts Institute of Technology (MIT) chemists and researchers tested using quantum dots in exploratory cancer surgery of test animals [96]. The semiconducting particles can be used to illuminate specific areas, allowing controlled lighting. The quantum dots at 10-20 nm, so that the fluorescence from the dots can be controlled using an external electromagnetic field. Further development of this technology can be used for smart roadway signs on highways.

Penn State University researchers have created a new hydrogen sensor made from titanium nanotubes that has the unique ability to self-clean [97]. The titanium nanotubes coated with a discontinuous layer of palladium can rid themselves of a variety of contaminants including stearic acid, cigarette smoke, and different types of oil via their photocatalytic properties. Furthermore, a wide variety of chemical sensors can be made from the titania nanotubes by doping them with trace amounts of different materials such as CO_2 or chemical agents in concrete. Therefore, TxDOT can use nanotubes for emission control and concrete analysis.

A. Flatau [98] takes inspiration from the transduction processes of the inner ear's cochlea and cilia to design acoustic sensors. Specifically, this project proposes to use nanowires of magnetostrictive material as hairlike sensors of ultrasonic and acoustic signals. The artificial cilia transducers have many advantages over the current sensors, as these magnetic hairs can be easily fabricated in arrays for enhanced sensitivity and/or spatial resolution as compared to current ultrasonic pressure detectors, and the diameters, length, and stiffness of the hairs can be tailored to a wide range of frequencies. Figure 69 shows the nanowires, which may be embedded into the tire of a testing vehicle to analyze noise effects of the pavement surface. It can also be used to analyze the tire/pavement interaction for various pavement surfaces.
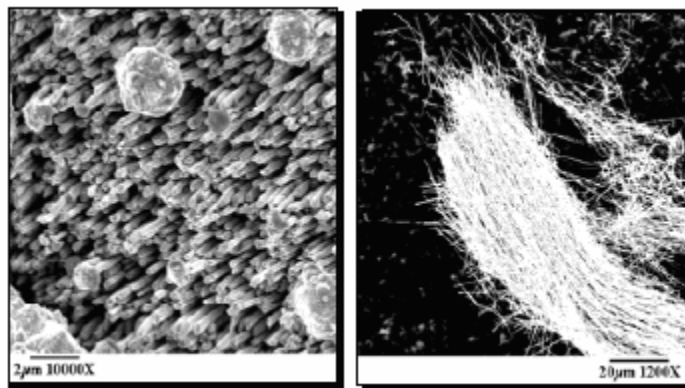
Figure 69 Nanowires (A. Flatau [98])

4.2 Microsensors in Transportation

Microsensor refers to a scale of 10^{-4} m to 10^{-2} m.

4.2.1 UH Wireless Moisture and Temperature Sensors [18] [99] [100] [101] [102]

The University of Houston team led by Dr. Ce Richard Liu is developing a wireless moisture and temperature sensor [18]. This sensor uses a single complementary metal oxide semiconductor (CMOS) chip and works at a 2-GHz frequency range. The sensor uses a novel microstrip transmission line-based moisture sensor developed by the principal investigator (PI). It uses the phase-shift measurement of an RF signal going through a transmission line buried in the soil to be measured. Our simulation has shown that the amplitude of the transmission measurement is a strong function of the conductivity (loss of the media), and the imaginary part of the dielectric constant, and the phase is mainly a strong function of the real part of the moisture content. Therefore, measuring phase shift in the transmission mode can directly obtain the soil moisture information. This moisture sensor utilizes the large difference between the water dielectric constant (about 80 times that of the air) and the surrounding medium (typically this is about 2-4 times of that of the air). The phase shift is largely dependent on the moisture content and the structure of the transmission line. In this particular project, we use the microstrip line as the transmission line structure due to its simplicity in

integrating it into a chip. The temperature sensor is embedded into the sensor using a single pin junction temperature sensor with digital self-calibration procedure.

When a transmission line is embedded into the medium, the equivalent dielectric constant ε_{eff} is equal to

$$\frac{\varepsilon_s + \varepsilon_m}{2} + \left(\frac{\varepsilon_s - \varepsilon_m}{2}\right)\left(\frac{1}{\sqrt{1 + 12d/w}}\right), \tag{1}$$

where d and w are the height and width of the transmission line as shown in Figure 70 (a). ε_s and ε_m are the dielectric constants for microstrip substrate and the surrounding medium, respectively [99]. The dielectric constant of the medium is governed by the mixture equation as

$$\sqrt{\varepsilon_m} = \sqrt{\varepsilon_d} + \rho_d \Psi(\sqrt{\varepsilon_w} - 1), \tag{2}$$

where ε_d and ε_w are, respectively, the permittivity of dry material and water, ρ_d is the dry density, and Ψ is defined as the absolute moisture content [100] [101].

Clearly, the moisture contents variation in Equation (2) will lead to the variation in ε_m and consequently alter the values of ε_{eff} in Equation (1). Since the phase of RF signal propagation on a microstrip transmission line is closely related to the value of ε_{eff}, the variation of the medium moisture contents can be observed from the phase variation in the RF signal propagation. The correlation [102] between the dielectric constant variation and the phase variation over a transmission line, which is only 1 cm in length (at 2.4 GHz) is shown in Figure 70 (b). We can clearly see that this novel sensor head is very sensitive to the moisture contents, and it has a monotonic relationship to the moisture contents as well.
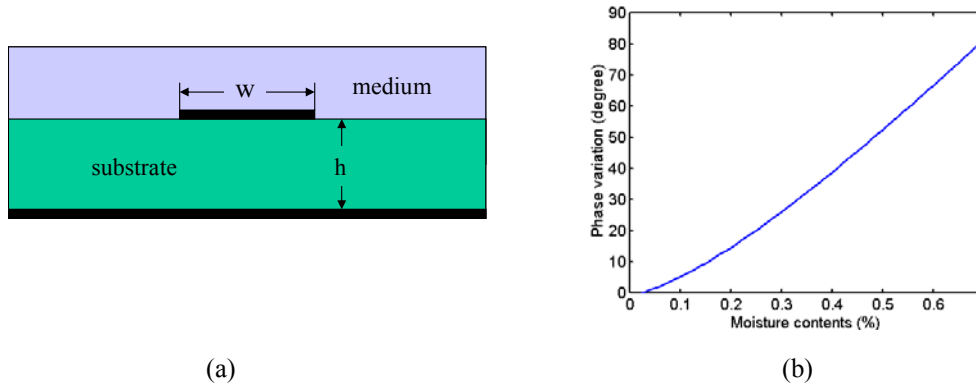
Figure 70 UH moisture sensor description. (a) Cross section of a microstrip transmission line sensor head; (b) correlation between the moisture contents and the phase variation for a 1 cm long microstrip transmission line on FR4 PCB (h/w = 0.5, ε_r = 4.2)

By properly designing a transmission line structure, the phase-shift range can be controlled so that the total phase shift at the highest moisture reading will be less than 90 degrees to avoid ambiguity. At frequencies over 1 GHz, the contribution to the phase shift from conductivity of the soil becomes small enough and can be ignored. In this research, we propose to use an on-chip microstripline-fringing field (MicroSLFF) sensor structure (Figure 71) as the sensor part of the system operating at a 2.4-GHz frequency. The other apparent advantage of the MicroSLFF sensor is that it can be easily integrated onto the top of the IC chip, which processes the data measured by the sensor (Figure 72). The other feature of the single-frequency sensor includes the simplicity of the sensor structure. The sensor will use part of the radio circuitry for moisture measurement instead of a separate sensor circuitry, which makes it possible to reduce the sensor cost to less than $5 each in quantities. Both lab and field tests show that this kind of sensor is very accurate.
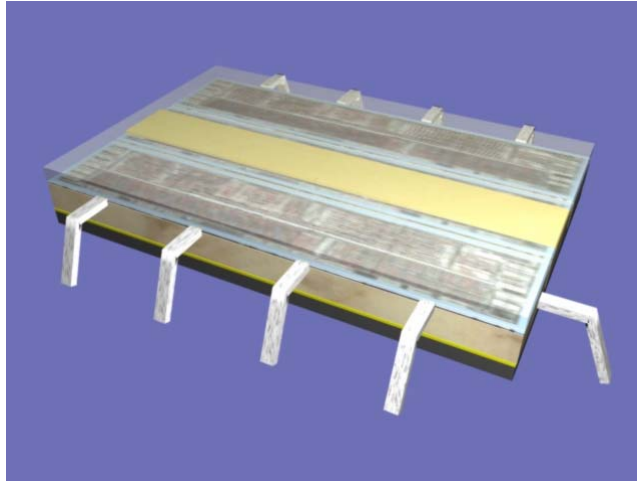
Figure 71 Structure of the single-chip wireless moisture sensor under development at UH. The center copper strip is used as the sensor head. An external antenna pin is at the right-hand side of the chip. Three sections are on the chip (from near side to far side): digital section, RF section, and analog/baseband section. This is a view without the packaging and corrosion protective layer on top of the sensor head. The actual chip is completely sealed for protection.
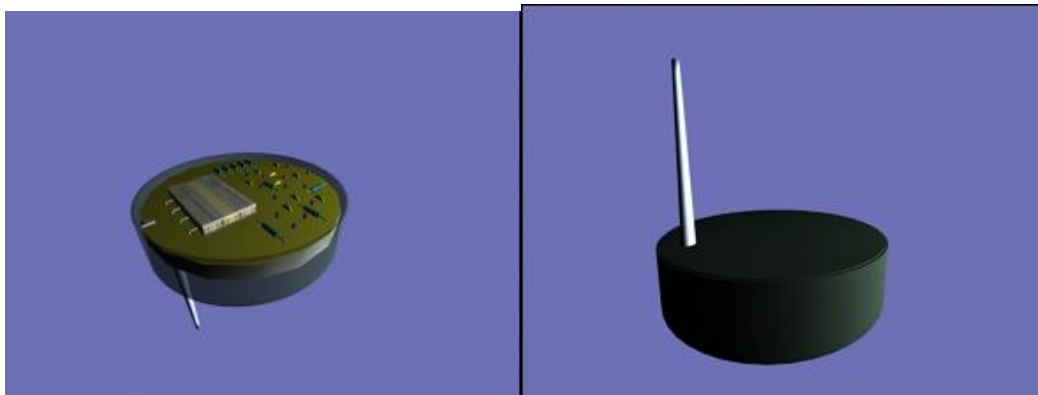
(a)   (b)

Figure 72 Structure of the wireless pavement temperature and moisture sensor. The diameter is about 1 in., and the height is ½ in. (a) Back view with cover removed; (b) packaged view

4.2.2 RFID System [103]-[110]

Longer reading distances, higher data rates, and smaller antenna sizes introduce a strong interest in RFID transponders operating in the UHF band. Figure 73 presents an overview of the proposed framework, allowing the functionality verification of individual components to reflect application-wide parameters.
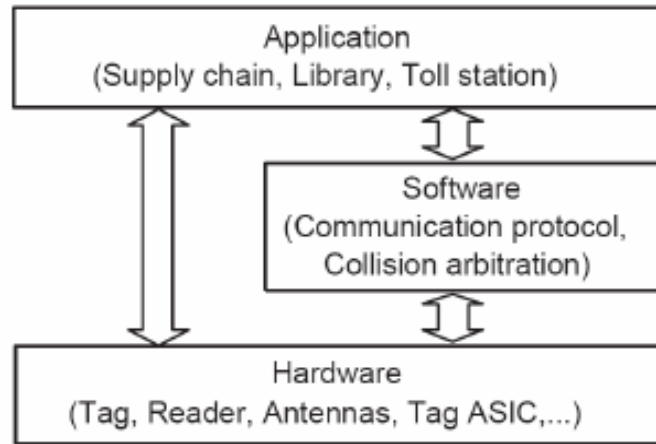
Figure 73 Overview of UHF RFID modeling framework (after V. Derbek et al. [103])
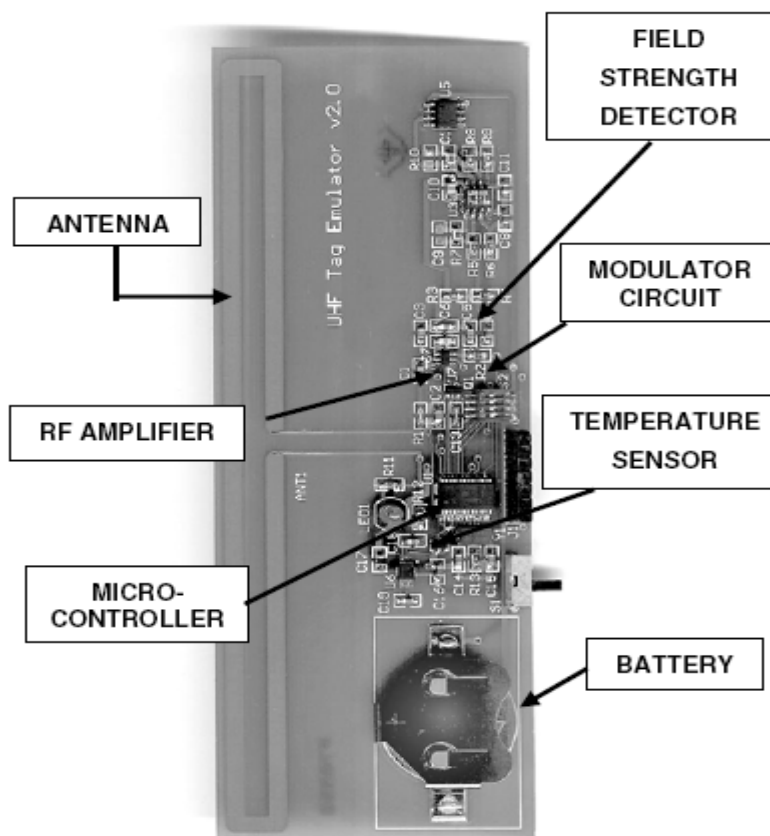
Figure 74 Active UHF RFID tag example (after R. Redemske and R. Fletcher [104])

Figure 74 shows the photograph of one of the tag emulator designs containing both a field-strength-sensor as well as a temperature sensor. Battery-powered backscatter tags have been used for many years as RFID transponders (e.g., for highway toll-collection systems or tracking radioactive materials as an example shown in Figure 75), such a device can be employed in many ways as a testing tool for RFID systems as well as a general-purpose communications link to other electronic devices. A variety of UHF antennas can be employed for this tag; however, for longer distances, precise impedance matching and a large scattering cross-section are preferred [105]. It is important to maximize the bandwidth of the antenna since UHF RFID systems typically implement frequency hopping over a range of frequencies (e.g., 902-928 MHz in North America). This bandwidth requirement for tag antennas is often difficult to achieve, but is necessary for consistent tag operation. In free-space, folded dipole designs are common, although more creative designs may be optimized to minimize total antenna size or improve readability when near certain materials such as metals or water.

Figure 75 Lab test of active UHF RFID tag (after R. Redemske and R. Fletcher [104])

The issue related with active UHF RFID is the battery, and more and more research interests are focused on passive UHF RFID. The most important part for a successful passive UHF RFID is its RF power-transmission system design. The key criteria for passive UHF RFID antenna design is the Friis Free-space Formula [106],

$$r = \frac{\lambda}{4\pi}\sqrt{\frac{P_t G_t G_r \tau}{P_{th}}}$$

where λ is the wavelength, P_t is the power transmitted by the reader, G_t is the gain of the transmitting antenna, G_r is the gain of the receiving tag antenna, P_{th} is the minimum threshold power necessary to provide enough power to the RFID tag chip, τ is the power transmission coefficient at the tag side, and r is the transmission distance.

For the passive UHF RFID tag, the signal modulation method can be amplitude-shift-keying (ASK), phase-shift-keying (PSK), and frequency-shift-keying (FSK). The commercial product from Texas Instruments is using FSK modulation. Figure 76 and 77 show examples of PSK and ASK UHF RFID tags.
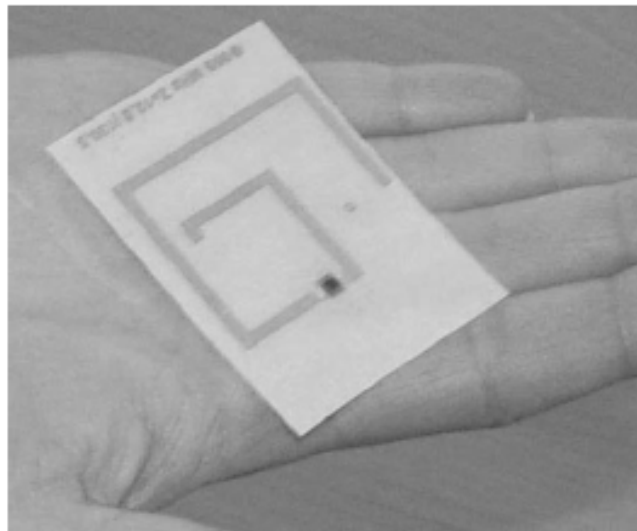
Figure 76 Example of a passive UHF PSK RFID tag (after U. Karthaus and M. Fischer [107])

The UHF PSK RFID tag shown in Figure 75 is assembled with the printed loop antenna. For details see References [107] section. Figure 76 shows an innovative double-frequency UHF ASK RFID tag.
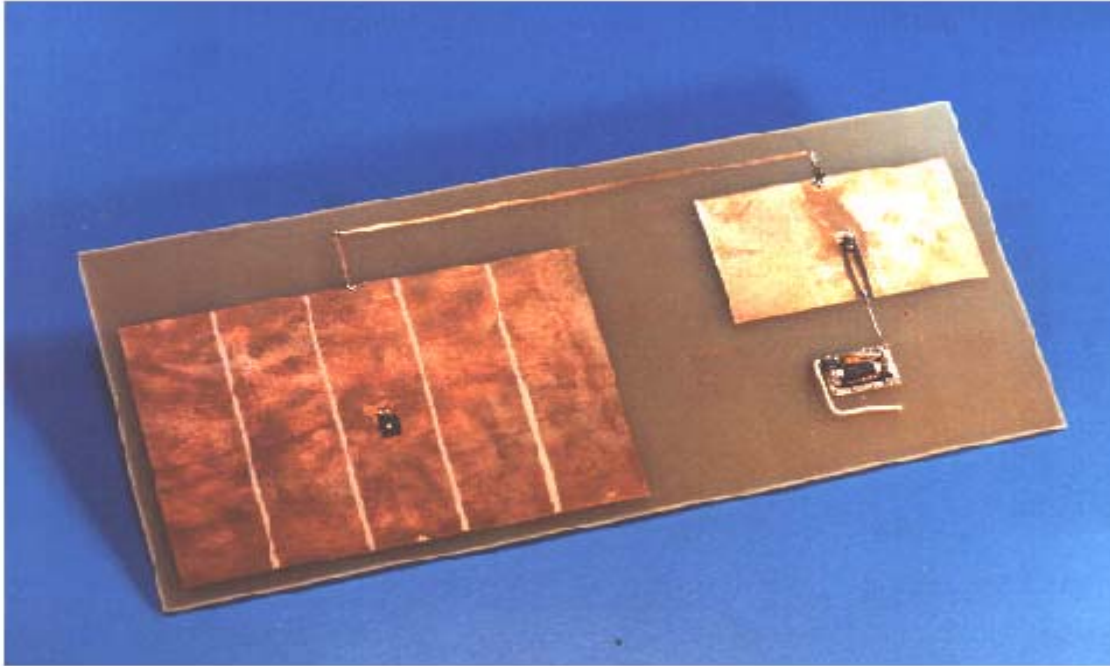
Figure 77 Example of a passive UHF ASK RFID tag (after R. Page [108])

The transponder's surprisingly low power requirement is due to its efficient means of rectification, frequency doubling, and modulation. All of these functions are accomplished by a single microwave diode. The 915-MHz patch antenna has two connections, a DC return path connected at the zero impedance point, and a transmission line matched to the 120-ohm impedance at the edge of the antenna. The transmission line routes the signal to CR1 for rectification. A DC tap on the 1830-MHz antenna provides the power connection for the microcontroller unit (MCU). Careful placement of CR1 along the transmission line is crucial in creating the proper alternating current impedances for efficient frequency doubling. The 1830-MHz antenna becomes a 90-degree open stub at 915 MHz at the cathode of CR1, effectively giving the 915-MHz signal a low-impedance trap to work against. Since the transmission line does not provide similar low impedance on the anode side of CR1, a 90-degree open stub at 1830-MHz must be added.

These UHF RFID tags can be used for TxDOT inventory tracking. For example, a vehicle can collect the inventory information while running on the street as shown in Figure 78.
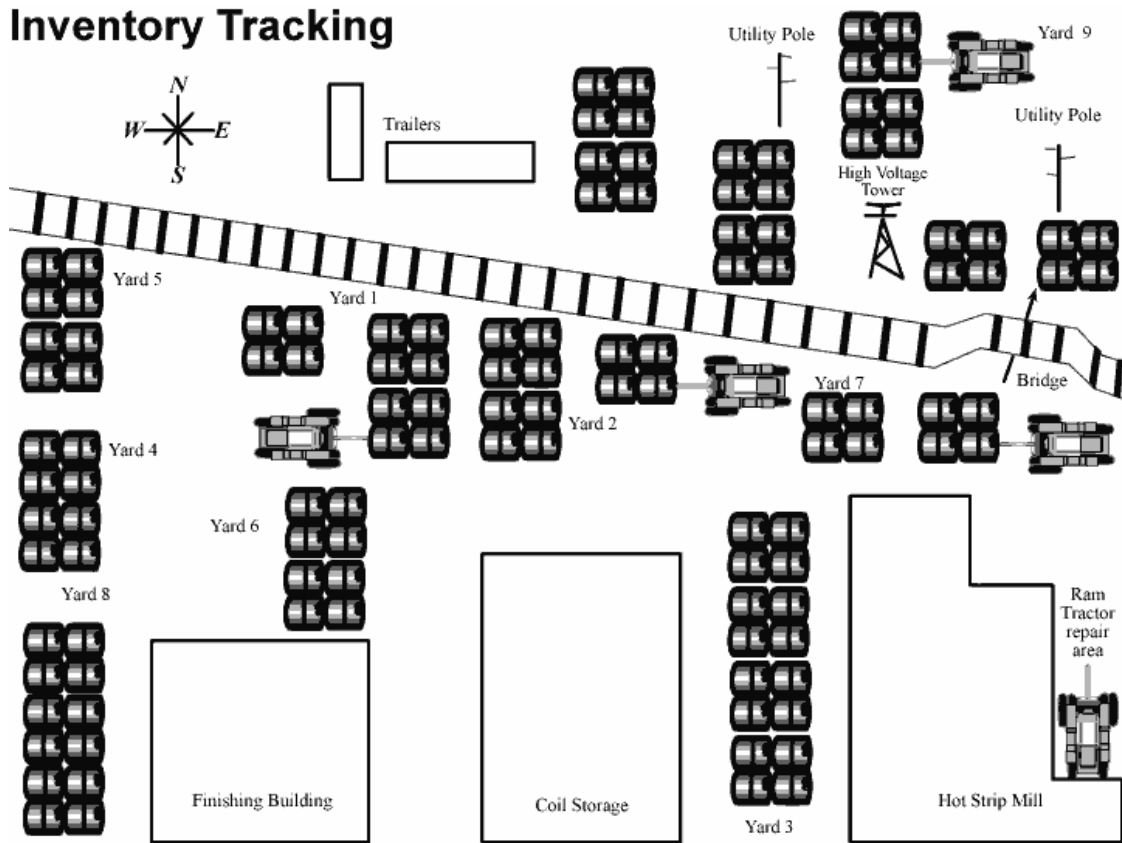
Figure 78 Demo of RFID inventory tracking (after Current Directions, Inc. [109])

Besides inventory tracking for TxDOT, RFID architecture can also be utilized as a highway or bridge monitoring system, as shown in Figure 79.
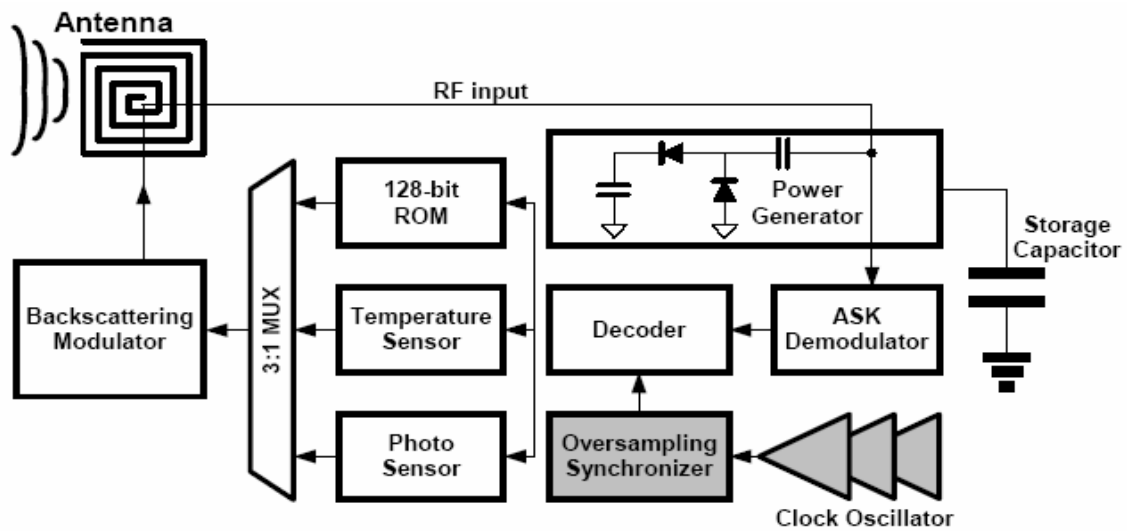
Figure 79 RFID sensor network (after N. Cho et al. [110])

Take the temperature measurement, for example. Figure 80 shows the results based on the RFID sensor network.
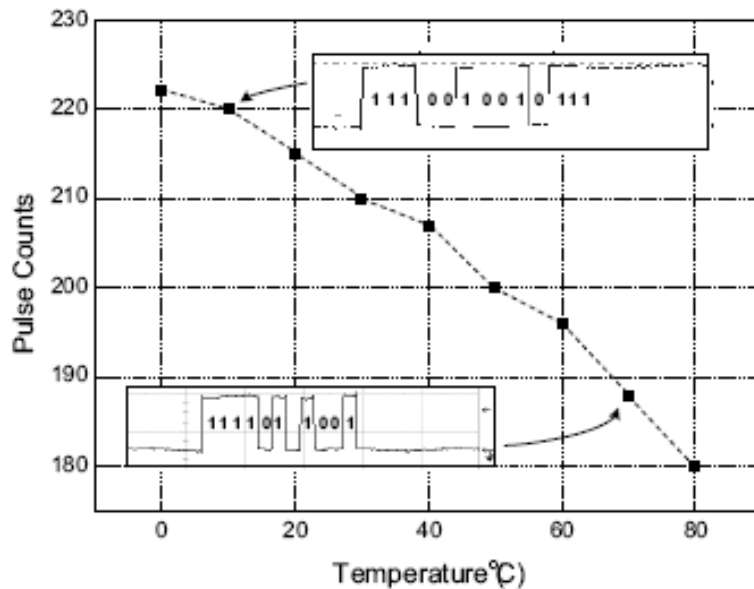
Figure 80 The measured characteristics of the temperature sensor (after N. Cho et al. [110])

The research team at the University of Houston is currently working on a passive RF MEMS sensor network. The sensor will be activated by the RF signal from a reader. These passive RF MEMS sensors will collect the pavement information and send it to the reader. The reader can even send commands to the MEMS sensors to perform simple tasks, such as emitting auto-healings for innovative materials to seal pavement cracks. Researchers at the University of Houston are currently testing these passive RF MEMS sensors. The sensor information can also be sent to the Internet and then stored at a central server. Because these sensors are passive, it makes maintenance low cost.

4.3 Bulky Sensors in Transportation

Bulky sensors usually come with a bulky radio module. Their dimension can not be smaller than 10^{-1} m.

4.3.1 Low-Cost Microwave WIM Sensor [111]

In TxDOT Project 0-4509 [111], the University of Houston team developed a low-cost WIM sensor using RF MEMS technology and filed a few patents. This WIM sensor can be made as short as a few millimeters or can be as long as a few meters. The cost of each sensor is less than $100, compared to a few thousand of dollars if conventional WIM sensors are used. This innovative WIM sensor is being developed and implemented in asphalt pavement for traffic load monitoring. Figure 81 is the field test setup of this low-cost WIM sensor.

a) Field test setup   b) Communication hub

Figure 81 Field test of low-cost microwave WIM sensor (after TxDOT Project 0-4509 [111])

Figure 82 shows the original WIM signal and the recovered WIM signal. This low-cost WIM sensor system also considers environmental influences, such as temperature and moisture, on the final results.
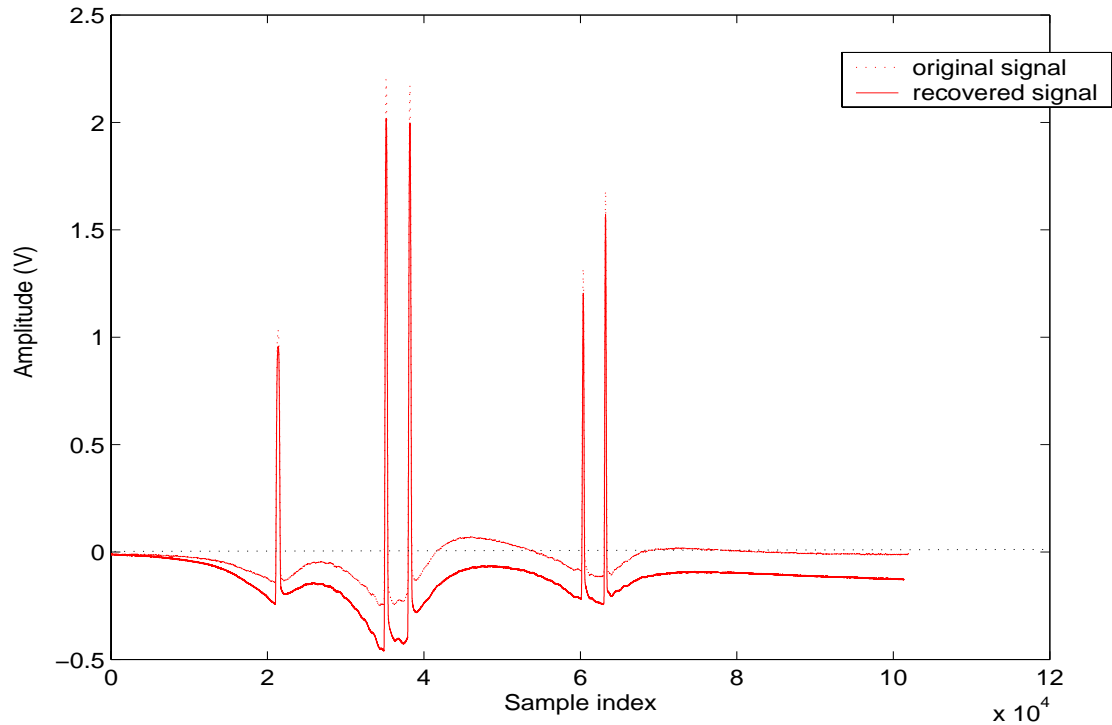
Figure 82 Low-cost WIM sensor results recovery (after TxDOT Project 0-4509 [111])

4.3.2 Sensor Networks with Communication and Control of Smart Materials and Sensors [112] [116]

Application of embedded nano and MEMS sensors entails burying them in the highway structure or pavement structures with no physical connection to the outside world. The MEMS and nanotechnology has the potential to integrate the wireless system, the microsensor, and the power supply together. Some wireless sensors are being studied.

The University of Houston research team developed a very low cost ($2) radio transceiver (see Figure 83). The wireless data transceiver operates at a 2.4-GHz frequency and can be tuned in the range from 0.9 GHz to 3.5 GHz by software. This radio device can transmit data at 2.3 Mbps, with an average power consumption of 6 mW. Transmission distance ranges are dynamically controlled up to 300 ft. The antenna of this

radio is printed on the printed circuit board (PCB). The size of this radio transceiver can be further reduced, and the research team is now working on a new version that is as small as a dime, including batteries. Due to the flexibility and low-power consumption, this radio can be directly used as a data transfer device for the sensors in pavements. A small battery will last for a couple of years.
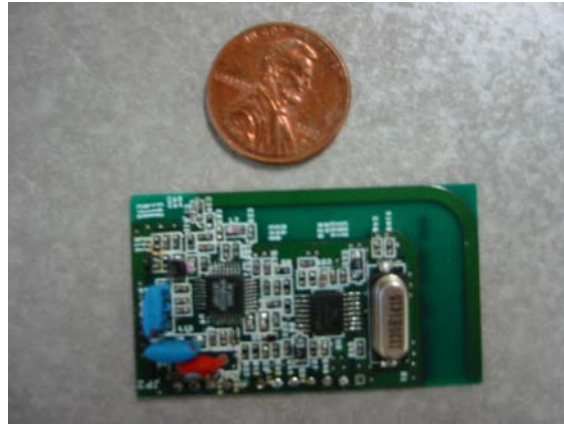
Figure 83 A low-cost, high-performance radio device developed at UH

This radio can transmit and receive data up to 300 ft, with an average power consumption of 6 mW in burst mode.

The University of California-Berkeley is experimenting with MEMS which they call motes [112]. The Golden Gate Bridge now has an experimental sensor network of approximately 200 small motes, each with an accelerometer that measures movement such as traffic, wind, or seismic loads. Using RF, sensor readings are wirelessly sent to more powerful computers for data analysis. Any anomalies might indicate a weakness in structural integrity, alerting engineers to repairs that can help keep the span safe in case of an earthquake or other natural disaster. Figure 84 shows the view of the mote sensor.

Figure 84 The motes sensor (after the University of California-Berkeley [112])

Jennifer Bernhard of the University of Illinois Urbana-Champaign is using electromagnetic finite element models to determine the range and spatial (area) resolution of wireless sensors embedded in concrete or soil under various conditions [112]. Researchers at Johns Hopkins University's Applied Physics Laboratory have developed a robust wireless embedded sensor suitable for long-term field monitoring of corrosion in rebar, particularly in bridge decks [113]. These Smart Aggregates sensors can be embedded throughout a structure during concrete construction, added right to the mix before placement. The system is made up of the Smart Aggregates and a data reader that can be mounted on a car or truck. The reader powers the aggregates as it passes over them and collects the sensor data onto a personal computer (PC). Each Johns Hopkins Smart Aggregate contains a wireless power receiver and data transmission coils, and it is designed using ceramic hybrid integrated circuit technology, to withstand mechanical stresses and the high-pH environment of concrete. The aggregates are built to have a lifetime of over 50 years. The wireless power transmission and data collection approach eliminates the need for and potential problem with batteries, cables, and connectors. Prototype Smart Aggregates have been manufactured and are undergoing reliability measurements.

Intel is testing sensor network technology by installing motes that monitor cooling equipment in one of its manufacturing plants [114]. In this project, sensors watch for abnormal vibrations that could indicate worn bearings or failing compressors in the

machines. Alerts are wirelessly transmitted to a central control system, keeping small mechanical problems from becoming costly production issues.

The research of F. G. Yuan seeks to develop a multisensor data fusion information framework for aerospace structural health monitoring (SHM) using smart sensors [115]. The smart sensors are capable of exciting a diagnostic signal, measuring physical parameters, interpreting and collaborating the data into information, and communicating with a monitoring station over a wireless link. The MICA platform developed at UC-Berkerley is used as a basis of this research [116]. The work is targeted at developing an active distributed smart sensing system for quantifying and visualizing location and sizing of damage in aerospace structures in near real time. The proposed research will lay the groundwork for a novel wireless smart sensor network technology for near real-time intelligent monitoring of complex aerospace systems and a broad set of physical phenomena.

From the review of the recent development on nano and MEMS techniques, we can see that almost all the techniques that have potential applications in transportation condition monitoring are being developed in other industrial fields. Some of them have been proved to be feasible and reliable. For the specific application environment in transportation infrastructure, we have to develop our specific sensors and systems. There will be a lot of challenges, and there also will be many opportunities.

CHAPTER 5 EXAMPLES OF NANOTECHNOLOGY

APPLICATIONS

Road and warning signs contribute significantly to the overall safety of transportation and other utilities. Oftentimes, needless accidents result due to incorrectly placed or missing warning signs. Lack of information is concluded as the ultimate cause of the accident, but this can easily be remedied. The purpose of this demo application is to develop a network of sensors which can easily communicate back to a central location about the whereabouts of a warning sign or damage sustained by a warning sign. Consider the following cases.

Case 1: Missing Stop Sign

Although efforts are made to decrease crime rates by large cities, many small crimes go unreported. Oftentimes part of pranks involve the removal of stop signs or other road signs which may adversely affect the safety of the drivers and passengers on the roadway. The removal of these signs can lead to serious accidents if, for example, stop signs are removed from an intersection.

Case 2: Military Base

Military bases are often storage sites for extremely hazardous materials and cargo such as land mines, warheads, and automatic weapons. Warning signs and fence posts are used to designate areas where civilians should not enter. The removal of these signs by perpetrators can seriously jeopardize the safety of nearby inhabitants.

Case 3: Natural Disaster

After a natural disaster or severe weather, no knowledge is known of the condition of road and warning signs. During a hurricane winds of up to 150 mph can sweep away road signs and traffic lights, or drive other debris through the signs, damaging them beyond function. Hurricanes are not the only natural disasters of significance. In the Midwest tornadoes wreak similar havoc with wind speeds reaching 300 mph. In the Northeast

winter storms can bring winds up to 50 mph and several feet of snow and ice. In the West Coast earthquakes can bring down large buildings and obliterate roads. After any severe weather recovery becomes a difficult process and citizen safety should be of first concern. Signs which can monitor their own condition can allow response crews to immediately replace lost warning signs. In addition to quicker response large amounts of money can be saved by preventing the need for safety crews to manually inspect each and every road and warning sign.

All of these dangerous situations can be avoided if monitoring of road and warning signs could be done on a real-time basis. In addition to potentially saving lives and preventing accidents this system could save money and maintenance time by removing the necessity for city workers to visually inspect road and warning signs after severe weather or natural disasters. Instead, a central monitoring station, ideally housed inside the same building as the emergency management headquarters for a city, would be able to have real-time monitoring of a sensor network and specifically identify any misplaced warning signs.

5.1 Demo Application Description

The overall demo system is shown in Figure 85. In this demo application, MEMS magnetic compass and accelerometer are used. The magnetic compass is used to detect the rotation of the stop sign and the accelerometer is used to detect the static tilt of the stop sign. A radio system is used to wirelessly acquire the data from both the magnetic compass and accelerometer.
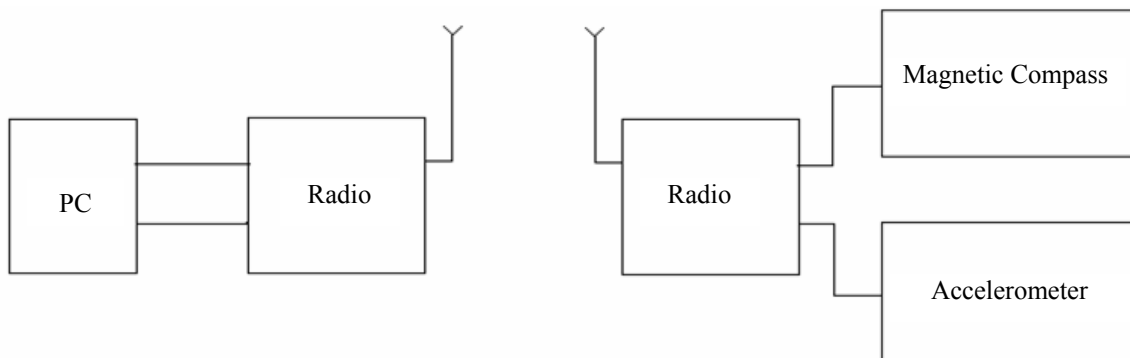
Figure 85 Overall demo application diagram

A demo prototype system is shown in Figure 86.
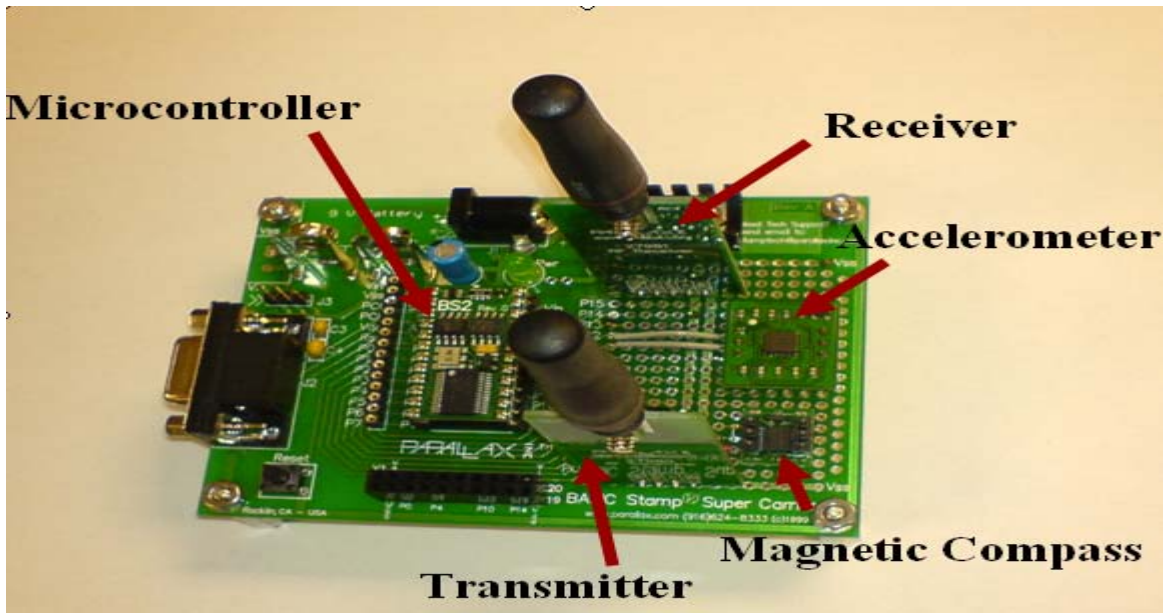
Figure 86 Prototype demo system

The working principle of magnetic compass is shown in Figure 87.
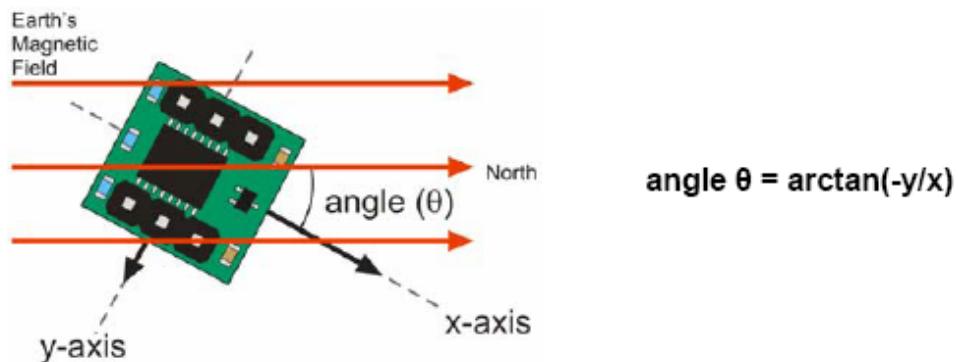
Figure 87 Working principle of magnetic compass

The MEMS compass sensor has two axes, x and y. Each axis reports the strength of the magnetic field's component parallel to it. The x and y components of the magnetic field are reported as the voltage difference (Vx and Vy) by the sensor. Vx and Vy are given by the following two equations,

$$Vx = (field\_strength) * \cos\theta$$

$$Vy = (field\_strength) * \sin\theta$$

Then the angle can be calculated using the equation given below

$$\theta = \tan^{-1}\left(\frac{-Vy}{Vx}\right)$$

When the magnetic compass points towards the north, Vx is at maxima and Vy is at its minima. Likewise, Vy is maximum when the compass points towards east or west.

The working principle of accelerometer is shown in Figure 88.
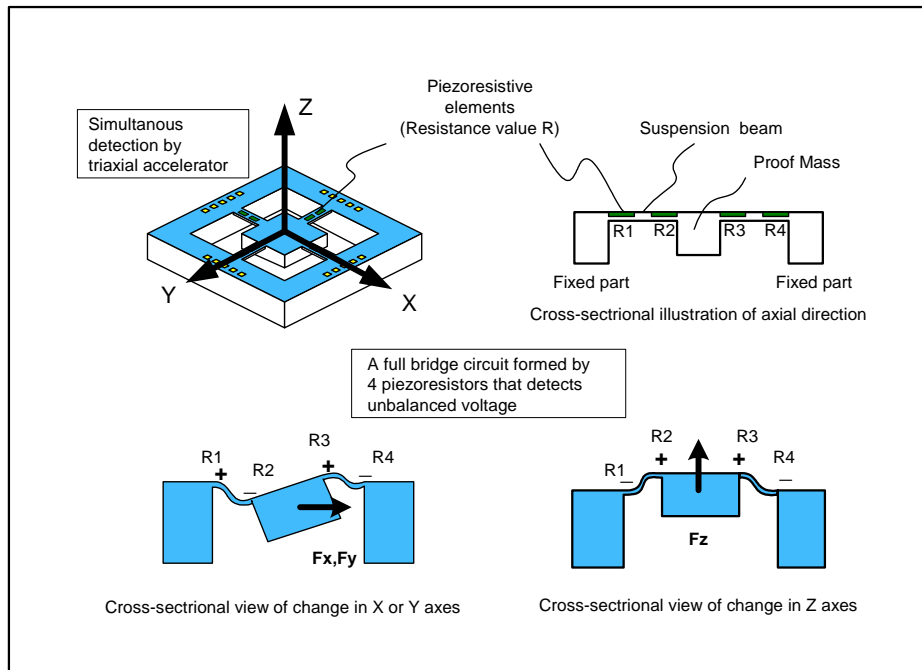
Figure 88 Working principle of three-axis piezoresistive accelerometer

The MEMS accelerometer uses piezoresistive strain gauges acting as arms of a Wheatstone bridge to convert mechanical strain to a DC output voltage. Deflection of the accelerometers proof mass (caused by an applied acceleration along the x axis) leads to bending around the suspension beam, in turn stretching two of the piezoresistors (R1 and R3) and compressing the others (R2 and R4). This leads to increased resistance in the

stretched piezoresistor and decreased resistance in the compressed piezoresistor. By detecting the change in resistance, the acceleration can be measured.

After measuring the DC acceleration in z direction of the sensor (see Figure 89), the static tilt of the stop sign can be calculated as below.

$$\theta = \tan^{-1}\left(\frac{-g_z}{g}\right)$$
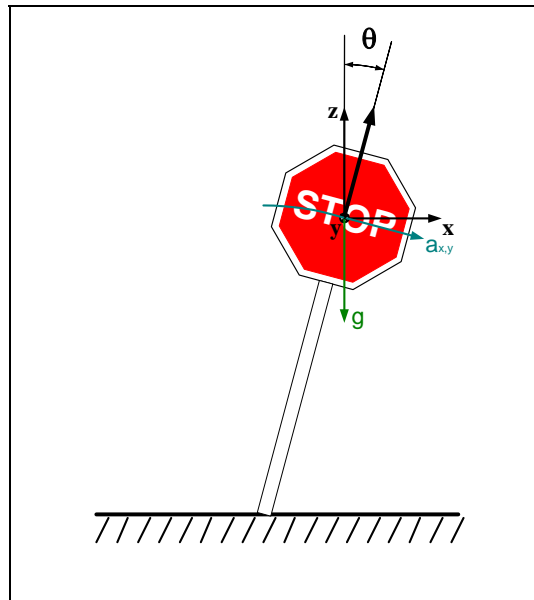
Figure 89 Tilt angle measurement using accelerometer

After the MEMS magnetic compass and accelerometer measure the rotation and tilt of the stop sign, the signal will be send out wirelessly by a radio chip to the PC. Software is developed to monitoring the rotation angle as well as the tilt angle of the stop sign in real time (see Figure 90). Figure 91 and Figure 92 show the demo hardware under test.
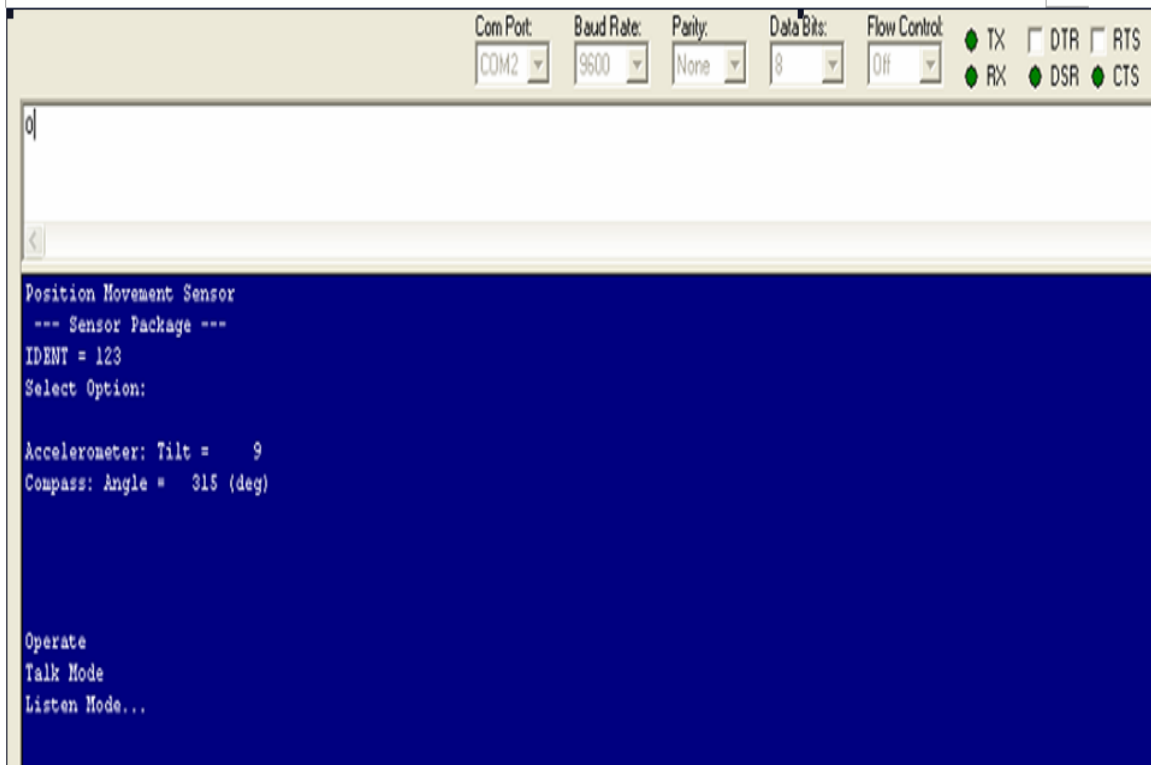
Figure 90 Demo software interface

Figure 91 Demo hardware under test.
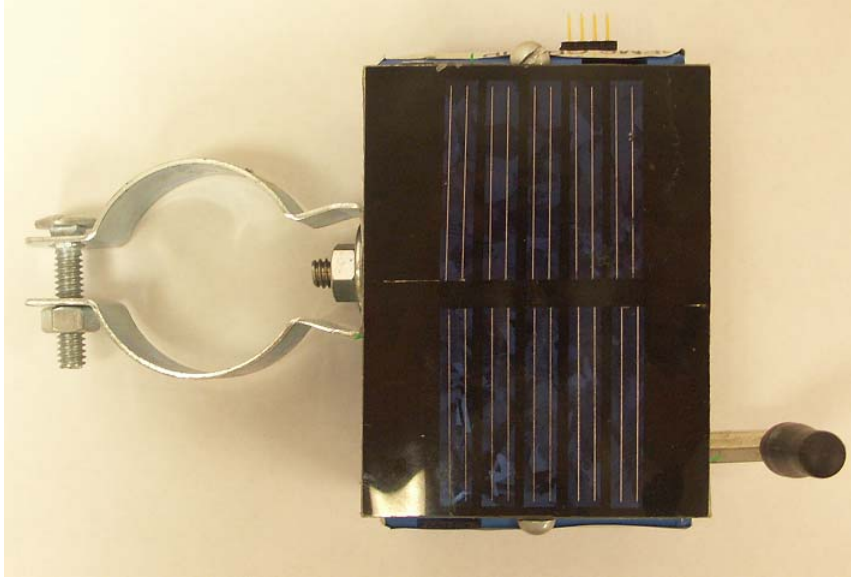
Figure 92 Top view of the demo MEMS sensor.

CHAPTER 6 CONCLUSIONS AND DISCUSSIONS

Based on the investigations performed in this project, we find that there are many aspects of nanotechnologies that can be applied to transportation systems. However, the successful nanotechnology application may need 5 or 10 years to be commercialized. Two categories of nano-products have great potential to transportation: 1) nanotechnology-based materials and 2) nanotechnology-based sensors. Smart materials are materials with sensors and actuators built in. Nano-based sensors are also called MEMS. In transportation applications, sometimes we prefer bigger sensors and actuators to small-scale ones. Therefore, many emerging sensors, even though they are not nano-based sensors, are useful, such as microwave and fiber-optic WIM sensors [111]. At the current stage, nano materials and smart materials are still in the lab stages. Practical applications will come 5 to 10 years from now. However nano-based sensors are getting to the implementation stages. Possible applications of nanosensors include the following:

1. Stop sign monitoring sensor network: a MEMS accelerometer and a magnetometer collects the rotation and tilt information of stop sign. And it is very useful in maintaining the safety of transportation. Details are discussed in the demo application.

2. RF tags: RF tags are mostly used for replacing bar codes for inventory purposes. The costs of RF tags are getting very low. Passive RF tags are in the sub-dollar range in quantities. The distance to which an RF tag can send signals is about a few feet to 100 ft. Passive RF tags have a sensing range of only a few feet. Active RF tags have a longer distance, up to about 100 ft, depending on the operating frequencies. TxDOT can use RF tags for pavement on-site monitoring, traffic sign position locations, monitoring to prevent signs from being moved, and materials inventory.

3. MEMS-based sensors: Examples of such sensors include MEMS-based accelerometers, which can be used in a profiler to replace costly coil-type accelerometers. Due to the low-cost nature of the MEMS accelerometer ($10 each in small quantities, in contrast to $800 for coil-type accelerometers), several MEMS accelerometers can be stacked for lower measurement noise, to extend a lower speed limit to the profiler. The current profiler has a low speed limit of 20 miles per hour, which is sometimes a problem.

4. Innovative sensors and actuators that are not based on nanotechnologies: There are emerging sensors and actuators that use advanced technologies, but not based on nanotechnologies. And that may have great application potentials to TxDOT, such as fiber-optic sensors and microwave WIM sensors [111].

In a few years, the sensors and actuators using nano and other technologies will have a lower cost and be in production. TxDOT is in a good position for applying these materials and sensors in Texas highways in the future to reduce maintenance costs, increase pavement lifespan, reduce accidents, and increase construction efficiency.

REFERENCES

[1]   R. Feynman. "There's Plenty of Room at the Bottom." Caltech's Engineering & Science Magazine, February, 1960. (Reprinted in Micromechanics and Mems: Classic and Seminal Papers to 1990, Edited by W. Trimmer, the IEEE Press PC4390-QCL, January 1997, page 3.)

[2]   R. G. Griffin. "The Future of MEMS, Microelectromechanical Systems in Transportation Engineering." Committee on Applications of Emerging Technology, October 2003.

[3]   Prime Faraday Technology Watch Group. "Introduction to MEMS." Prime Faraday Technology Watch, 2001.

[4]   M. Madou. "Fundamentals of Microfabrication" 2nd edition, CRC Press, 2002.

[5]   Daniel C. S. Bien. "Membrane Valve." Northern Ireland Semiconductor Research Center, 2004.

[6]   G. T. Kovacs. "Micromachined Transducers Sourcebook." WGB/McGraw-Hill, 2000.

[7]   M. Elwenspoek and H. Jansen. "Silicon Micromachining." Cambridge, 1998.

[8]   The Micro and Nano Systems Research Group. "Bulk Machining Figure." TIMA Laboratory, Grenoble, France, 2005.

[9]   R. C. Jaeger. "Introduction to Microelectronic Fabrication" 2nd edition, Prentice Hall, 2001.

[10]   "Tutorial on MEMS and Micromechanics," www.trimmer.net.

[11]   MEMS Foundry Services, http://www.memsservices.com/ms-foundry.shtml.

[12]   J. Woodard, N. Ferrell, and D. Hansford. "Design, Fabrication, and Optimization of a Polymer MEMS Cell Force Sensor for Measuring Single Cell Biomechanics." The IASTED Conference on Biomedical Engineering, 2005.

[13]   G. M. Atkinson, R. E. Pearson, Z. Ounaies, C. Park, J. S. Harrison, W. C. Wilson, and J. A. Midkiff. "Piezoelectric Polyimide MEMS Process." Proceedings of the NASA VLSI Symposium, May 2003.

[14]   X. F. Wang, J. Engel, and C. Liu. "Liquid Crystal Polymer (LCP) for MEMS: Processes and Applications." Hournal of Micromechanics and Microengineering 13:5, pp. 628-633, September 2003.

[15]   J. Xie, J. Shih, and Y.-C. Tai. "Integrated Surface-Micromachined Mass Flow Controller." in MEMS '03, 2003. Kyoto, Japan.

[16]   C. Liu. "Foundations of MEMS." University of Illinois at Urbana-Champaign, 2005.

[17]   Long-Range Research Plan and Project Information, RMC 1, Texas Department of Transportation, Spring, 1998.

[18]   C. Liu et al. "Investigation of Short Range Sensing Devices for Use in Non-Destructive Pavement Evaluation." Final Technical Report to Texas Department of Transportation, October 2000.

[19]   T. Kuennen. "Small Science Will Bring Big Changes To Road." Better Roads, 2004, http://www.betterroads.com/articles/jul04a.htm.

[20]   T. A. Plaisted, A. V. Amirkhizi, D. Arbelaez, S. C. Nemat-Nasser, and S. Nemat-Nasser. "Self-Healing Structural Composites with Electromagnetic Functionality." www.ceam.ucsd.edu.

[21]   M. Oles, E. Nun, G. Dambacher, and B. Schleich. "Learning From Nature - Polymer Surfaces with a Nano Structure That Utilize the Lotus-Effect and Clean Themselves." lst Annual International IEEE-EMBS Special Topic Conference on Microtechnologies in Medicine & Biology, 2000.

[22]   W. Barthlott and C. Neinhuis. "The Purity of Sacred Lotus or Escape from Contamination in Biological Surfaces." Planta 202: 1-8, 1997.

[23]   B. Brooks. "Nanotechnology Will Change Our Roads." Washington State Technology Transfer, 2005.

[24]   J. Y. Kim, C. Cohen, M. L. Shuler, and L. W. Lion. "Use of Amphiphilic Polymer Particles for In Situ Extraction of Sorbed Phenanthrene from a Contaminated Aquifer Material." Environmental Science & Technology, Vol. 34, 2000, pp. 4133-4139.

[25]   W. Tungittiplakorn, L. W. Lion, C. Cohen, and J. Y. Kim. "Engineered Polymeric Nanoparticles for Soil Remediation." Environmental Science & Technology, Vol. 38, 2004, pp. 1605-1610.

[26]   A. K. El Wahed, J. L. Sproston, and G. K. Schleyer. "Electrorheological and Magnetorheological Fluids in Blast Resistant Design Applications." Materials and Design, Vol. 24, No. 4, 2002, pp. 391-404.

[27]   C. S. Cai, W. Wu, S. Chen, and G. Voyiadjis. "Applications of Smart Materials in Structural Engineering." Louisiana Transportation Research Center, 2004.

[28]   S. R. Sharp "State-of-the-Art Survey of Advanced Materials and Their Potential Application in Highway Infrastructure." Virginia Transportation Research Council, 2004.

[29]   Jsemmens@cox.net "Transportation Research Digest." Arizona Transportation Institute, 2005.

[30]   L. S. Ingram, K. D. Herbold, T. E. Baker, J. W. Brumfield, M. E. Felag, T. R. Ferragut, M. G. Grogg, L. R. Lineman, and R. O. Rasmussen. "Superior Materials, Advanced Test Methods, and Specifications in Europe." Office of International Programs, Office of Policy, Federal Highway Administration, U.S. Department of Transportation, 2004.

[31]   N. Adams and D. B. Strokes. "Using Advanced Lithium Technology to Combat ASR in Concrete." Concrete International, 2002.

[32]   T. Kuennen. "FHWA Research Zeroes in on Concrete Nanotechnology." Concrete Products,   2004. http://concreteproducts.com/mag/concrete_fhwa_research_zeroes/index.html

[33]   Research groups in Michigan Tech Transportation Institute, Michigan Technological University Civil and Environmental Engineering Department. "Guidelines for Detection, Analysis, and Treatment of Materials-Related Distress in Concrete Pavements." Federal Highway Administration Turner-Fairbank Highway Research Center, 2002.

[34]   M. Collepardi. "Delayed Ettringite is an Internal Sulfate Attack on Concrete." http://www.uwm.edu/~ymchun/CBU/Collepardi.DEF.pdf.

[35]   M. Heinrich and Michael Janauschek. "Improvements in Pavement Research with Accelerated Load Testing." EPFL-LAVOC, Switzerland, 2003.

[36]   D. H. Timm and A. L. Priest. "Dynamic Pavement Response Data Collection and Processing at the NCAT Test Track." National Center for Asphalt Technology, 2004.

[37]   C. Ozyildirim. "Evaluation of Continuously Reinforced Hydraulic Cement Concrete Pavement at Virginia." Virginia Department of Transportation and the University of Virginia, 2004.

[38]   S. M. J. G. Erkens, A. Scarpas, and A. A. A. Modlenaar. "Asphalt Concrete Response Evaluation: Analytical and Experimental Aspects." Delft University of Technology, 2000.

[39]   N. Garg and G. F. Hayhoe. "Asphalt Concrete Strain Responses at High Loads and Low Speeds at the National Airport Pavement Test Facility (NAPTF)." 1 Galaxy Scientific Corporation, 2000.

[40] J. C. Duke. "Health Monitoring of Post Tension Tendons." Department of Engineering Science and Mechanics, Virginia Polytechnic and State University, 2002.

[41] L. Lin, A. P. Pisano, and R. T. Howe. "A Micro Strain Gauge with Mechanical Amplifier." *Journal of Microelectromechanical System,* vol. 6, no. 4, December 1997.

[42] K. Wang, J. K. Cable, and G. Zhi. "Investigation into Improved Pavement Curing Materials and Techniques." Center for Transportation Research and Education, Iowa State University, 2002.

[43] S. Mindess and J. F. Young. *Concrete*. Prentice-Hall, Englewood Cliffs, N.J., 1981.

[44] K. Kupfer. "Material Properties, Measuring Methods, Applications." Materialforschungs- und -prüfanstalt an der Bauhaus-Universität Weimar, Germany, 2001.

[45] T. L. Yeo, D. Eckstein, B. McKinley, L. F. Boswell, T. Sun, and K. T. V. Grattan. "Demonstration of a Fibre-Optic Sensing Technique for the Measurement of Moisture Absorption in Concrete." *Smart Materials and Structures*, 2006.

[46] W. Xie, T. Sun, K. T. V. Grattan, D. McPolin, P. A. M. Basheer, and A. E. Long. "Fibre Optic Chemical Sensor Systems for Internal Concrete Condition Monitoring." Proc. 2nd European Workshop on Optical Fibre Sensors, vol. 5502, pp. 334–7, 2004.

[47] C. -Y. Lee and G. -B. Lee. "MEMS-based Humidity Sensors with Integrated Temperature Sensors for Signal Drift Compensation." Sensors, 2003. Proceedings of IEEE.

[48] K. Govardhan and Z. C. Alex. "MEMS Based Humidity Sensor." Department of Electronics and Instrumentation, Vellore Institute of Technology, Vellore, INDIA , 2005.

[49] T. J. Harpster, B. Stark, and K. Najafi. "A Passive Wireless Integrated Humidity Sensor." Center for Wireless Integrated Microsystems, University of Michigan, Micro Electro Mechanical Systems, the 14th IEEE International Conference on (MEMS), 2001.

[50] T. Harpster, S. Hauvespre, M. Dokmeci, B. Stark, A. Vosoughi, and K. Najafi. "A Passive Humidity Monitoring System for In-Situ Remote Wireless Testing of Micropackages." Center for Wireless Integrated Microsystems, University of

Michigan, Micro Electro Mechanical Systems, the 13th Annual International Conference on (MEMS), 2000.

[51]   T. J. Harpster, S. Hauvespre, M. R. Dokmeci, and K. Najafi. "A Passive Humidity Monitoring System for In Situ Remote Wireless Testing of Micropackages." Center for Wireless Integrated Microsystems, University of Michigan, *Journal of Microelectromechanical Systems*, 2002.

[52]   A. D. DeHennis and Khalil Najafi, "A Wireless Microsystem for the Remote Sensing of Pressure, Temperature, and Relative Humidity."   *Journal of Microelectromechanical Systems,* 2005.

[53]   U. Kang and K. D. Wise. "A High-Speed Capacitive Humidity Sensor with On-Chip Thermal Reset." *IEEE Trans. Electron Devices*, vol. 47, Apr. 2000.

[54]   A. J. Helmicki, A. E. Aktan, and V. J. Hunt. "Issues in Implementation of Structural Monitoring to Constructed Facilities for Serviceability with Damageable Considerations." Ohio Department of Transportation, Proceedings of American Control Conference, 1995.

[55]   A. Iraqi, R. Z. Morawski, A. Barwicz, and W. J. Bock. "Distributed Data Processing in a Telemetric System for Monitoring Civil Engineering Constructions." *IEEE Transactions on Instrumentation and Measurement,* vol. 48, no. 3, 1999.

[56]   C. H. McGogney. "Magnetic Flux Leakage for Bridge Inspection." *Nondestructive Testing Methods for Civil Infrastructure,* ASCE, 1995, pp. 31–44.

[57]   S. B. Chase and G. Washer. "Nondestructive Evaluation for Bridge Management in the Next Century." Federal Highway Administration Publication, July 1997.

[58]   J. P. Lynch, Y. Wang, and K. H. Law. "Validation of a Large-Scale Wireless Structural Monitoring System on the Geumdang Bridge." Stanford University, University of Michigan, 2005.

[59]   Y. Wang, J. P. Lynch, and K. H. Law. "Wireless Structural Sensors Using Reliable Communication Protocols for Data Acquisition and Interrogation." Proceedings of the 23rd International Modal Analysis Conference, 2005.

[60]   J. P. Lynch, A. Sundararajan, K. H. Law, A. S. Kiremidjian, E. Carryer, H. Sohn, and C. R. Farrar. "Field Validation of a Wireless Structural Monitoring System on the Alamosa Canyon Bridge." SPIE's 10th Annual International Symposium on Smart Structures and Materials, San Diego, CA, USA, March 2-6, 2003.

[61]   C. R. Farrar, S. W. Doebling, P. J. Cornwell, and E. G. Straser. "Variability of Modal Parameters Measured on the Alamosa Canyon Bridge." Proceedings of the 15th International Modal Analysis Conference – IMAC, pp. 257-263, 1997.

[62]   S. W. Doebling, C. R. Farrar, and P. J. Cornwell. "A Statistical Comparison of Impact and Ambient Testing Results from the Alamosa Canyon Bridge." Proceedings of the 15th International Modal Analysis Conference – IMAC, pp. 264-269, 1997.

[63]   S. W. Doebling, C. R. Farrar, and R. S. Goodman. "Effects of Measurement Statistics on the Detection of Damage in the Alamosa Canyon Bridge." Proceedings of the 15th International Modal Analysis Conference – IMAC, pp. 919-929, 1997.

[64]   V. DeBrunner, M. Ta, Student, and D. Zhou. "On the Design of Structural Vibration Control Systems for Highway Bridges." 2004 IEEE Intelligent Vehicles Symposium.

[65]   N. Yazdi, F. Ayazi, and K. Najafi. "Micromachined Inertial Sensors." *Proc. IEEE,* vol. 86, pp. 1640–1659, Aug. 1998.

[66]   L. J. Ristic. "Surface Micromachined Polysilicon Accelerometer." Motorola, INC., IEEE Solid State Sensors and Actuators Workshop, Hilton Head, 1992.

[67]   L. -P. Wang, K. Deng, L. Zou, R. Wolf, R. J. Davis, and S. Trolier-McKinstry. "Microelectromechanical Systems (MEMS) Accelerometers Using Lead Zirconate Titanate Thick Films." *IEEE Electron Device Letters*, vol. 23, no. 4, 2002.

[68]   G. J. O'Brien and J. Hammond. "Outrigger: Solid Outer Frame Lateral Accelerometer Design." Solid-State Sensors, Actuators and Microsystems, 2005.

[69]   J. Wu, G. K. Fedder, and L. R. Carley. "A Low-Noise Low-Offset Capacitive Sensing Amplifier for a 50-µg/Hz Monolithic CMOS MEMS Accelerometer." *IEEE Journal of Solid-State Circuits,* vol. 39, no. 5, 2004.

[70]   S. Timoshenko and S. Woinowsky-Krieger. *Theory of Plates and Shells*, 2nd ed. New York: McGraw-Hill, 1959.

[71]   A. Leissa. "Vibration of Plates." Washington, DC: Sci. Tech. Inform. Div., NASA, 1993.

[72]   F. Mohad-Yasin, C. E. Korman, and D. J. Nagel. "Measurement of Noise Characteristics of MEMS Accelerometer." Semiconductor Device Research Symposium, 2001 International.

[73]   J. Chang, A. A. Abidi, and C. R. Voswanathan. "1/f Noise Sources." *IEEE Transactions on Electron Devices*, Vol. 41, no. 11, November 1994.

[74]   P. Singh, X. Wang, R. LaFollette, and D. Reisner. "RF-Recharged Microbattery for Powering Miniature Sensors." Sensors, 2004. Proceedings of IEEE.

[75]   J. N. Harb, R. M. LaFollette, R. H. Selfridge, and L. L. Howell. "Microbatteries for Self-Sustained Hybrid Micropower Supplies." *Journal of Power Sources,* 2002.

[76]   M. Krüger and Christian U. Grosse. "Structural Health Monitoring with Wireless Sensor Networks." Structural Health Monitoring with Wireless Sensor Networks, 2005.

[77]   C. U. Grosse, F. Finck, J. Kurz, and H. W. Reinhardt. "Monitoring Techniques Based on Wireless AE Sensors for Large Structures in Civil Engineering." Proc. EWGAE 2004 Symposium in Berlin, DGZfP: Berlin, BB90 (2004), pp 843-856.

[78]   A. E. Aktan, A. J. Helmicki, and V. J. Hunt. "Issues in Health Monitoring for Intelligent Infrastructure." University of Cincinnati Infrastructure Institute, University of Cincinnati, Cincinnati, 1998.

[79]   A. E. Aktan, A. J. Helmicki, V. Hunt, A. Levi, B. Sobecks, and R. Barrish. "Instrumentation, Testing and Monitoring of Reinforced Concrete Deck-on-Steel Girder Bridges." UCII Report UC-CII-9, 1996.

[80]   National Transportation Library, http://ntl.bts.gov//data/FY99_2.pdf.

[81]   C. B. Yun. "Recent R&D Activities on Structural Health Monitoring for Civil Infra-structures in Korea." Smart Infra-Structure Technology Center, Korea Advanced Institute of Science and Technology, Daejeon, KoreaLee, 2004.

[82]   J. D. Kim, C. B. Yun, J. H. Yi, and J. M. Shim. "Health-Monitoring Method for Bridges under Ordinary Traffic Loadings." *Journal of Sound and Vibration*, vol. 257(2), pp. 247-264, 2002.

[83]   G. Meltz, W. W. Morey, and W. H. Glenn. "Foxmation of Bragg Gratings in Optical Fibres by a Transverse Holographic Method." Opt. Lett., 14,823-825, 1989.

[84]   W. W. Morey, G. Meltz, and W. H. Glenn. "Fibre Optic Bragg Grating Sensors." *Proc. SPIE* 1169, 98-107, 1989.

[85]   J. A. J. Fells, M. J. Goodwin, C. J. Groves-Kirkby, D. C. J. Reid, J. E. Rule, and

M. B. Snell. "Fibre Optic Sensing for Military Bridge Health and Load Monitoring." IEE Colloquium on Optical Techniques for Smart Structures and Structural Monitoring (Digest No. 1997/033), 1997.

[86]   M. Nagayama, H. Tamura, and K. Shimozawa. "Corrosion Monitoring Using Embedded Minisensors on Rebars in Concrete Rehabilitated with a VCI." General Building Research Corporation of Japan, March 1997.

[87] I. J. Oppenheim, A. Jain, and D. W. Greve. "MEMS Ultrasonic Transducers for the Testing of Solids." *IEEE Transactions on Ultrasonics, Ferroelectrics, and Frequency Control,* vol. 50, no. 3, 2003.

[88]   K. B. Jacobson. "Biosensors and Other Medical and Environmental Probes." http://www.ornl.gov/info/ornlreview/rev29_3/text/biosens.htm.

[89]   Baverstam Associates' Electronic Newsletter, May 2004, vol. 4, issue 4.

[90] O. T. C. Chen, C. W. Lin, S. Wang, and C. Y. Jen. "A Multi-Function Amperometric Microsensor for Medical Application." Proceedings of the 40th Midwest Symposium on Circuits and Systems, vol. 2, 3-6 August 1997, pp. 1461–1464.

[91]   M. Mayer, O. Paul, D. Bolliger, and H. Baltes. "Integrated Temperature Microsensors for Characterization and Optimization of Thermosonic Ball Bonding Process." Components and Packaging Technologies, *IEEE Transactions*, vol. 23 , no. 2, June 2000, pp. 393 – 398.

[92]   H. Nam, G. S. Cha, T. D. Strong, J. Ha, J. H. Sim, R. W. Hower, S. M. Martin, and R. B. Brown. "Micropotentiometric Sensors." *Proc. IEEE*, vol. 91, no. 6, June 2003, pp. 870–880.

[93]   I. Stiharu, S. Rakheja, and L. Wang. "Humidity Microsensor in CMOS Mitel15 Technology." IEEE Canadian Conference on Electrical and Computer Engineering, vol. 3, 9-12 May 1999, pp. 1652 – 1657.

[94]   J. Tieman, J. Schmalzel, and R. Krchnavek. "Design of a MEMS-based, 3-axis Accelerometer Smart Sensor." Sensors for Industry Conference, 2002. 2nd ISA/IEEE, 19-21 November 2002, pp. 19 – 23.

[95]   O. Tohyama, M. Kohashi, M. Fukui, and H. Itoh. "A Fiber-optic Pressure Microsensor for Biomedical Applications." International Conference on Solid State Sensors, Transducers and Actuators, vol. 2, 16-19 June 1997, Chicago, pp. 1489 – 1492.

[96]   Nano News Now Premium Newsletter 3, September 2003.

[97] R. W. Bogue. "Nanotechnology: What Are the Prospects for Sensors?" Sensor Review, 2004.

[98] A. Flatau. *Structural Control and Health Monitoring*. John Wiley & Sons, Ltd, 2005.

[99] D. M. Pozar. *Microwave Engineering*, 2nd Edition, John Wiley, 1998.

[100] D. S. McLachlan, A. Priou, I. Chenerie, and E. Issac. "Modeling the Permittivity of Composite Materials with a General Effective Medium Equation." *Journal of Electromagnetic Waves Applications*, vol. 6, 1992, pp. 1099–1131.

[101] F. T. Ulaby, R. K. Moore, and A. K. Fung. "Microwave Remote Sensing Active and Passive, Artech House." Reprint Edition, 1990, vol. 3, Appendix E.

[102] S. O. Nelson. "Correlating Dielectric Properties of Solids and Particulate Samples through Mixture Relationships." *Transactions ASAE*, vol. 35, 1992, pp. 625–629.

[103] V. Derbek, C. Steger, J. Preishuber-Pfluegl, and M. Pistauer. "Architecture for Model-Based UHF RFID System Design Verification." Proceedings of the 2005 European Conference on Circuit Theory and Design, 2005.

[104] R. Redemske and R. Fletcher. "Design of UHF RFID Emulators with Applications to RFID Testing and Data Transport." Fourth IEEE Workshop on Automatic Identification Advanced Technologies, 2005.

[105] P. H. Cole, M. Y. Loukine, and D. M. Hall. "Integral Backscattering Transponders for Low Cost RFID Applications." Fourth Annual Wireless Symposium and Exhibition, Santa Clara, pp. 328-336, 1996.

[106] K. V. Seshagiri Rao, P. V. Nikitin, and S. F. Lam. "Antenna Design for UHF RFID Tags: A Review and a Practical Application." *IEEE Transaction on Antennas and Propagation*, vol. 53, no. 12, 2005.

[107] U. Karthaus and M. Fischer. "Fully Integrated Passive UHF RFID Transponder IC with 16.7-µW Minimum RF Input Power." *IEEE Journal of Solid-State Circuits*, vol. 38, no. 10, 2003.

[108] R. Page. "A Low Power RF ID Transponder." Wenzel Associates. www.wenzel.com/pdffiles/rays.pdf.

[109] "Inventory Tracking." Current Directions, Inc. http://www.currentdirections.com/success/mfg-steel--inventory-tracking.html.

[110]   N. Cho, S. -J. Song, S. Kim, S. Kim, and H. -J. Yoo. "A 5.1-µW UHF RFID Tag Chip Integrated with Sensors for Wireless Environmental Monitoring." Proceedings of ESSCIRC, Grenoble, France, 2005.

[111]   R. Liu et al. "Evaluation of Innovative Sensors and Techniques for Measuring Traffic Loads." Final Project Report, TxDOT Project 0-4509, 2006.

[112]   "Nanotech Hits the Roads." Roland Piquepaille's Technology Trends. http://radio.weblogs.com/0105910/2004/08/04.html.

[113]   T.Kuennen. "Small Science Will Bring Big Changes to Roads." Road Science, 2004. http://www.betterroads.com/articles/downloads/br07-04rdsci2.pdf.

[114]   "The Promise of Wireless Sensor Networks". Intel. http://www.intel.com/pressroom/archive/backgrnd/20040316backgrounder.pdf.

[115]   Mechanical and Aerospace Engineering Research Projects 2004-05, http://www.engr.ncsu.edu/research/projects/media/pdf/mae.pdf.

[116]   M. Tomizuka. "Sensor and Control Technology in the Engineering of Modern Civil and Mechanical Systems." Department of Mechanical Engineering, University of California, 2005. http://3icee.njut.edu.cn/download/paper/ch1/ch1_03.pdf.